Universidade de Aveiro Departamento de Física
2006

Martinho
Marta Almeida

Interacções Físico Biológicas que Controlam a Dispersão de Larvas: Aplicação às Zonas Adjacentes aos Estuários do Norte de Portugal

Physical Biologycal Interactions Controlling Larvae Dispersion: Application to Regions in the Neighbourhood of the Estuaries of North Portugal

Universidade de Aveiro Departamento de Física
2006

Martinho
Marta Almeida

Interacções Físico Biológicas que Controlam a Dispersão de Larvas: Aplicação às Zonas Adjacentes aos Estuários do Norte de Portugal

dissertação apresentada à Universidade de Aveiro para cumprimento dos requisitos necessários à obtenção do grau de Doutor em Física, realizada sob a orientação do Doutor Jesús Dubert, Professor Auxiliar Convidado do Departamento de Física e do Doutor Henrique Queiroga, Professor Auxiliar com Agregação do Departamento de Biologia

Apoio financeiro da FCT e do FSE no âmbito do III Quadro Comunitário de Apoio através da bolsa SFRH/BD/5439/2001

o júri

presidente

Doutor Amadeu Mortágua Velho da Maia Soares
Professor Catedrático do Departamento de Biologia da Universidade de Aveiro

Doutor Carlos Souto Torres
Professor Titular do Departamento de Física Aplicada da Universidade de Vigo

Doutora Teresa Paula Gonçalves Cruz
Professora Auxiliar do Departamento de Biologia da Universidade de Évora

Doutor António Miguel Piecho de Almeida Santos
Investigador Auxiliar do Instituto de Investigação das Pescas e do Mar – Ipimar-Iniap

Doutor João Miguel Silva Sequeira Dias
Professor Auxiliar do Departamento de Física da Universidade de Aveiro

Doutor Henrique José de Barros Brito Queiroga
Professor Auxiliar com Agregação do Departamento de Biologia da Universidade de Aveiro
Co-orientador

Doutor Jesús Manuel Pedreira Dubert
Professor Auxiliar Convidado do Departamento de Física da Universidade de Aveiro
Orientador

palavras-chave

Oceanografia da Plataforma Continental Portuguesa, Modelação Numérica, Onda de Maré, Dispersão e Recrutamento de Larvas, Migração Vertical Diária.

resumo

Um modelo numérico tridimensional oceânico foi usado para estudar a influência das condições físicas na dispersão e recrutamento de larvas com migração vertical diária (MVD) activa na plataforma continental noroeste de Portugal. As primeiras simulações foram forçadas por marés e verificou-se que a interacção entre MVD e correntes de maré não é importante para o transporte de larvas na plataforma continental oeste portuguesa. O trabalho realizado com forçamento de marés incrementou o presente conhecimento da dinâmica da maré na região. A análise da variação vertical dos parâmetros das elipses de maré mostra uma separação clara entre os harmónicos diurnos e semi-diurnos, e entre a circulação oceânica quase barotrópica e as correntes com dependência vertical na plataforma. Desprezando a interacção entre MVD e as marés, o próximo passo foi a construção e validação dum modelo realístico forçado por fluxos atmosfera-oceano, capaz de reproduzir as correntes dominantes, geradas pelo vento, na plataforma continental. Na configuração criada a MVD das larvas foi simulada com quatro cenários de distribuição e migração vertical. Foram feitas duas simulações, uma para o final do Inverno e outra para a Primavera, abrangendo os meses de Fevereiro a Abril e Abril a Junho de 2002. Estes períodos foram escolhidos pois exibem diferentes regimes de vento, não favorável e favorável ao afloramento costeiro. Os resultados mostram que as partículas com MVD sofreram maior retenção na plataforma continental interna durante condições de afloramento do que em qualquer outra combinação de cenário de migração e regime de vento. Na costa noroeste da Península Ibérica, que não exibe irregularidades topográficas que poderiam criar áreas de concentração e retenção, a MVD pode constituir um mecanismo importante para evitar a dispersão de larvas em direcção ao mar aberto.

keywords

Portuguese Shelf Oceanography, Numerical Modelling, Tidal Wave, Larvae Dispersion and Recruitment, Diel Vertical Migration.

abstract

A three-dimensional ocean numerical model was used to study the influence of physical conditions on the dispersion and recruitment of larvae with active diel vertical migration (DVM) at the northwestern Portuguese shelf region. In the first simulations the model was forced by tides and it was verified that the interaction between DVM and tidal currents is not important in the western Portuguese shelf for the transport of horizontally passive larvae. The extensive work done with tidal modelling allowed an increment in the knowledge of tidal dynamics in the region. The tidal currents are dominated by the semi-diurnal harmonic M_2 and are amplified over the shelf. The diurnal components suffer a greater amplification specially K_1 over the Lisbon Promontory. The analysis of vertical parameters of tidal ellipses showed a clear separation between semi-diurnal and diurnal components, and between the almost barotropic open sea circulation and depth dependent shelf currents. Neglecting the interaction of DVM with the tidal currents, the next step was to build and validate a realistic model forced by air-ocean fluxes, able to reproduce the prevailing wind-driven shelf currents. This new model configuration created was again used to study larvae DVM, simulated with four different scenarios of distribution and vertical migration of larvae. Two simulations were performed, one for the late winter and the other for the spring, covering the months of February to April and April to June 2002. These periods were chosen because they show contrasting wind regimes, between non-upwelling and upwelling season. The results showed that particles with DVM were more retained in the inner shelf during upwelling conditions than in any other combination of migration scenario and wind regime. In the coast of northwest Iberia, which lacks topographic irregularities that may originate concentration and retention areas, DVM may constitute an important mechanism to avoid seaward dispersal of the larvae.

Contents

List of Figures

List of Tables

Chapter 1

Introduction

The present work is focused on the northwestern Iberian shelf oceanography with the aim of studying larvae dispersion and recruitment. The larvae of interest are those hatched inside the estuaries eventually reaching the shelf where they will be dispersed by the tidal and wind driven currents. The importance of the extension and methodology of the dispersion lie in the fact of some larval species need to come back inside the estuaries to continue its development, after spend some time in the shelf. Many of these species, during the larval stage, exhibit diel vertical migration (DVM) which can be a mechanism for the recruitment process.

There are several physical mechanisms to explain larvae dispersion on the shelf, one of them is the interaction between tidal currents and DVM of larvae. This mechanism had been studied by Hill [1991a,b, 1995], who describes a series of situations where planktonic organisms migrating vertically in the water column on a background of tidal currents would experience considerable horizontal transport, provided the period of the migration is a multiple, or close to a multiple, of the tidal period. To test this hypothesis many model simulations were done. In these simulations the tidal forcing was implemented and the particles were introduced in the model as drifters. A description of the simulations and the results are shown in the appendix of chapter 3. In spite of a large number of studies and observational programs on this region, most of them were devoted to subinercial aspects of the circulation at the shelf/slope and only few studies about the tidal dynamics in this region can be found. Previous tidal works in the

western Iberian shelf consist on the three-dimensional modelling of Fanjul et al. [1997] and bidimensional finite elements modelling by Sauvaget et al. [2000] and Fortunato et al. [2002]. The main feature of those works is an accurate comparison of amplitudes and phases of the main tidal constituents with observational data. The tidal simulations done to test drifters transport inspired a deeper analysis of the tidal dynamics in the Western Iberian region, which is the subject of chapter 3. The main emphasis of the work presented here is on some three-dimensional aspects of the adjustment of the tidal ellipses at the shelf/slope. That chapter was accepted for publication in the journal *Continental Shelf Research*. Related to this work studying tides, it was created a web page dedicated to tidal predictions in the studied region. It is a free utility where users can obtain the tidal heights for a chosen period at several locations. The title of the page is *Tidal Prediction for the Western Iberian Peninsula* and the address is `http://neptuno.fis.ua.pt/tidal`.

As shown is the appendix of chapter 3, the interaction of diel vertical migration with the tidal currents is not an important mechanism for larvae dispersion in the studied region. Thus, the next step was to build and validate a realistic model forced by air-ocean fluxes, able to reproduce the prevailing wind-driven shelf currents. The influence of the oceanic circulation onto the shelf was not considered because the shelf break and slope act as an insulator [Peliz et al., 2003a], limiting the influence of external forcings in the middle and inner shelf, which is our region of interest. It is thence assumed that the circulation on the shelf is solely forced by wind and air-ocean heat fluxes. For this purpose, a fine resolution model was created for the northwestern Portuguese shelf, and was validated with hydrological and currentmeter observations collected in a cruise during May 2002, in the framework of the ProRecruit project. The model was forced with wind and bulk fluxes taken from the NCEP reanalysis database which were interpolated for the model grid. The simulated period was characterised by the end of the winter regime and the beginning of the spring/summer regime, typically upwelling favourable, with the onset of the stratification. A description of the simulation and the validation with currentmeter and hydrological data is done in chapter 4.

The successful validation of the model created allowed to apply it in the study of

larvae dispersion. In the model built, larvae were again introduced as drifters with Lagrangian horizontal movement and, in order to examine the influence of vertical migration pattern on dispersal, four scenarios of distribution were implemented and analysed. Those different scenarios were chosen to contrast two with active daily vertical migration and two scenarios without vertical migration. In the first, the particles were dropped at the surface and constrained to remain there. In the second they were released with an uniform distribution between the surface and the bottom and left to change vertical position according to the vertical currents of the model. In the third, diel vertical migration was imposed on the particles, making them migrate daily between a surface and a bottom layer. In the last scenario, vertical migration was also imposed, but the pattern of migration was more complex in agreement with observation of the variation of decapod larvae distribution in the water column in the Western Portuguese shelf. Such observations were also done during the ProRecruit cruise in a fixed point at the shelf off Ria de Aveiro [dos Santos et al., in preparation]. The numerical model has been adapted to reproduced these scenarios of drifters vertical distribution and migration. Two simulations were performed, one for the late winter and the other for the spring, covering the months of February to April and April to June 2002. These periods were chosen because they show contrasting wind regimes, between non-upwelling and upwelling season. The interaction between the migration scenarios and the shelf circulation conducted to the discovery of a retention mechanism for larvae with vertical migration. The main conclusion of this study is that upwelling conditions do not necessarily lead to offshore transport of larvae. They would do in the case of larvae that do not exhibit vertical migration behaviour and would either remain at the surface or be passively redistributed along the water column by the vertical component of the currents. Larvae with diel vertical migration were more retained in the inner shelf during upwelling than in any other combination of migration scenario and wind regime. This study is done in chapter 5 and has been accepted for publication in the journal *Marine Ecology Progress Series*. Moreover, it was distinguished as feature article of the journal.

The tools for creation of the model forcings used, both tidal and air-ocean forcings,

as well as the tools used in the tidal harmonic analysis and visualisation of all the simulations results were created by me and consist in a large set of functions gathered in m_pack, a free Matlab package available at the site `http://neptuno.fis.ua.pt/~mma`.

In the next chapter (chapter 2) is done a description of the numerical model used in all the simulations. Chapter 3 is devoted to the work done in the study of tides in the Western Iberian region. In chapter 4 is described the model created for the northwestern Portuguese shelf, and the validation of the model with hydrological and currentmeter observations is done. Chapter 5 explores the dispersion and recruitment of larvae at the shelf, namely the influence of the vertical migration on the inner-shelf retention, under different wind regimes. At the end, chapter 6 summarises the work.

Chapter 2

The Numerical Model

This chapter provides a description of the main features of the numerical model used in this work, the Regional Ocean Modeling System (ROMS), a community code developed at Rutgers University (USA) and at University of California Los Angeles (USA).

2.1 Model description

ROMS is a a three-dimensional model that solves the free-surface, hydrostatic, primitive equations of the ocean dynamics over a variable topography. In the horizontal it uses orthogonal curvilinear coordinates and, in the vertical, stretched terrain-following coordinates. It is the successor of the S-coordinate Rutgers University Model, SCRUM, including many numerical improvements, like high-order advection schemes, several subgrid scale parameterizations, atmospheric, oceanic and benthic boundary layer, accurate pressure gradient, radiation boundary layer and assimilation of data. For computational economy, the hydrostatic primitive equations for momentum are solved using a split-explicit time stepping scheme which requires a special treatment and coupling between barotropic (fast) and baroclinc (slow) modes. A finite number of barotropic time steps, within each baroclinic step, are carried out to evolve the free-surface and vertically integrated momentum equations. In order to avoid the errors associated with the aliasing of frequencies resolved by the barotropic steps but unresolved by the baroclinic step, the barotropic fields are time averaged before they replace those values

obtained with a longer baroclinic step. A cosine-shape time filter, centred at the new time level, is used for the averaging of the barotropic fields. In addition, the separated time-stepping is constrained to maintain exactly both volume conservation and constancy preservation properties which are needed for the tracer equations [Shchepetkin and McWilliams, 2005]. Currently all 2D and 3D equations are time discretized using a third-order accurate predictor (Leap-Frog) an corrector (Adams-Molton) time-stepping algorithm which is very robust and stable. The enhanced stability of the scheme allows larger time steps, by a factor of about four, which more than offsets the increased cost of the predictor-corrector algorithm.

2.2 Governing equations

In the Boussinesq and hydrostatic approximations, the governing equations in Cartesian coordinates are:

$$\frac{Du}{Dt} = fv - \frac{\partial \phi}{\partial x} + \mathcal{F}_u + \mathcal{D}_u \tag{2.1}$$

$$\frac{Dv}{Dt} = -fu - \frac{\partial \phi}{\partial y} + \mathcal{F}_v + \mathcal{D}_v \tag{2.2}$$

$$\frac{DT}{Dt} = \mathcal{F}_T + \mathcal{D}_T \tag{2.3}$$

$$\frac{DS}{Dt} = \mathcal{F}_S + \mathcal{D}_S \tag{2.4}$$

$$\rho = \rho(T, S, P) \tag{2.5}$$

$$\frac{\partial \phi}{\partial z} = -\frac{\rho g}{\rho_0} \tag{2.6}$$

$$\nabla.\mathbf{v} = 0 \tag{2.7}$$

with vertical boundary conditions at the top, $z = \zeta$:

$$K_M \frac{\partial u}{\partial z} = \tau_s^x \tag{2.8}$$

$$K_M \frac{\partial v}{\partial z} = \tau_s^y \tag{2.9}$$

$$K_T \frac{\partial T}{\partial z} = \frac{Q_T}{\rho_0 C_p} \tag{2.10}$$

$$K_S \frac{\partial S}{\partial z} = (E - P)S \tag{2.11}$$

$$w = \frac{\partial \zeta}{\partial t} \tag{2.12}$$

and at the bottom, $z = -h$:

$$K_M \frac{\partial u}{\partial z} = \tau_b^x \tag{2.13}$$

$$K_M \frac{\partial v}{\partial z} = \tau_b^y \tag{2.14}$$

$$K_T \frac{\partial T}{\partial z} = 0 \tag{2.15}$$

$$K_S \frac{\partial S}{\partial z} = 0 \tag{2.16}$$

$$w = \mathbf{v}.\nabla h \tag{2.17}$$

where

- x, y, z are the Cartesian coordinates
- u, v, w are the velocity components
- f is the Coriolis parameter
- ϕ is the dynamic pressure
- $\mathcal{F}_u$, $\mathcal{F}_v$, $\mathcal{F}_T$, $\mathcal{F}_S$ are the forcing terms
- $\mathcal{D}_u$, $\mathcal{D}_v$, $\mathcal{D}_T$, $\mathcal{D}_S$ are the diffusive terms
- T is the potential temperature
- S is the salinity
- P is the total pressure
- $\rho_0 + \rho$ is the total *in situ* density

- g is acceleration of gravity
- ζ is the surface elevation
- K_M, K_T, K_S are the vertical turbulent mixing coefficients
- τ_s^x, τ_s^y are the surface wind stress components
- Q_T is the surface heat flux
- $E - P$ is the evaporation minus precipitation
- τ_b^x, τ_b^y are the bottom stress components
- h is the bottom depth

The equations 2.1 and 2.2 express the momentum balance in the x- and y-directions, respectively. Equations 2.3 and 2.4 are the advective-diffusive equations and express the time evolution of temperature and salinity. Equation 2.5 is the equation of state. Under the hydrostatic approximation, the momentum balance in the vertical direction limits itself to a balance between the pressure gradient and the buoyancy forces. In the Boussinesq approximation, density variations are neglected in the momentum equations except in their contribution to the buoyancy forces in the vertical momentum equation (2.6). Equation 2.7 is the continuity equation for an incompressible fluid.

2.3 Coordinates system and discretization

In the horizontal, the primitive equations are evaluated using a boundary fitted, orthogonal curvilinear coordinates on a staggered Arakawa C grid (Figure 2.1), through second-order finite difference approximation. This system can conform to irregular lateral boundaries or allows the placement of more computational resolution in regions of interest [Ives and Zacharias, 1987]. The Arakawa C grid is well suited for problems with horizontal resolution that is fine compared to the first radius of deformation [Arakawa and Lamb, 1977; Wilkin and Headström, 1998]. These new coordinates are introduced by a transformation in the horizontal coordinate from the Cartesian coordinates x, y to

ξ, η. The new coordinates are orthogonal and the boundaries of the physical domain lie along lines of constant ξ and η. The metric coefficients m, and n of the orthogonal curvilinear coordinate system relate differential distances in the ξ, η directions to actual physical arc lengths:

$$(ds)_\xi = \frac{d\xi}{m} \tag{2.18}$$

$$(ds)_\eta = \frac{d\eta}{n} \tag{2.19}$$

A line element of length ds therefore satisfies:

$$ds^2 = \frac{d\xi^2}{m^2} + \frac{d\eta^2}{n^2} \tag{2.20}$$

And m and n can be computed from Cartesian coordinates defined as functions of ξ and η:

$$m = (x_\xi^2 + y_\xi^2)^{-1/2} \tag{2.21}$$

$$n = (x_\eta^2 + y_\eta^2)^{-1/2} \tag{2.22}$$

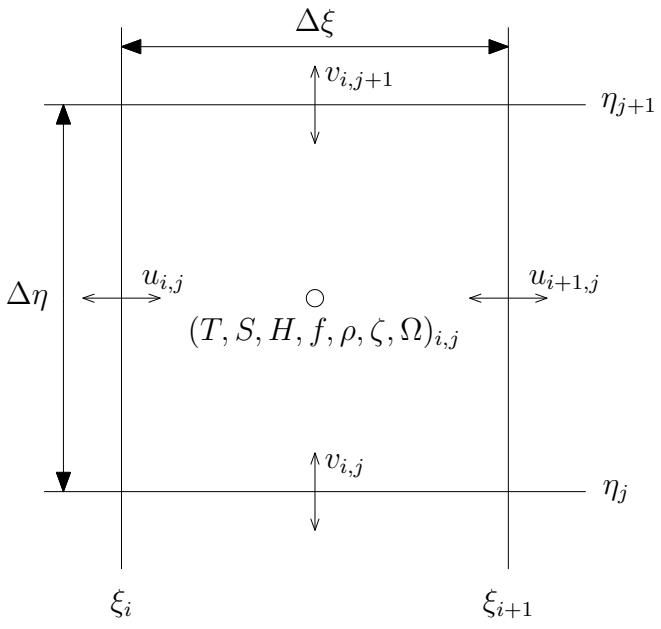

Figure 2.1: Placement of variables on the Arakawa C grid.

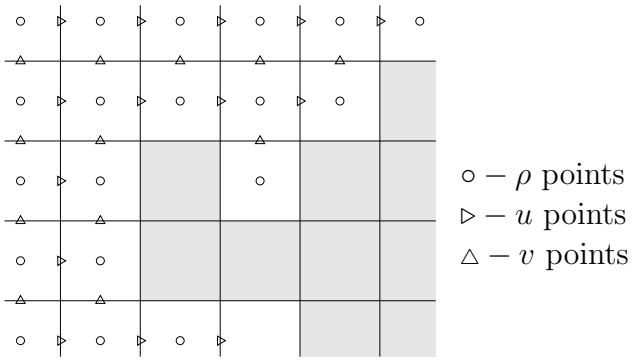

Figure 2.2: Land/sea mask.

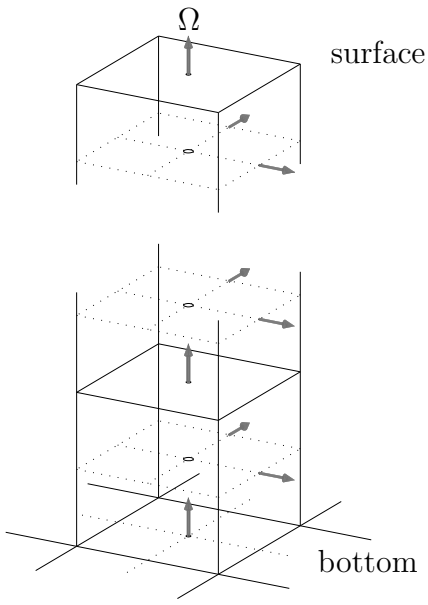

Figure 2.3: Placement of variables on the staggered vertical grid.

Coastal boundaries can also be specified as a finite-discretized grid via land/sea masking (example in Figure 2.2). The model has the ability to work with interior land areas, although the computations occur over the entire model domain.

The vertical discretization also uses a second-order finite difference approximation. As well as in the horizontal, the model also uses a staggered vertical grid (Figures 2.3 and 2.4). These choices are traditional for second-order, finite differences models, and provide for conservation of the first and second moments of momentum and tracers [Haidvogel et al., 2000].

The stretched terrain-following coordinates [Song and Haidvogel, 1994] allow the increase of resolution in depths of interest along the water column. Standard sigma coordinates subdivide the vertical into an equal number of points:

$$s = \frac{z}{h} \tag{2.23}$$

As an extension of this, a nonlinear stretching of the vertical coordinate can be applied that depends on local water depth. This option can be used to generate a more uniform vertical resolution near the surface and consequently a better representation of the mixed layer and thermocline. The strong, and sometimes undesirable, coupling between s-coordinate surfaces and local water depth is also reduced. The original transformation as defined by Song and Haidvogel [1994] is:

$$z = \zeta(1+s) + \underbrace{h_c s + (h - h_c)C(s)}_{A} \tag{2.24}$$

where h_c is a constant chosen as a typical surface mixed layer depth, and

$$C(s) = (1-\theta_b)\frac{\sinh(\theta_s s)}{\sinh(\theta_b)} + \theta_b \frac{\tanh[\theta_s(s+0.5)] - \tanh(\theta_s/2)}{2\tanh(\theta_s/2)} \tag{2.25}$$

The parameter θ_s controls the resolution near the surface, for large θ_s the coordinate lines are more tightly confined to the surface ($20 < \theta_s < 1$). θ_b is the bottom control parameter, if it approaches 1, resolution at the bottom boundary layer is enhanced ($0 < \theta_b < 1$).

Currently ROMS uses a modified version of equation 2.24, with consequent numerical improvements [Shchepetkin and McWilliams, 2005]:

$$z = \zeta(1 + \frac{A}{h}) + A \tag{2.26}$$

The vertical velocity in this coordinate system is defined as:

$$\Omega = \frac{\partial s}{\partial t} = \frac{\partial s}{\partial z}\left[w - (1+s)\frac{\partial \zeta}{\partial t} - mu\frac{\partial z}{\partial \xi} - nv\frac{\partial z}{\partial \eta}\right] \tag{2.27}$$

and the kinematic boundary conditions 2.12 and 2.17, at the surface ($s = 0$) and at the bottom ($s = -1$) simplify to:

$$\Omega = 0 \tag{2.28}$$

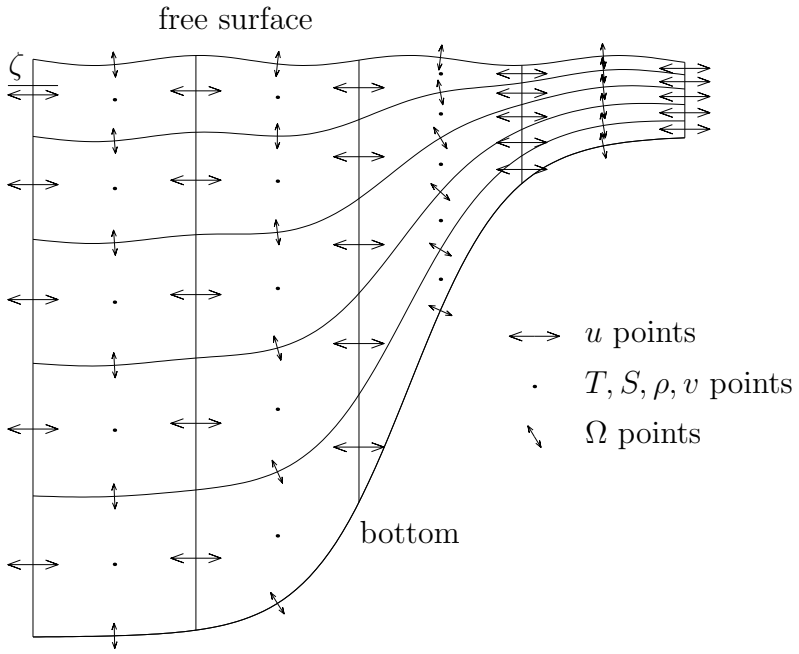

Figure 2.4: Placement of the variables on a cross section.

2.4 The pressure gradient scheme

Terrain-following coordinate models exhibit stronger sensitivity to topography which results in pressure gradient errors. These errors arise due to the splitting of the pressure gradient term into a component along the s-surface and the hydrostatic correction:

$$\left.\frac{1}{\rho_0}\frac{\partial P}{\partial x}\right|_{z=const} = \left.\frac{1}{\rho_0}\frac{\partial P}{\partial x}\right|_{s=const} - \left.\frac{1}{\rho_0}\frac{\partial P}{\partial z}\frac{\partial z}{\partial x}\right|_{s=const} \tag{2.29}$$

Unfortunately, both terms are large, and cancellation of the hydrostatic resting pressure is not exact due to imbalanced numerical truncation errors in the two terms. The resulting pressure gradient errors depend on the steepness of the topography, the horizontal and vertical resolution and the strength of the stratification. When using realistic topography, some smoothing is required before it can be used. In ROMS, empirical studies have shown that reliable results are obtained if the smoothing parameter,

$$r = \frac{\Delta h}{2h} = \frac{h_{+1/2} - h_{-1/2}}{h_{+1/2} + h_{-1/2}} \tag{2.30}$$

does not significantly exceed 0.2 [Haidvogel and Beckmann, 1999].

Several alternate forms of the s-coordinate pressure gradient have been formulated with the aim of reduce errors, each with slightly numerical properties. The scheme

implemented in ROMS is the weighted Jacobian formulation proposed by Song [1998]. The pressure gradient force, equation 2.29, can be written in the Jacobian form:

$$\frac{1}{\rho_0}\frac{\partial P}{\partial x}\bigg|_{z=const} = \rho_s g\frac{\partial \zeta}{\partial x} + g\int_z^{\zeta} \mathcal{J}(\rho, z)ds \tag{2.31}$$

where

$$\mathcal{J}(\rho, z) = \frac{\partial z}{\partial s}\,\frac{\partial \rho}{\partial x}\bigg|_{s=const} - \frac{\partial \rho}{\partial s}\,\frac{\partial z}{\partial x}\bigg|_{s=const} \tag{2.32}$$

and ρ_s is the density at the surface. Thence, vertical variations in the pressure gradient are expressed in terms of a vertical integral of the Jacobian of density and depth with respect to the vertical computational coordinate. Two discrete schemes were proposed by Song [1998], using standard centred differencing in the generalised vertical coordinate, and using a vertical weighting such that the finite differences are centred with respect to the Cartesian z coordinate. In an idealised case the standard Jacobian outperforms the weighted Jacobian when the hydrostatic condition is satisfied. When not, the weighted Jacobian gives superior results, which is often the case in realistic configurations. The conservation of momentum and energy and the accurate representation of the bottom pressure has been validated [Song and White, 1998] and the conservation of these properties can constrain model errors.

More recently the pressure gradient scheme proposed by Shchepetkin and McWilliams [2003] has also been introduced in ROMS. The new algorithm is based on the reconstruction of the density field and the physical z coordinate as continuous functions of transformed coordinates with subsequent analytical integration to compute the pressure gradient force. This scheme achieves more accurate hydrostatic balance between the two components of equation 2.29 and does not loose much accuracy with nonuniform vertical grids at relatively coarse resolution.

2.5 The advection scheme

ROMS has various options for advection schemes: second- and fourth-order centred differences, and third-order upstream biased. These schemes are stable for the predictor-corrector methodology of the model. The advection operator for the momentum and

tracer variables has been redesigned to reduce dispersive errors. Explicit smoothing of the fields is no longer mandatory, enhancing the effective resolution of the solution for a given grid [Shchepetkin and McWilliams, 1998]. In addition there is an option for conservative parabolic splines representation of the vertical advection which has dispersion properties similar to an eight-order accurate conventional scheme [Shchepetkin and McWilliams, 2005].

2.6 The turbulent closure scheme

Several subgrid-scale parameterizations are available in ROMS. The horizontal mixing of momentum and tracers can be along vertical levels, geopotential surfaces or isopycnic surfaces. The mixing operator can be harmonic or biharmonic and the vertical mixing parameterization can be done via local or nonlocal closure schemes. The local closure scheme is based on the level 2.5 turbulent kinetic energy equations by Mellor and Yamada [1982] (M-Y). The nonlocal closure scheme is based on the K-profile planetary (KPP) boundary layer formulation by Large et al. [1994]. KPP matches separate parameterizations for vertical mixing of the surface boundary layer and the ocean interior. The boundary layer depth depends on the surface forcing, the buoyancy and the velocity profile and is determined by equating a bulk Richardson number relative to the surface to a critical value. Below the boundary layer the vertical mixing is regarded as the superposition of three processes: vertical shear, internal wave breaking and double diffusion. In the surface layer, the diffusivity is formulated to agree with a similarity theory of turbulence. At the base of the surface layer, both diffusivity and its gradient have to match the interior values. The KPP has been expanded to include both surface and bottom oceanic boundary layers. For additional information about KPP and comparison with M-Y see Durski et al. [2004].

Chapter 3

The Structure of Tides in the Western Iberian Region

A s-coordinate three-dimensional model, ROMS (Regional Ocean Modeling System), was implemented in the Western Iberian region ranging from the coast to 11° W aiming high resolution tidal simulations for an homogeneous ocean. The features for tidal heights and ellipses for the principal constituents, M_2, S_2, N_2, K_2, K_1, O_1, P_1 and Q_1, were imposed at the boundaries of the model. A tidal analysis for heights and tidal currents was done allowing to calculate two-dimensional distribution of amplitudes and three-dimensional structure of tidal currents. The amplitudes and phases for heights agrees with previous results and observations, showing a good precision on the tidal propagation in the interior of the domain.

Tidal kinetic energy is dominated by the semi-diurnal components, mainly M_2, and increases on the shelf. Over the Lisbon Promontory the diurnal component K_1 is however the second more energetic harmonic. Vertical variation of tidal ellipse parameters evidences the different structure of semi-diurnal and diurnal tidal components, as well as differences between the open sea and shelf tidal circulation.

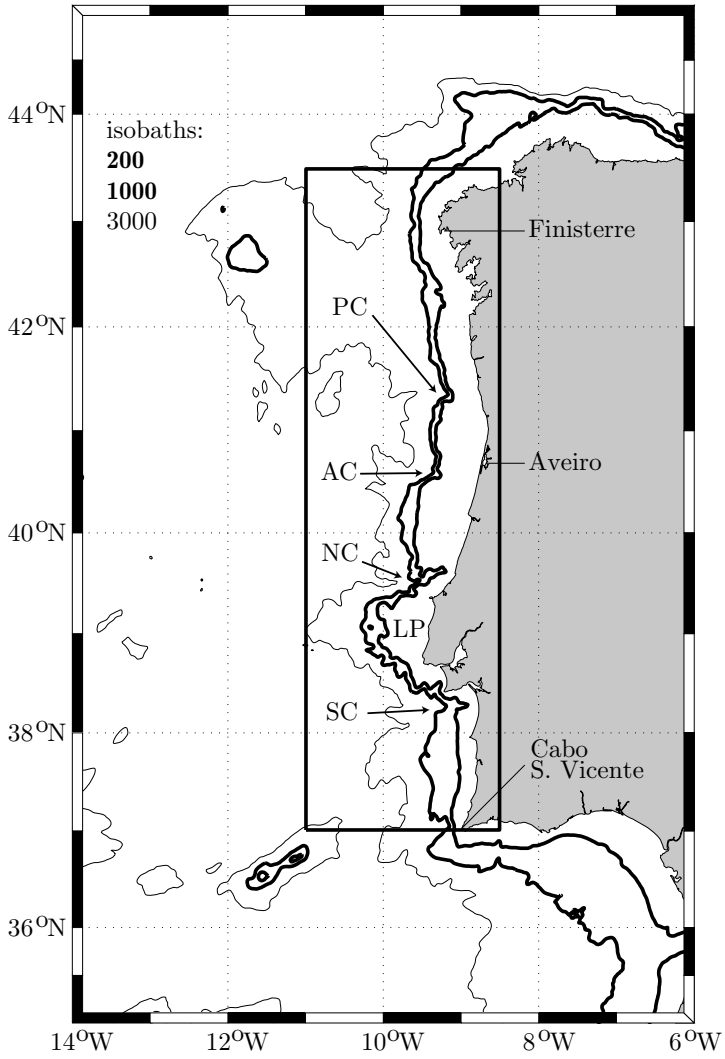

Figure 3.1: Region of study with modelling area (inner rectangle). Slope is given by isobaths 200 m and 1000 m (bold isobaths). Isobath 3000 is also included. The main bathymetric irregularities are shown, namely the Setúbal Canyon (SC), the Lisbon Promontory (LP), the Nazaré Canyon (NC), Aveiro Canyon (AC) and the Porto Canyon (PC). The dimensions of the modelling area are 720 km in the south-north direction and 210 km in the west-east direction.

3.1 Introduction

The main aim of this work is to study the tides and its associated currents in the shelf/slope of Western Iberian Peninsula based on a three-dimensional model. In spite of a large number of studies and observational programs on this region were (and are)

devoted to subinercial aspects of the circulation at the shelf/slope, much less studies about the tidal dynamics in this region can be found.

The Western Iberian Peninsula (Figure 3.1) extends approximately south-north along the meridian 9° W, between 37° N and 43° N. The shelf width is approximately 40 km unless in the southernmost region, until Lisbon, where it is half of this value. The region is characterised by the presence of several irregularities determinant for the tidal dynamics, namely the Lisbon Promontory and four main canyons: Setúbal, Nazaré, Aveiro and Porto. The bathymetry profile from cape S. Vicente to Setúbal Canyon is characterised by the lack of a clear shelf break and the depth increases in a near exponential manner.

Previous work has already been done in this region using also a three-dimensional finite differences model [Fanjul et al., 1997] and using bidimensional finite elements models [Sauvaget et al., 2000; Fortunato et al., 2002]. Fanjul et al. [1997] performs a very extensive analysis of the tidal propagation for the eastern North Atlantic region. They put a special emphasis in comparison with observational data (tidal gauges and currentmeters on the French shelf) and achieve a very accurate description in terms of the propagation of the tidal wave. However, their model configuration is not designed to study the details of the adjustment of the tidal wave in the shelf/slope region. Bidimensional modelling study of Sauvaget et al. [2000] is centred mainly on the numerical formulation of the finite elements model and the comparison of amplitudes and phases with tidal gauges registers. Fortunato et al. [2002] also with finite element modelling approach, give emphasis to the generation of barotropic shelf waves arising from diurnal tides at the Lisbon Promontory. The main feature of the above cited works is an accurate comparison of amplitudes and phases of the main tidal constituents with observational data (tidal gauges). The main emphasis of this work will be to carry out a study of some three-dimensional aspects of the adjustment of the tidal ellipses at the shelf/slope. Namely its horizontal structure (amplitude and polarisation) and its vertical structure in the water column. However, some comparisons of tidal heights and tidal currents is done to assure the model results validation.

For several years, two-dimensional models gave adequate results for predictions of

tidal elevations. However because of much small scale variability of tidal currents, in comparison with elevations, a rigorous study of tidal dynamics on the shelf requires an high resolution 3-D numerical model [Prandle, 1997b; Davies et al., 1997]. This is a consequence of the higher bottom and internal frictional influence in these regions [Prandle, 1997a]. Because diurnal currents are more sensitive to friction than the semi-diurnals currents of the same magnitude [Prandle, 1997b], this may be a justification to the fact that in the above mentioned previous studies, diurnal constituents exhibit larger deviations when compared with available data.

Many results of this work are build upon previous theoretical and observational works on tidal dynamics. A good explanation of the vertical tidal ellipse variation was made by Prandle [1982] for the homogeneous case and some other studies for the stratified ocean also exist [Souza and Simpson, 1996; Simpson, 1997; Xing and Davies, 1997, 1998].

The stratification is not considered in this study, neglecting the internal tide associated with the interaction between steep topography and the barotropic tide. Although we do not expect that the influence of internal wave propagation to be so large as in Bay of Biscay [New and da Silva, 2002] or in Malin-Hebrides region [Xing and Davies, 1998], some evidences from internal tide tidal currents can be found in Vitorino et al. [2002], which reports bottom intensification and cross-shore polarisation of currents along the Porto Canyon axis, over the shelf. However the comparison of tidal ellipses of stations located in the inner shelf reported in this work indicates that the effects of stratification in tidal currents is not important in that region. Also it is not expected that the amplitude and phase of tidal wave be significantly affected by stratification, similarly to the Xing and Davies [1998].

The following section describes the model setup and parametrization. Section 3.3 includes the results and its analysis being divided in analysis of tidal heights, analysis of tidal currents, analysis of the vertical structure of tidal ellipse parameters and analysis of sensitivity of the results to the bottom friction. In section 4 the results are summarised.

Table 3.1: Model setup parameters

L	280	Number of points points E–W
M	360	Number of points points N–S
N	10	Number of s-levels
h_{max}	5125 m	Maximum region depth
h_{min}	5 m	Minimum region depth
θ_s	3	S-coordinates surface control parameter
θ_b	0.4	S-coordinates bottom control parameter
Δx	0.75 km	Resolution in the zonal direction
Δy	2 km	Resolution in the meridional direction
Δt	60 s	Baroclinic time step
Δt_f	3 s	Barotropic time step
ν	15 $m^2\ s^{-1}$	Laplacian horizontal viscosity
ν_t	15 $m^2\ s^{-1}$	Laplacian horizontal diffusivity
κ	5×10^{-6} $m^2\ s^{-1}$	Background vertical viscosity
κ_t	5×10^{-6} $m^2\ s^{-1}$	Background vertical diffusivity
r	3×10^{-4} m s^{-1}	Linear bottom drag coefficient (run II)
T	14 °C	Constant temperature
S	35 psu	Constant salinity

3.2 Model setup and parameterization

A three-dimensional model was used to simulate tidal dynamics in the Western Iberian Peninsula Coast. The model is ROMS [Haidvogel et al., 2000], a free surface, hydrostatic, primitive equations model, with vertical s-coordinates [Song and Haidvogel, 1994].

The grid used covers the longitudes between 8.5° W and 11° W and the latitudes 37° N to 43.5° N (Figure 3.1), thus 720 km in the south-north direction and 210 km in the west-east direction. Grid resolution is constant with ~ 0.75 km in the zonal (W–E)

direction and ~ 2 km in the meridional (S–N) direction, consisting in 280 by 360 grid points. Ten vertical s-levels were used, with $\theta_s = 3$ and $\theta_b = 0.4$, as defined by Song and Haidvogel [1994], indicating that vertical resolution is increased in surface and bottom.

In this study it was used homogeneous conditions for temperature and salinity, with values $T = 14°\text{C}$ and $S = 35$ psu.

Grid topography was taken from GEBCO — General Bathymetric Chart of the Oceans — 1-minute global bathymetric grid, with some corrections on the continental shelf.

ROMS was forced at the open boundaries with tidal parameters for elevations (amplitudes and phases) and for current ellipses (semi-major axis, semi-minor axis, inclination and phase). Tidal data was obtained from OSU TOPEX/Poseidon Global Inverse Solution, TPXO [Egbert and Erofeeva, 2002]. TPXO is a global model of ocean tides which best fits the Laplace tidal equation and data from the TOPEX/Poseidon orbit cycles. It uses a inversion scheme [Egbert et al., 1994] developed for assimilating the altimetric data into a global barotropic model. That model provides elevations and tidal currents for the main semi-diurnal and diurnal constituents (M_2, S_2, N_2, K_2 and K_1, O_1, P_1, Q_1, respectively) with a resolution of 1/6 degrees for the North Atlantic. As a first approach, barotropic initial conditions were used. The model was run for sixty days and the output time series of ocean surface heights and ocean currents was analysed, using harmonic least squares fit, to retrieve harmonic parameters of tides. The output time series were separated by 5 grid points, in both south-north and west-east direction, ie, with a resolution of 10 per 3.75 km respectively.

The simulation period was smaller than synodic period of some pairs of constituents, following Rayleigh criterion. In the case of S_2 and K_2, or K_1 and P_1, the time series length should be at least 182 days. However, using Fourier analysis it was realised that shallow water tidal constituents are not important in the studied region. For this reason, the least squares fit done only with the forcing frequencies becoming the Rayleigh criterion unnecessary.

Model setup parameters are shown in Table 3.1. The vertical mixing scheme is based on the vertical closure turbulent model proposed by Large et al. [1994] (K–profile

Table 3.2: Simulations performed to test the sensitivity of the bottom friction parameterization on the tidal dynamics. The parameter r is the linear bottom drag coefficient and z_0 is the bottom roughness of the quadratic formulation.

run	bottom frict. parametriz..	friction parameter
I	linear	$r = 1.5 \times 10^{-4}$ m s^{-1}
II	linear	$r = 3 \times 10^{-4}$ m s^{-1}
III	linear	$r = 6 \times 10^{-4}$ m s^{-1}
VI	quadratic	$z_0 = 0.005$ m

parameterization, KPP).

Due to the importance of the bottom friction for the tidal currents on the shelf, four simulations were performed in order to test the sensitivity of the parameterization of the bottom friction on the tidal dynamics (Table 3.2). In three simulation it was used a linear bottom friction condition, ($\tau_b = rv_b$, where v_b stands for the velocity at the deepest level) with different bottom drag coefficients, r. In one simulation it was used a typical value of $r = 3 \times 10^{-4}$ m s^{-1}, and in the other two, half and the double of this value. In the fourth simulation it was used a quadratic formulation, $\tau_b = C_d v_b U_b$, where v_b is an horizontal current component at the deepest level, U_b is the horizontal speed at the same level and $Cd = (K/\ln(z_b/z_0))^2$, with $K = 0.4$ von Kármán's constant, z_b the height of the deepest level and z_0 the bottom roughness. For z_0 was used a typical value of 0.005 m.

3.3 Results

The characteristics of the slope and the latitudinal variations in bathymetry lead to important modifications in the offshore tidal wave, originally moving northwards as a Kelvin wave. Acting as a barrier to the tidal wave propagation, the relatively wide Lisbon Promontory (see Figure 3.1) is an important topographic feature in the studied region. In this area, different relative amplification of tidal constituents originates an

Table 3.3: Simulated and observed amplitudes and phases of tidal heights for Cascais and Vigo. Observed data is taken from Tables 3 and 4 of Fanjul et al. [1997]. Empty field is employed where no data is available.

	Cascais				Vigo			
	amplitude (cm)		phase (degrees)		amplitude (cm)		phase (degrees)	
	obs	sim	obs	sim	obs	sim	obs	sim
M_2	112.3	113.2	65.0	64.8	112.3	113.2	76.7	80.0
S_2	35.0	35.3	91.0	90.3	38.8	39.7	106.2	109.9
N_2		21.3		47.0	23.8	23.9	58.1	61.1
K_2		9.5		88.6	11.0	10.8	103.8	106.7
K_1	7.0	7.7	54.0	60.1	7.6	8.1	59.4	67.6
O_1	5.8	5.9	313.0	317.6	6.5	6.1	318.7	323.1
P_1		2.3		47.7	2.5	2.4	48.4	55.7
Q_1		1.8		262.7		1.9		267.8

interesting horizontal tidal currents pattern, with currents in opposite directions at points separated by few dozens of kilometres at the shelf, analysed below.

Tides in the Western Iberian Coast are dominated by the semi-diurnal tidal components M_2 and S_2 (Figures 3.2 and 3.3), which give rise to clear spring-neap cycles modulated by other constituents. In some parts of the shelf like Lisbon Promontory, however, diurnal harmonics, especially K_1, assume a great importance and modifies significantly the tidal currents pattern.

The results presented hereafter, namely the tidal heights, tidal currents and vertical structure are the results of the main simulation (Table 3.2, run II), with linear drag coefficient $r = 3 \times 10^{-4}$ m s^{-1}. At the end of this section, the sensitivity to bottom friction is analysed by comparing the results of the main simulation with the other simulations, with different bottom friction parameterizations (Table 3.2).

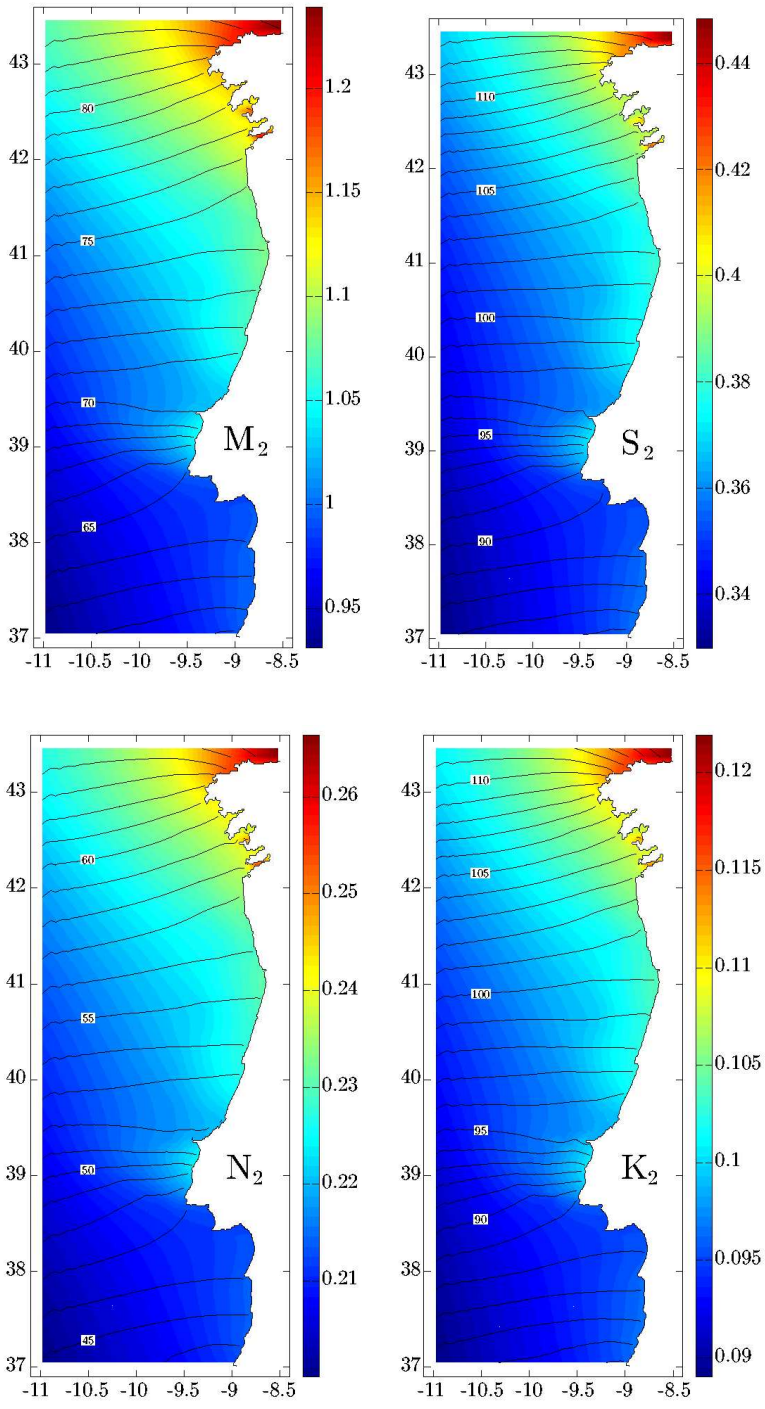

Figure 3.2: Amplitudes (m) and phases (deg) of the semi-diurnal tidal components: M_2, S_2, N_2 and K_2.

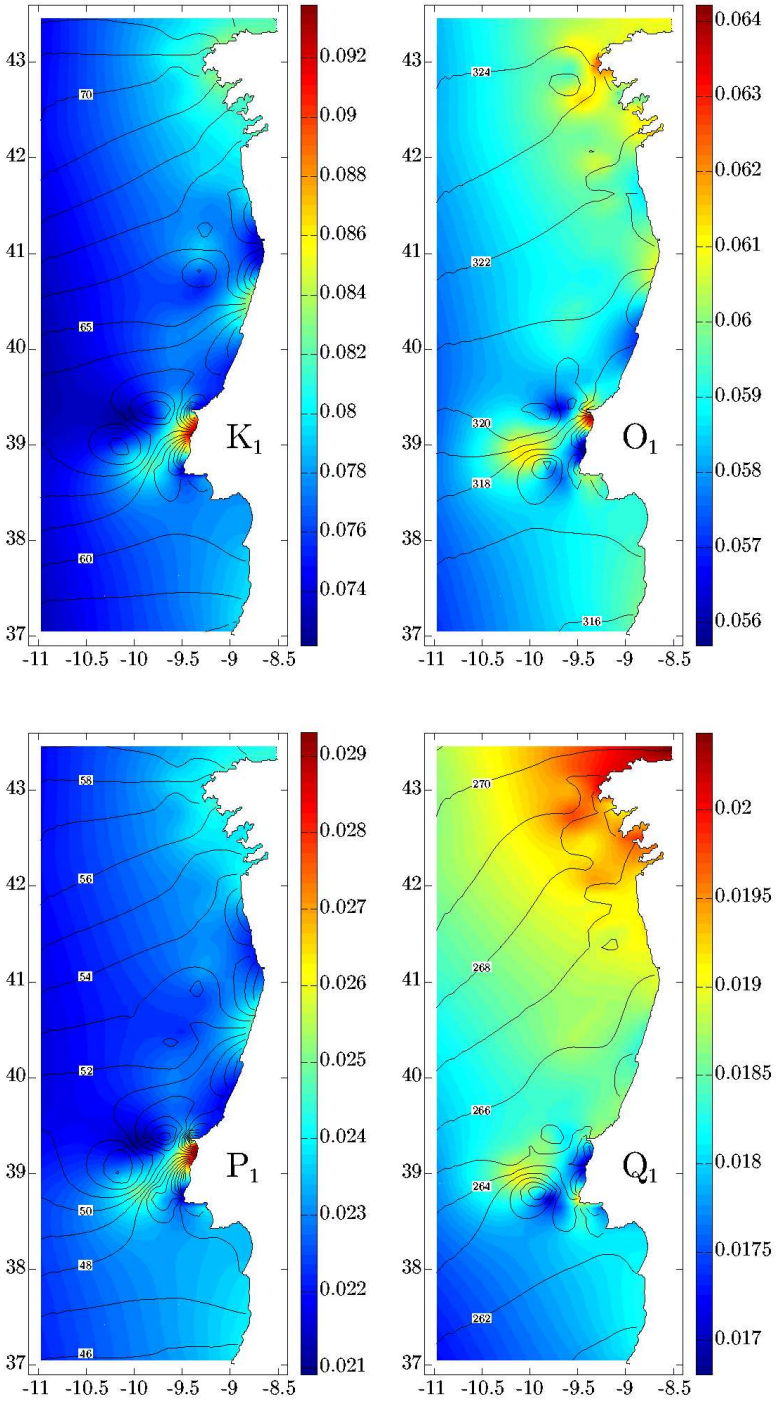

Figure 3.3: Amplitudes (m) and phases (deg) of the diurnal tidal components: K_1, O_1, P_1 and Q_1.

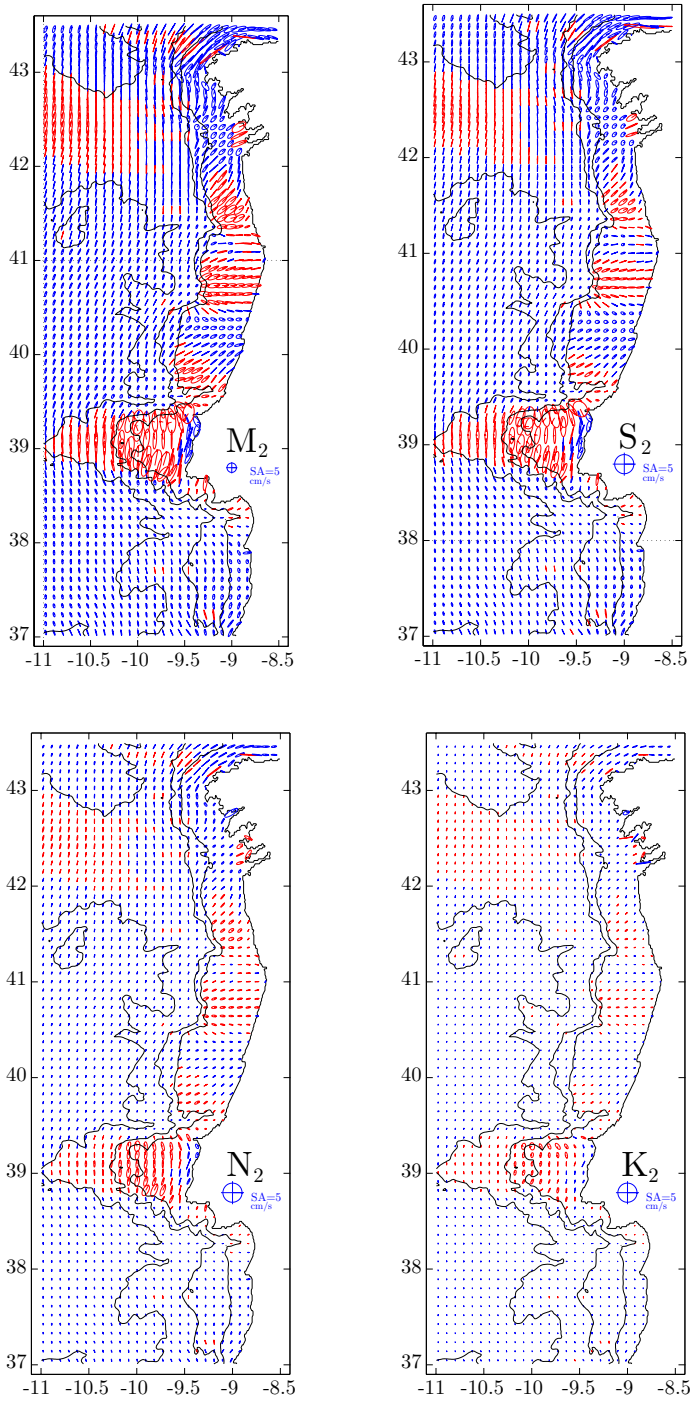

Figure 3.4: Barotropic tidal ellipses of the semi-diurnal tidal components: M_2, S_2, N_2 and K_2. Blue ellipses are counterclockwise, while red ones have clockwise rotation. The radial line inside the ellipses gives the Greenwich phase. Over the Lisbon Promontory M_2 and S_2 ellipses are more disperse for clarity. Notice the ellipses scale. It represents a circular ellipse with semi-axis of 5 cm/s, but its size is half for M_2. Bold bathymetric lines represent the shelf break (200 and 1000 metres); the thick line is the isobathymetric 3000 m.

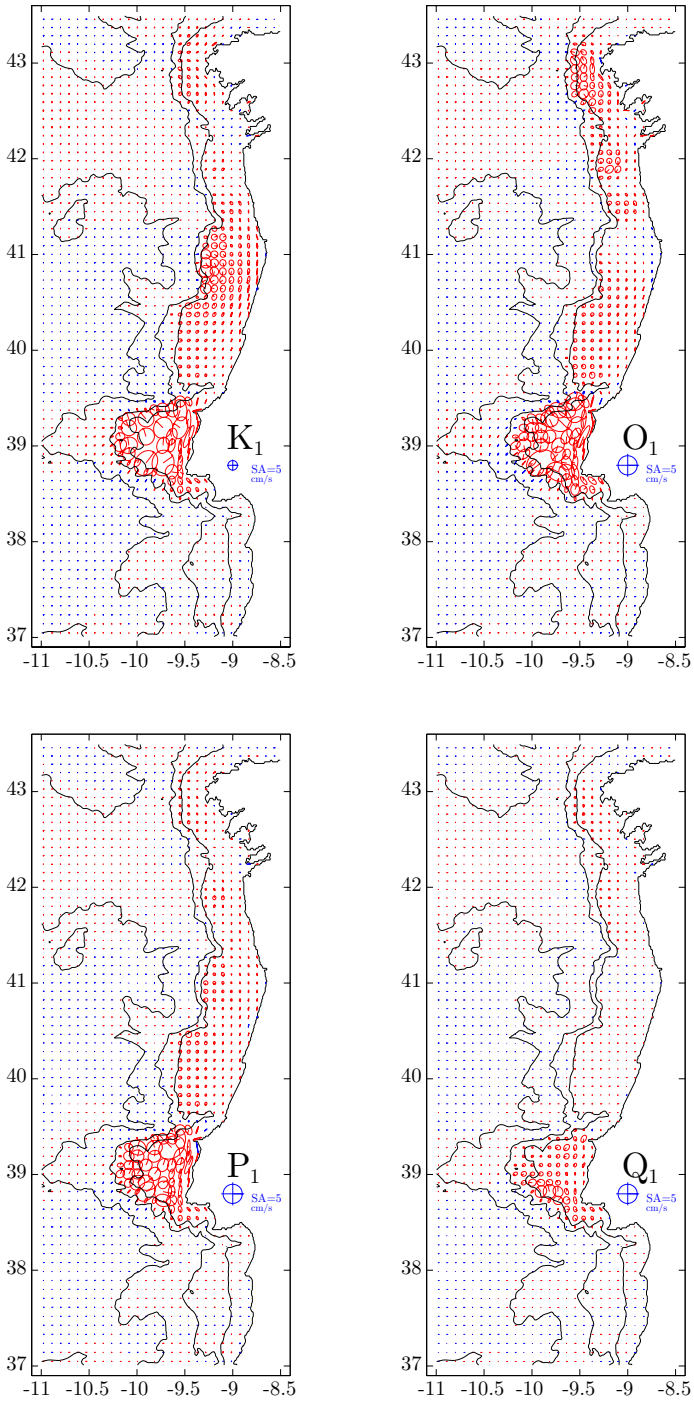

Figure 3.5: Barotropic tidal ellipses of the diurnal tidal components: K_1, O_1, P_1 and Q_1. Blue ellipses are counterclockwise, while red ones have clockwise rotation. The radial line inside the ellipses gives the Greenwich phase. Notice that K_1 ellipse scale is the double or the others.

3.3.1 Tidal heights

Figures 3.2 and 3.3 show cotidal charts for the semi-diurnal and diurnal tidal components. Results are in agreement with Fanjul et al. [1997]. Tidal wave propagates from south to north as a Kelvin wave with amplitudes decreasing offshore. Highest tidal amplitudes are found in the north of the region. M_2 is the main harmonic with amplitudes around 1 m, followed by S_2 with less than half of this value, N_2 with 0.25 m and K_2 with 0.1 m. Diurnal components show relative small values, around 0.08 m for K_1, 0.06 m for O_1, 0.02 m for P_1 and less than 0.02 m for Q_1. Exponential increase of amplitude towards the coast is found in all semi-diurnal charts for the generality of the region, and phase lines are perpendicular to the coast, while diurnal components do not show such behaviour. These components exhibit an amplification over Lisbon Promontory and over the Galician shelf.

Table 3.3 shows a comparison of the simulated amplitudes and phases of tidal heights with analysis of observations done in Tables 3 and 4 of Fanjul et al. [1997], for two locations of the west coast of the Iberian Peninsula: Vigo and Cascais ports. We consider this comparison satisfactory, with amplitude differences of O(1 cm) and typical phase errors of 3° for semidiurnal components and 6° for diurnal ones, and provides confidence for the results analysed in this work.

3.3.2 Tidal currents

Figures 3.4 and 3.5 show the tidal ellipses for the semi-diurnal and diurnal components calculated from the vertically integrated currents. The blue ellipses are conterclockwise and the red ones are clockwise.

Pure Kelvin wave dynamics expects current ellipses rotating counterclockwise and aligned parallel to the coast. By these figures we realise that if this happens approximately in the open sea, it is not the case of the shelf region. Bathymetric irregularities have large influence in the adjustment of the velocity field. It is responsible for amplification of tidal currents, inversion of the direction of rotation of the tidal ellipses and its polarisation in certain directions.

The south-north orientation of tidal currents changes in presence of the shelf features. In southern region, where slope is smooth this influence is not relevant. On the other hand, because of the steep slope of northern region, semi-diurnal components suffer amplification and ellipses become polarised orthogonally to bathymetric lines. This behaviour has been observed in other places, recently by de Mesquita [2003] and Pereira et al. [2002], for instance, and it happens in places were the wave front crosses the slope. Associated with the depth increase or decrease, the change of wave speed leads to wave refraction which make the wave front to become oriented parallel with isobaths [Pugh, 1987]. This phenomena is more clear in places with larger slope, that is, between Lisbon Promontory and Galicia and is not a feature of diurnal tides.

Of special interest when referring to diurnal tides in the studied area, is the Lisbon Promontory. This is the place where larger ellipse amplification of diurnal components occurs, associated with the intensified tidal amplitudes in this region (Figure 3.3).

Diurnal currents amplification in the Western Iberian shelf has been studied in terms of topographic waves [Sauvaget et al., 2000]. In what concerns tidal currents structure, four regimes are noticeable: open sea/shelf and semi-diurnal/diurnal currents. Shelf tidal circulation completely differs from open sea dynamics for all tidal components; all semi-diurnal current ellipses exhibits similar behaviour with different scales and the same statement is valid for diurnal current ellipses.

To quantify the relative importance of tidal components currents and the differences between open sea and shelf regimes, the kinetic energy density averaged over the tidal period was calculated for each tidal component. This calculus was done as $\frac{1}{T_i}\int_0^{T_i}\frac{1}{2}\rho(U_i^2+V_i^2)dt$, where T_i is the period of the tidal component i, $U_i = U_{0i}\cos(\frac{2\pi}{T_i}t+\phi_{ui})$ and $V_i = V_{0i}\cos(\frac{2\pi}{T_i}t+\phi_{vi})$. This integral results in $\rho(U_{0i}^2+V_{0i}^2)$. Considering the absence of spatial density differences and because we are interested in relative values (rates), the expression used for the kinetic energy density was $U_{0i}^2+V_{0i}^2$. Notice that the integral is independent of the number of periods used, ie, the result is the same if we use nT, instead of T, for integer $n \geq 1$.

Table 3.4 shows these values for the barotropic velocities. The first column represents the rate between energy on shelf/upper slope (inshore of isobath 1000 m) of each

Table 3.4: Relative percentage of kinetic energy density of depth averaged velocities. First column: rate between energy on shelf/upper slope of each component and energy of whole domain region for that component. Second column: rate between energy on Lisbon Promontory (LP) of each component and energy of whole domain region for that component. Third column: rate between energy on shelf/upper slope of each component and total energy of whole domain. Fourth column: rate between energy on LP of each component and total energy of whole domain.

	Shelf/Region	LP/Region	Shelf/Total	LP/Total
All	62.02	30.71	62.02	30.71
SD	51.92	15.87	40.48	12.38
D	97.79	83.28	21.53	18.34
M_2	51.78	15.71	33.41	10.14
S_2	51.91	16.92	5.13	1.67
N_2	54.28	15.31	1.52	0.43
K_2	54.28	17.78	0.42	0.14
K_1	97.69	82.23	15.25	12.84
O_1	97.95	83.84	3.82	3.27
P_1	98.40	89.53	2.14	1.94
Q_1	96.38	84.81	0.33	0.29

component and energy of whole domain for that component. The second one gives the rate between energy on Lisbon Promontory (LP) of each component and energy of whole domain for that component. LP is here defined as the section of shelf between latitudes 38.5° N and 39.5° N. The third column represents the rate between energy on shelf/upper slope of each component and the total energy (all components) of whole domain. The fourth column is the rate between energy on LP of each component and total energy of whole domain.

The distribution of energy from each component (columns 1 and 2) show that between 96 and 98% of the diurnal energy is on the shelf, mainly over LP (second column,

82 to 90%). For the semi-diurnal components these values decrease to about 50% over the shelf and 15 to 18% over LP. Comparing the energy of each component with the total energy (columns 3 and 4) we see that M_2 represents 33.41% of the energy distribution and one third of it is found over LP (10.14%). In the case og K_1 this proportion increases to almost one, 15.25% for the shelf and 12.84% for LP, indicating a concentration of diurnal energy on LP. The diurnal components dominate over LP (last column), where K_1 is the strongest component followed by M_2, O_1 and P_1.

Similar analysis has been done for surface and bottom velocities (not shown). For the surface, the shelf energy density shows higher values, mainly for the semi-diurnal components where the rate between the shelf and the full region for each component is now about 67% (it was about 52% in the case of barotropic velocities). Diurnal components remain closer to the barotropic value, about 99%. Over LP (second column), the diurnals have approximately the same value but the semi-diurnals, however, decrease to about one third of the barotropic case. The bottom velocities follow very close (qualitatively and quantitatively) what happens at the surface.

An example of the complex behaviour of the tidal currents is reported in Figure 3.7 in which the tidal elevation during 10 days is represented in the upper side of the figure for two stations, located at the positions P1 and P2, of Figure 3.6. Both graphics of tidal elevations are almost coincident because both stations are close. However the tidal currents present rather different patterns. Even if the stations are separated by ~ 50 km in the shelf of Lisbon Promontory, the time evolution of the tidal current is almost opposite in intensity and direction, in such a way that during rising tide the currents in the offshore station P1 is in the northward direction and rotating clockwise whereas in the coastal station P2 the flow has southward direction and it turns mainly in the counterclockwise direction, opposing to the surrounding flow. This occurs because at P1 diurnal currents are similar in amplitude to semi-diurnal currents, generating a pattern essentially diurnal, while in location P2, diurnal currents are much smaller than at P1 and the typical semi-diurnal modulation is observed.

The validation of tidal heights is basically based on previous studies for this region as was done in Table 3.3, indicating a good agreement between observation and modelling.

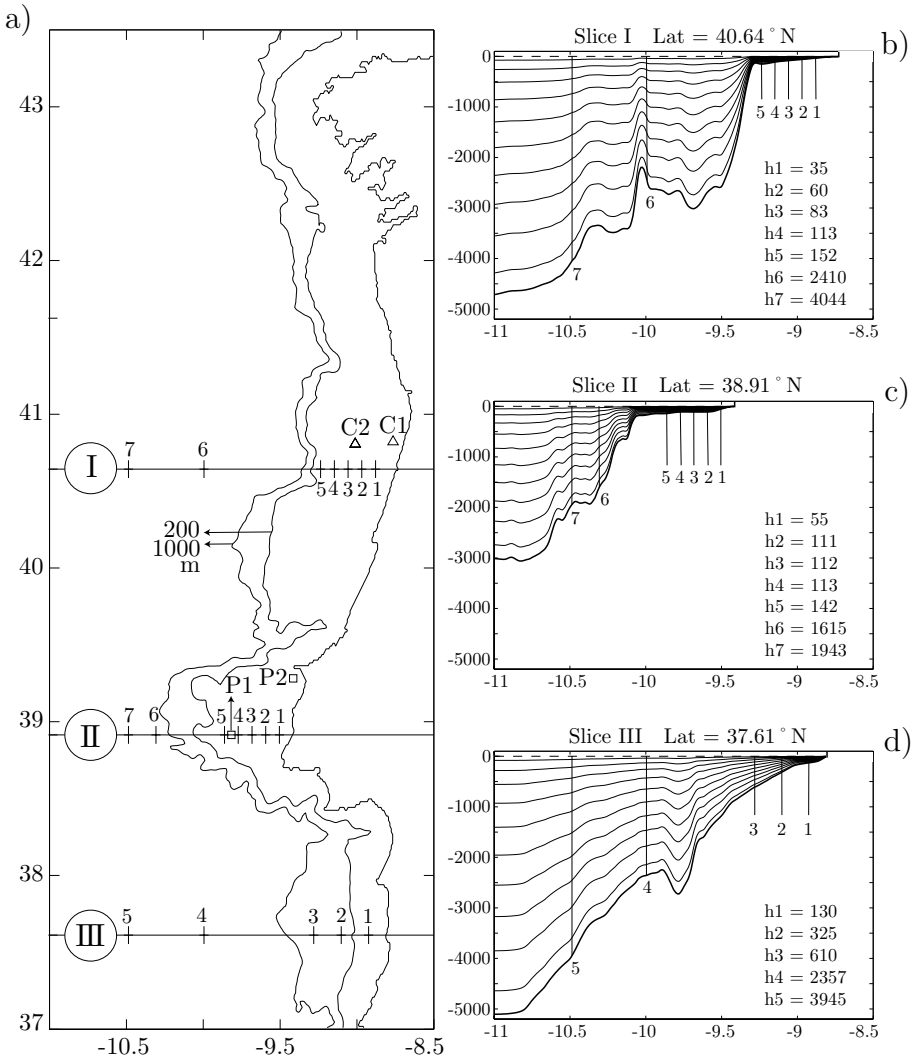

Figure 3.6: Studied area (at left) with locations referenced through the text, namely the slices I, II and III in which vertical variation of ellipses parameters was analysed (Figures 3.9, 3.10 and 3.11); the currentmeters locations C1 and C2 (Figure 3.8); the sites P1 and P2, for current inversion feature over Lisbon Promontory (Figure 3.7). At right are shown the vertical slice I, II and III. The deepest line, bold, is the bathymetry. Other solid lines correspond to the s-coordinates levels. Upper dashed line is the surface ($z = 0$ m). The numbered vertical lines are the sites where vertical analysis is done. The correspondent depths are also shown.

For currents validation there are some available data from currentmeters. Figure 3.8 is a comparison between M_2 ellipses obtained through analysis of data collected during

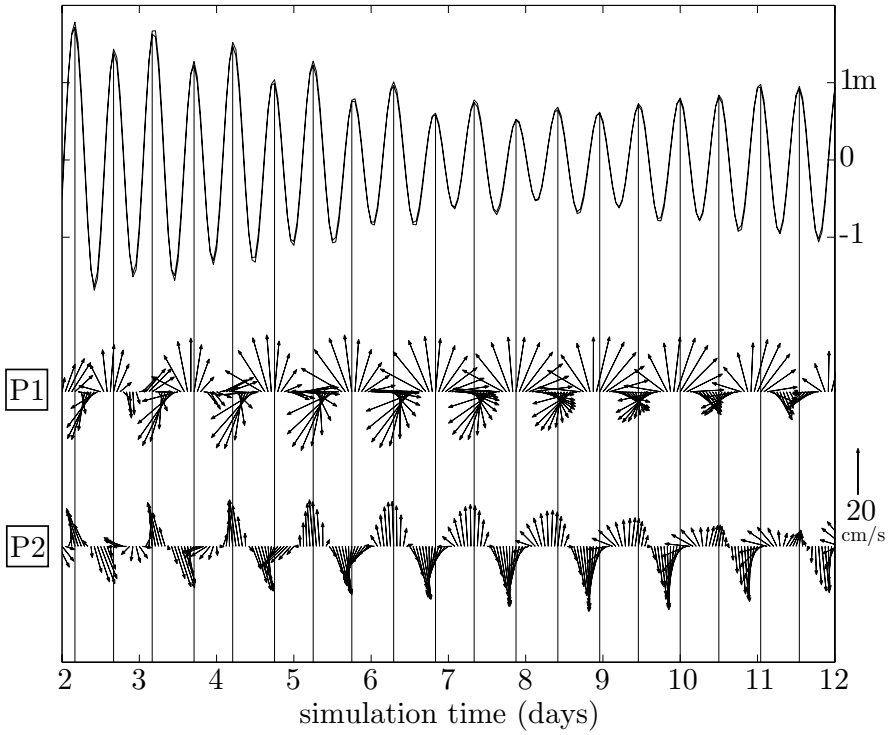

Figure 3.7: Tidal heights and currents at the points P1 and P2 (see Figure 3.6). Heights are superposed and are almost coincident. The vertical lines indicate the high tides.

the Survival cruise, described in Santos et al. [2004], during two weeks of February 2000. The harmonic analysis of these time series was done with the T_TIDE package from Pawlowicz et al. [2002]. The currentmeters location is shown in Figure 3.6 as C1 and C2. C1 was placed at 10 metres depth, being the total depth 30 m. At C2 there were two currentmeters at depths 20 and 45 metres, being the total depth 80 m. Taking into account the small length of the data series and the current variance, this comparison is considered quite good, giving confidence to the results obtained in this work.

3.3.3 Vertical structure

The vertical structure of tidal ellipses parameters — semi-major axis, eccentricity, inclination and phase angle — will now be discussed. Three region slices were chosen for this analysis according to its tidal circulation behaviour. In each slice were selected a variable number of sites either on open sea and shelf, where twenty equally spaced

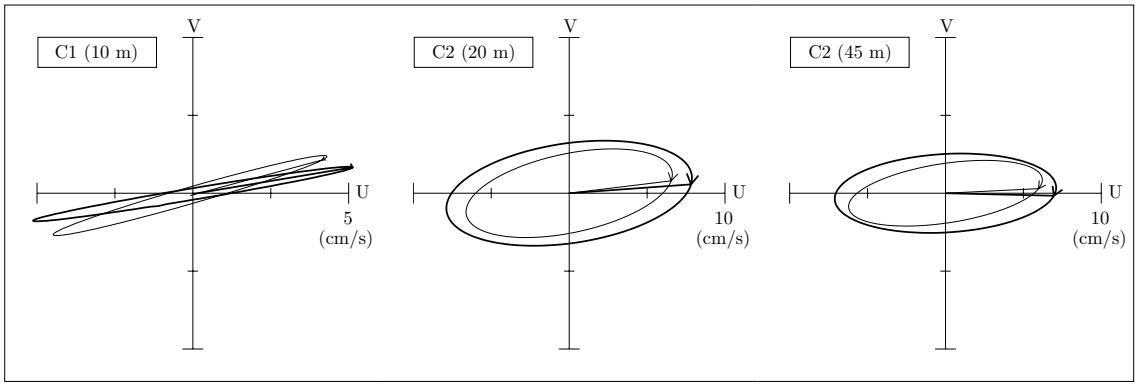

Figure 3.8: Comparison of model results with currentmeters (bold line) for M_2. Currentmeters data was collected in February 2000 during the Survival campaign for 15 days at the sites C1 and C2 (see Figure 3.6). These two points are located at 30 m and 80 m isobaths.

in depths harmonic analysis of currents (obtained through interpolation between the s-levels) was performed.

Slices locations are shown in Figure 3.6a by I, II and III. Figure 3.6b–d shows the grid vertical slices at these locations, together with position of the analysed sites — numbered vertical lines. S-coordinate levels are also shown. This figure is particularly useful to see the topographic differences of the slices. We remark the nonexistence of shelf break in the slice III, corresponding to southern region, in contrast with the steep slope in the other slices — Lisbon Promontory (II) and northern region (I).

In Figures 3.9 and 3.10 are represented the vertical profile of ellipse parameters for M_2 and K_1, respectively. Numbered (bold) lines correspond to the sites at the shelf and numbers increase in the offshore direction. Open sea sites were not numbered because the lines in these figures are very close, indistinguishable in some cases. Only M_2 harmonic, as semi-diurnal, and K_1 harmonic, as diurnal, are shown, because other semi-diurnal and diurnal components follow qualitatively the same analyses. Notice that in these figures, the mean value of the ellipse parameters was removed. In the vertical, relative depth is used, being 0 the surface and -1 the bottom.

These figures evidence the distinction between open sea and shelf. Offshore vertical structure of the velocity field is independent of the depth. Indeed, for the offshore

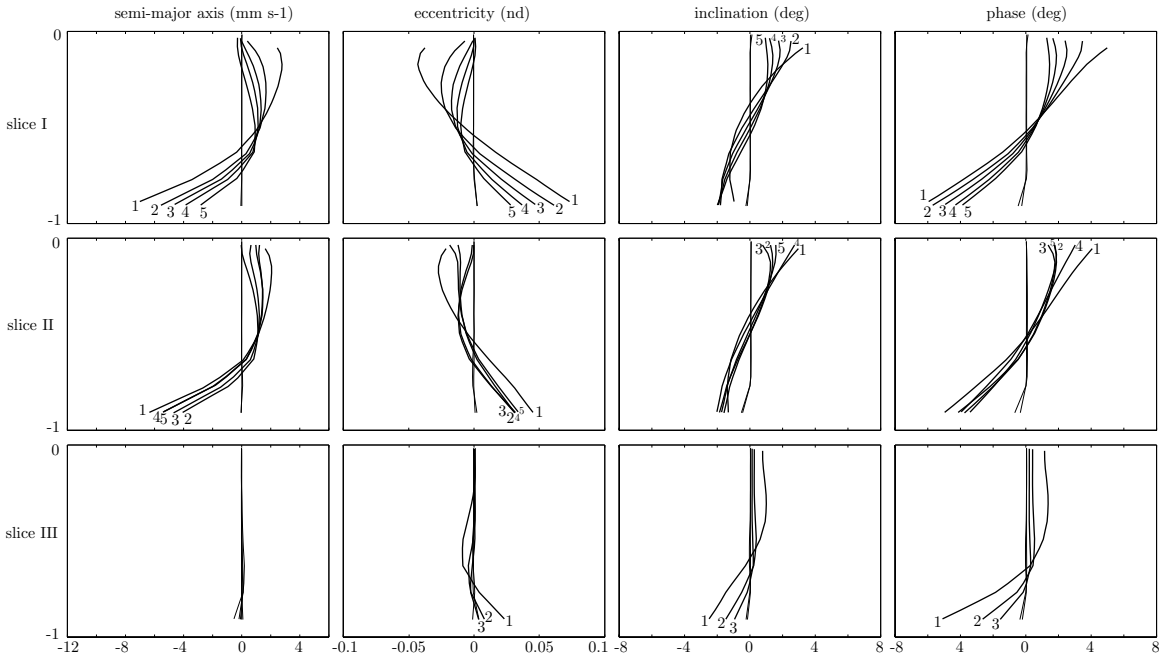

Figure 3.9: Vertical structure of M_2 tidal ellipse parameters. Slice I is in front of Aveiro — first row; slice II crosses the Lisbon Promontory — second row; slice III is in the middle of the southern part of the modelled region — third row. See Figure 3.6 for the location and properties of the slices. Variation with depth of ellipse parameters is represented: semi-major axis — first column; eccentricity — second column; ellipse inclination — third column; phase, relative to Greenwich — forth column. Relative depth is used being 0 the surface and -1 the bottom. The mean of all ellipse parameters was removed for clarity. Units are m/s for semi-major axis, degrees for inclination and phase. Eccentricity has no units.

stations, vertical variations in ellipses parameters occurs usually only near the bottom. On the other hand, in the shelf, the vertical modification of ellipses occurs in all the water column, also associated with spacial variations from slice to slice. Differences in the way diurnal and semi-diurnal tidal components change, not only spatially but vertically, are also shown.

Tidal components have larger semi-major axis (Figures 3.9 and 3.10, first column) usually below the surface decreasing with depth. A typical variation of O(1) cm/s in semi-major axis is found in all slices, for both M_2 and K_1, on the shelf except in slice

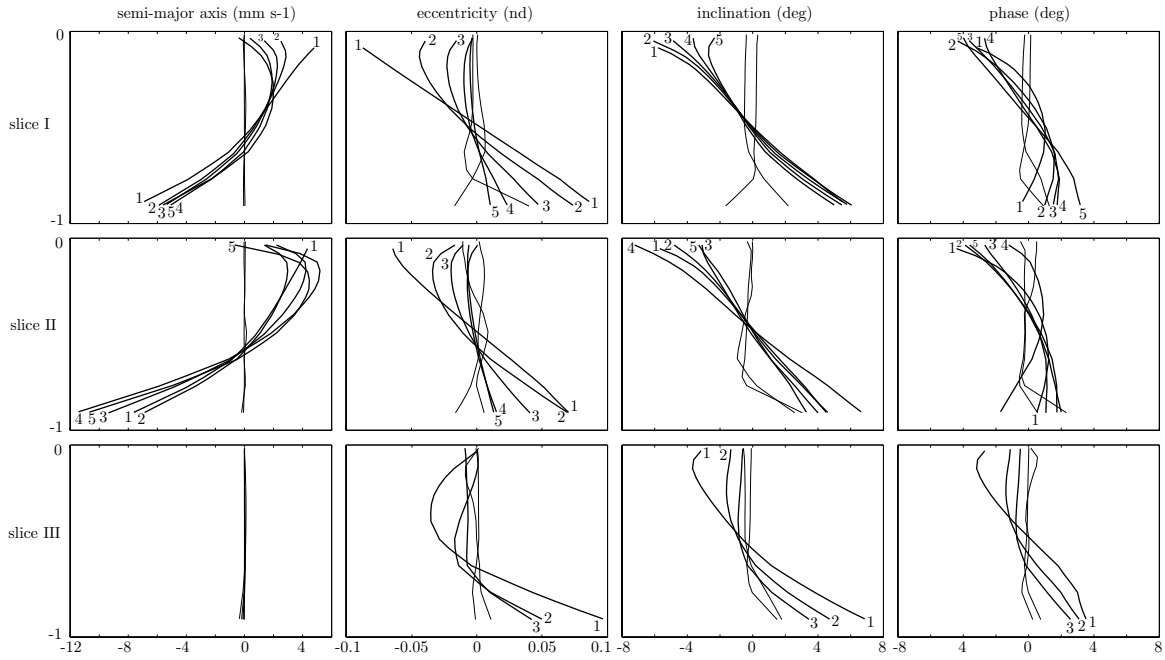

Figure 3.10: Same as Figure 3.9 but for the diurnal harmonic K_1.

III, located in the southern region, where the slope is very smooth (see Figure 3.6). The largest surface to bottom variation occurs for the diurnal harmonic at the slices II, over the Lisbon Promontory, where highest tidal current amplification exist. The vertical variation of ellipse amplitude and other parameters generally decrease offshore, until the shelf break, becoming the tidal structure essentially barotropic in the open-sea.

Ellipse eccentricity (rate between semi-major and semi-minor axis; if 0 the ellipse is degenerated, a line segment; if 1 the ellipse is a counterclockwise circumference; if -1, the ellipse is a clockwise circumference) behaves in opposite way to semi-major axis. Highest eccentricity is found at the bottom indicating that ellipses become more counterclockwise with depth (positive eccentricity means counterclockwise ellipse rotation). Once again, variation with depth has a minimum below the surface (in the case of semi-major axis it was a maximum). Larger amplitude of vertical variation also increases onshore. K_1 eccentricity at offshore sites seem to be less barotropic than for M_2.

Ellipse inclination (angle between semi-major axis, in the first or second quadrant, and u-axis) also evidences difference between semi-diurnal and diurnal components. Semi-diurnal ellipses inclination show smaller difference between open sea and shelf

than diurnal ones. Also should be noticed that diurnal inclinations in open sea are more depth dependent than semi-diurnal, increasing in the last third of water depth, near the bottom. If slice III is almost barotropic respecting semi-major axis, it is not in terms of inclination which shows a variation comparable to the other slices. Inclination vertical profile of diurnal components is opposite to the semi-diurnal one.

Tidal ellipses phase (the angle, relative to Greenwich meridian, the ellipse need for currents reach the maximum in the first or second quadrant) evidences similar behaviour. Semi-diurnal components have bigger vertical variation in the shelf than diurnal components phases. A typical variation of O(10) degrees almost linear between bottom and surface is found in the slice I and II for the semi-diurnal component. The variation in the diurnal K_1 component is about two thirds of the semi-diurnal M_2 phases vertical variation. In the slice III the phases are almost constant in the first half of the water column (from surface to bottom).

3.3.4 Sensitivity to bottom friction

The vertical structure of tidal currents, mainly in shelf regions, is sensitive to bottom friction, which should be responsible for many of the features described until here. Figure 3.11 shows the vertical variation of the tidal ellipses parameters at the shelf station I.4, shown in Figure 3.6a. Each row corresponds to one of the four runs done to test the sensitivity of the model to bottom friction (Table 3.2). The bold lines correspond to the semi-diurnal harmonics M_2, S_2, N_2 and K_2 (with numbers 1 to 4), and the thin lines correspond to the diurnal components K_1, O_1, P_1 and Q_1 (with numbers 5 to 8). Like in previous figures, here again the mean value of the parameters was removed.

In the rows one to three, the linear bottom friction was used with the drag coefficient increasing twice from run I to run II and from run II to run III (run II used a typical parameterization and was the one analysed until here). In the last run it was used a quadratic bottom friction parameterization, as described previously. We realise that runs I to III are qualitatively very similar but the variation of the ellipse parameters with depth increases with the bottom drag coefficient. This leads to an higher distinction

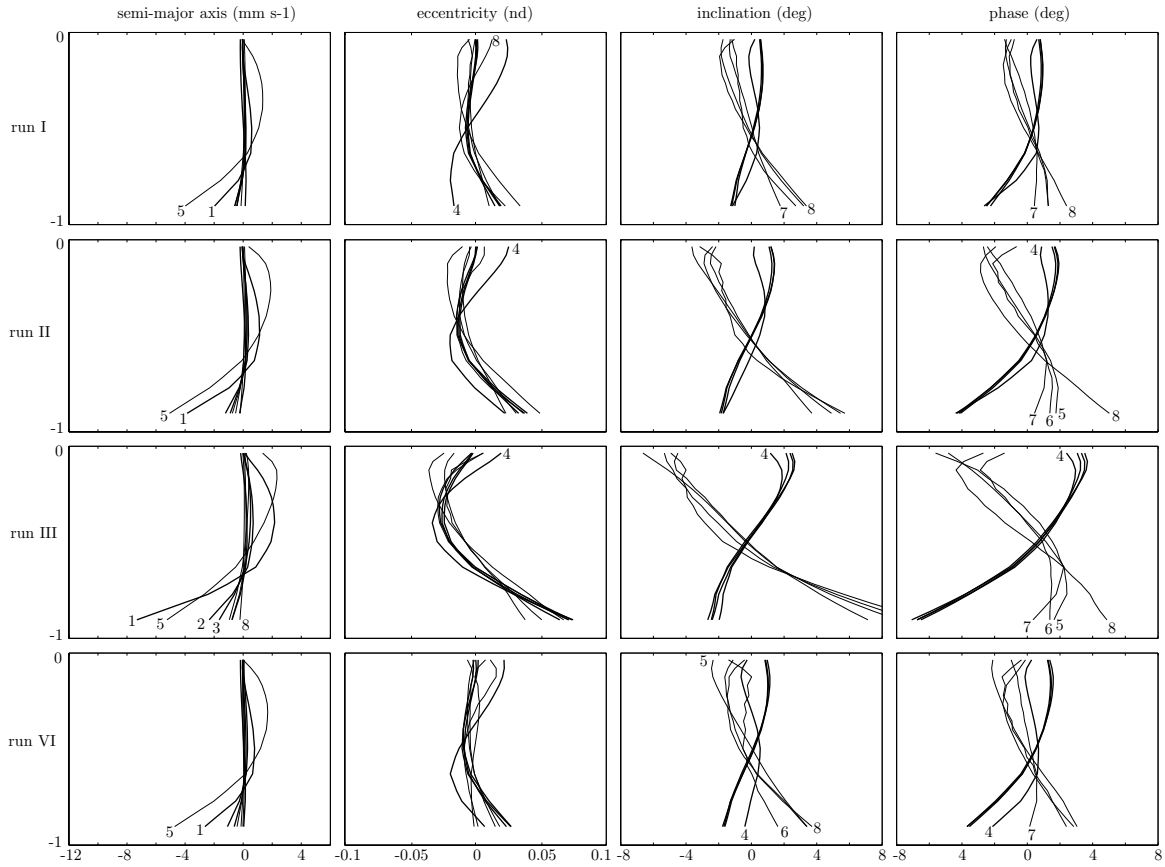

Figure 3.11: Vertical structure of the tidal ellipses parameters at the shelf station I.4 (shown in Figure 3.6a). The bold lines correspond to the semi-diurnal harmonics M_2, S_2, N_2 and K_2 (with numbers 1 to 4), and the thin lines correspond to the diurnal components K_1, O_1, P_1 and Q_1 (with numbers 5 to 8). Rows correspond to runs I to IV (see Table 3.2).

between the behaviours of the diurnal and semi-diurnal components, mainly in terms of the ellipse inclination and phase angle. The run IV, is in general more similar with run two, without quantitatively significative differences. This result was expected since run two and four correspond to typical parameterizations used in ocean modelling, in spite of the first (run II) be linear and the other (run VI) quadratic. One final simulation without bottom friction was also done. As result, the tidal currents became barotropic in all the region. Also no distinction between semi-diurnal and diurnal vertical variation of parameters was noticeable.

3.4 Discussion and conclusions

A description of tidal dynamics of the Western Iberian Peninsula was obtained by means of numerical modelling, putting emphasis on the study of the vertical structure of tidal ellipses for the homogeneous case. Stratification effects were beyond the scope of this study. It is well known that the stratification has influence on tidal ellipses [Souza and Simpson, 1996; Simpson, 1997; Xing and Davies, 1997, 1998]. However, in this study it has not been considered to avoid to study the many different situations concerning the stratification along the year for this region. Thus, the obtained results describe the winter situation in which the shelf is nearly homogeneous [Oliveira et al., 2004]. As the main results for tidal heights amplitude and phase are similar to the previous literature [Fanjul et al., 1997] and compares well with the observations, no large efforts in validation for these results has been done. However, comparison of tidal ellipses for two points in the inner and middle shelf with currentmeters registers show a good agreement. The tidal currents in the domain are dominated by the semi-diurnal M_2 component and are amplified in the shelf. The diurnal components suffer a greater amplification, specially K_1 over the Lisbon Promontory. The analysis of vertical parameters of tidal ellipses allows a clear separation between semi-diurnal and diurnal components, and between the almost barotropic open sea circulation and the depth dependent, due to bottom friction, shelf currents.

3.5 Appendix: tides and diel vertical migration

The periodic vertical movement of larvae in a background of tidal currents may lead to significative horizontal transport of these organisms [Hill, 1991a,b, 1995]. To measure the importance of this mechanisms in the dispersion and retention of larvae, some simulations were done with the tidally forced model. In these simulations, the larvae were introduced as drifters with passive horizontal movements but with diel vertical migration, i.e., a vertical movement was imposed on the drifters with a daily periodicity. The timing of the vertical movement was such that the particles were close to the

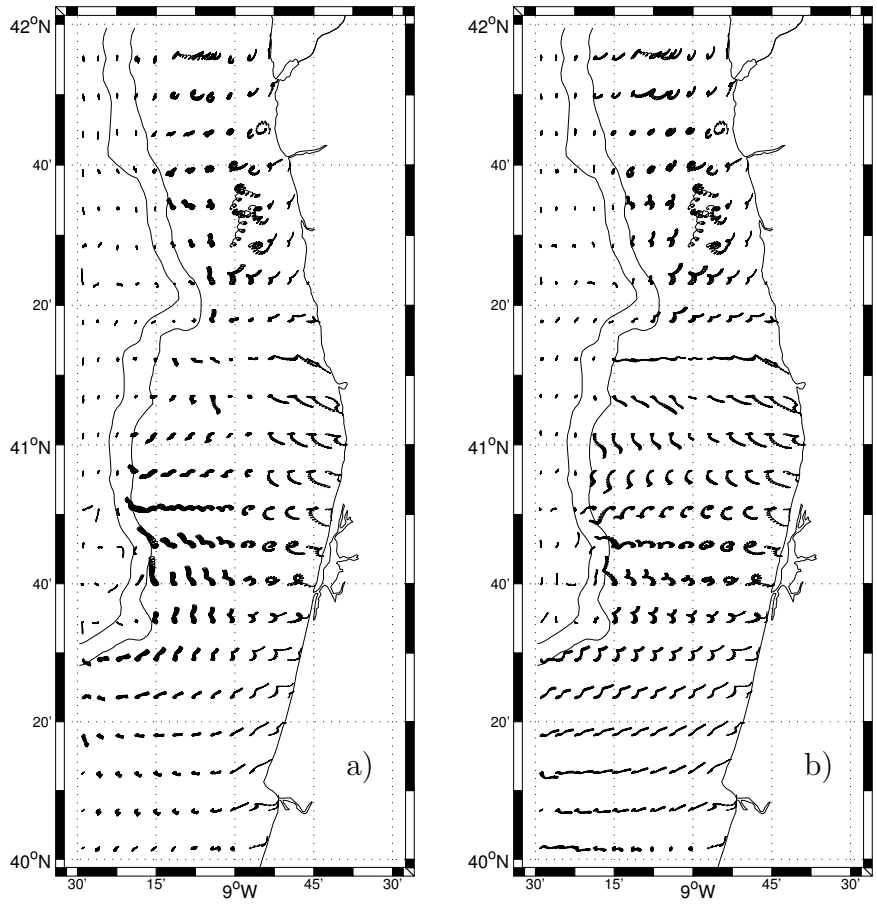

Figure 3.12: Dispersion of larvae with diel vertical migration (DVM) by the tidal currents on the northwestern Portuguese shelf: a) with maximum migration depth of 50 m and b) with migration until the bottom. Besides the coastline are shown the isobaths 200 and 1000 m.

surface during the night and in deeper layers during the day, considering the duration of the night of about 6 hours, and the day, 14 hours. The other 4 hours were spent in the ascending and descending drifters' movement. Figure 3.12 show two results of the simulations for the case of migration until a maximum depth of 50 m (a) and for migration until the bottom (b). The horizontal trajectory of the drifters is shown for 20 days of simulation. The absence of an effective horizontal transport is clear. During the 20 days the total distance travelled by the drifters was in general lower than 10 km, which is very small compared with typical shelf wind driven currents of dozens of cm s^{-1}.

As conclusion, the interaction between active diel vertical migration and tidal currents is not important in the Western Portuguese shelf for the transport of horizontally passive larvae.

Chapter 4

Observations and Modelling of the 2002 Spring Transition at the NW Portuguese Shelf

A modelling study and comparison with hydrological and currentmeter observations during spring transition is presented here for the northwestern Portuguese shelf region. The data was collected during a cruise in May 2002 and a three-dimensional fine resolution ocean circulation model driven by the main shelf forcings was created. The studied period was characterised by the end of the winter regime and the onset of the shelf stratification.

The Portuguese shelf is characterised by a fresher surface layer of riverine origin and by a circulation with a high degree of independence from open ocean being mainly controlled by the wind. The model was able to simulate these shelf features and its results compare well with the hydrological and currentmeter observations.

4.1 Introduction

Ocean modelling studies in the West Iberian region are mostly concentrated on the slope region [Peliz et al., 2003a,b], on tidal dynamics [Sauvaget et al., 2000; Fortunato et al., 2002] large scale studies [Stevens et al., 2000; Batteen et al., 2000]. Also modelling

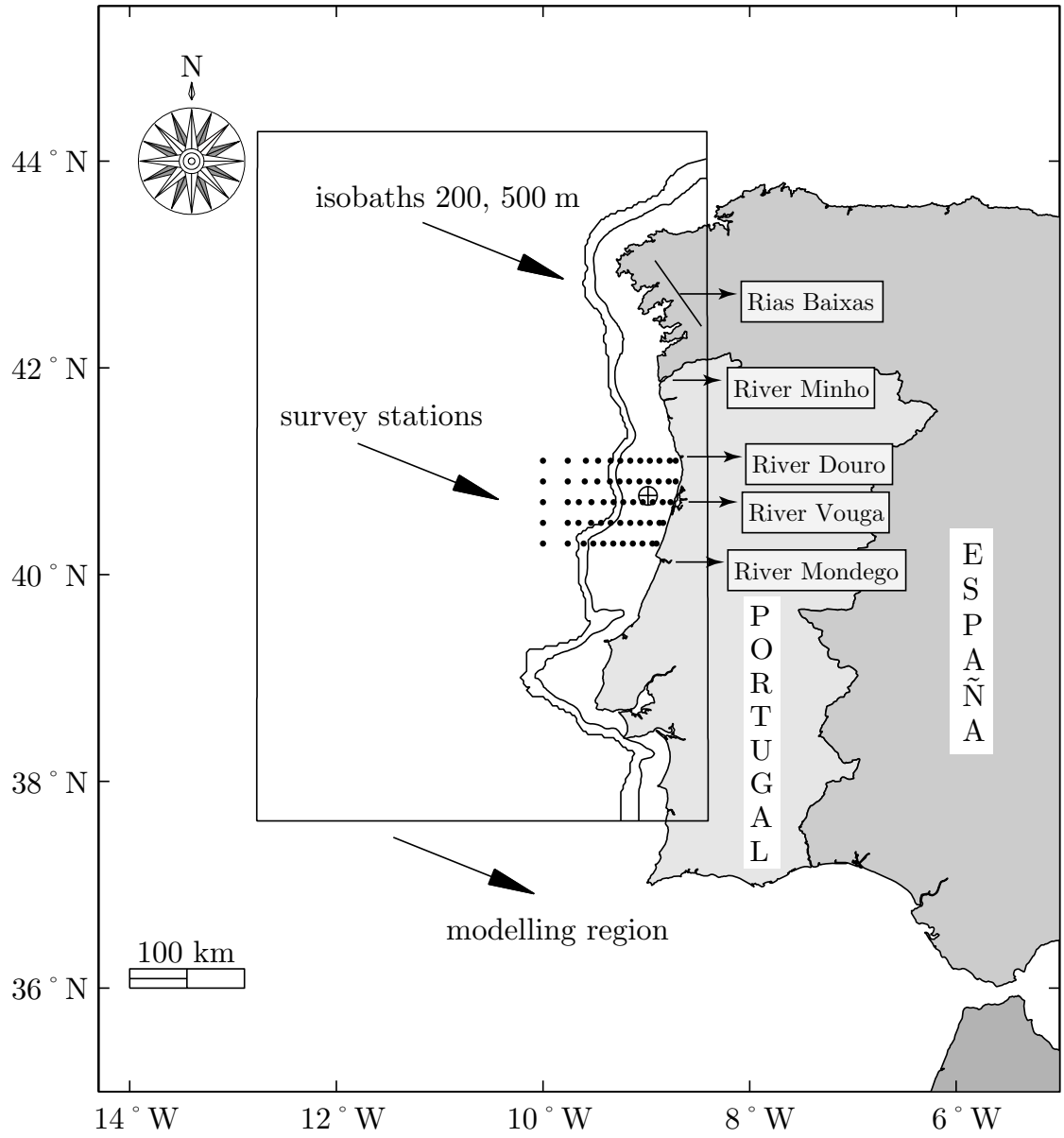

Figure 4.1: Region of study with modelling region and main land runoff sources of the northwestern Portugal and Galicia. The survey hydrological stations and mooring site are shown by the matrice of points and by the symbol $\oplus$, respectively.

across a vertical section applied to sediment transport in the Iberian shelf has been done by Xing and Davies [2002], and studies of summer upwelling dynamics, based on 1–1/2 layer model was done by Røed and Shi [1999]. It is however remarked the lack of numerical and observational studies of the shelf dynamics, and particularly for the period of the spring transition. From the observational point of view the existent

works are based mainly on currentmeter recordings. Vitorino et al. [2002] studied the dynamics of one point at mid-shelf during three years (July 1996 to June 1999), and many aspects of subinertial and high frequency flow are discussed for that point.

This work intend to contribute to the study of the hydrology and dynamics of the shelf circulation in the mid-region of the Iberian shelf.

The wind in the Western Iberia is the main forcing of the shelf currents and exhibits high interannual variability. During the winter the Azores anticyclone is in its southernmost position (27° N) and the Iceland cyclone is strong. During summer the Azores anticyclone is over the central North Atlantic at a latitude of about 33° N and the Iceland cyclone is week. These conditions produce weak westerly winds and frequently northward, downwelling favourable winds during winter and northerly winds, upwelling favourable, during the spring and summer. The upwelling intensity is greatest in July, August and September but has high variability [Fiúza et al., 1982; Vitorino et al., 2002].

Vitorino et al. [2002] describes the typical winter and non-winter conditions and the transition between them in the north Portuguese shelf: during the winter regime the southerly downwelling winds leads to an increase of the temperature at the mid-shelf, a consequence of shoreward movement of warmer surface oceanic waters, and gives rise to poleward currents often higher than 20 cm/s. The mid-shelf becomes very homogeneous due to radiative loss and the strong waves activity. The mixed layer depth can reach 80 m. In the non-winter regime, characterised by northerly winds, the upwelling leads to a decrease of the mid-shelf water temperature and the development of a thermal front at the break separating the warmer oceanic waters from the cooler shelf waters. At mid-shelf an equatorward jet develops with a speed that can overtake 30 cm/s. The mid-shelf stratification is a result of river outflow of cooler and fresher water, and limited to a 20 m surface layer. The increase on the northerly wind events typical during April characterises the transition from the winter to the summer regimes.

The northwestern Portuguese and Spanish shelf is characterised by the presence of a surface low salinity layer [Fiúza et al., 1998; Stevens et al., 2000; Vitorino et al., 2002; Oliveira et al., 2004]. Its origin is the several land runoff sources in the region being the main ones the rivers Mondego, Vouga, Douro, Lima, Minho and the Galician Rias (see

Figure 4.1). Among these the most important are the rivers Douro and Minho. The fresh water input is more intense during winter, but the low salinity layer persists during all year as a buoyant plume. It has been called as Western Iberian Buoyant Plume, WIBP [Peliz et al., 2002]. The extension and depth of this plume has high variability being very dependent on the wind regime. It stretches offshore in upwelling favourable winds and remains in the inner shelf during non-upwelling conditions. Offshore, it is trapped by the Iberian Poleward Current, IPC [Peliz et al., 2002; Santos et al., 2004; Ribeiro et al., 2005], which is present during all year in the northwestern Iberian slope, being more evident in the winter [Frouin et al., 1990; Peliz et al., 2003b, 2005].

This work describes a modelling study for the spring transition in the northern Portuguese shelf. The model simulates the end of April and the month of May 2002 and the results are compared with hydrological and currentmeter cruise observations. The cruise took place in front of Aveiro, (mouth of river Vouga, see Figure 4.1) during that period. The wind over the survey region (more precisely, at the mooring site, to be described in the next section, indicated in Figure 4.1 by the symbol $\oplus$) is shown in Figure 4.2. It is upwelling favourable in the first two and half weeks of simulation, then it becomes variable but essentially northward for two weeks and until the end of May it becomes southward again. In March and first half of April (not shown) the wind was very variable with a main two weeks downwelling episode between days 9 and 23 of March. In April the northerly upwelling winds started in the second week and persist until May with a relaxation period during the third week.

The wind-driven shelf currents respond rapidly to the wind regime and are very independent from the slope density-driven poleward current, IPC, [Peliz et al., 2003a]. This independence between the shelf and offshore dynamics allowed this simulation study to be focused on the shelf region. In parallel with cruise observations, model simulations are an important tool to understand and complement the observations.

Next section describes the simulation and the cruise observations. Then the results are shown and discussed.

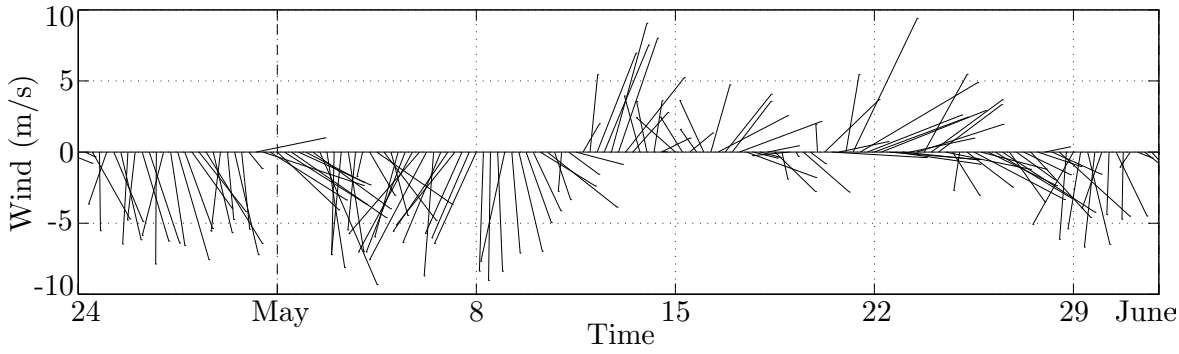

Figure 4.2: Wind at the mooring site (indicated in Figure 4.1) during the simulation period.

4.2 Data and methods

4.2.1 Observations

The observations were done during a cruise which consisted in an hydrological and planktonic survey in the framework of the ProRecruit project. The cruise took place on board RV Noruega in northwest Portugal and collected planktonic, hydrological and currentmeter data.

The hydrological measures were done in a grid of stations and in a fixed point (Figure 4.1). Mooring data used in this work was obtained with currentmeters at 15 and 35 m depth measuring currents and another at 5 m depth, with a temperature sensor, measuring temperature. It was also used a temperature chain which collected data at 11 different depths between 2 and 39 m, namely, 2, 5, 8, 11, 14, 17, 20, 24, 29, 34 and 39 m, being the total depth 64 m. The currentmeters and the temperature chain were located at the fixed point (longitude 8.98° W and latitude 40.77° N).

The timetable of the different measurements is outlined in Figure 4.3.

4.2.2 Simulation

The model used in this work was the Regional Ocean Modeling System, ROMS [Haidvogel et al., 2000], a three-dimensional model that solves the free-surface, hydrostatic, primitive equations of the ocean dynamics over a variable topography. It uses orthogo-

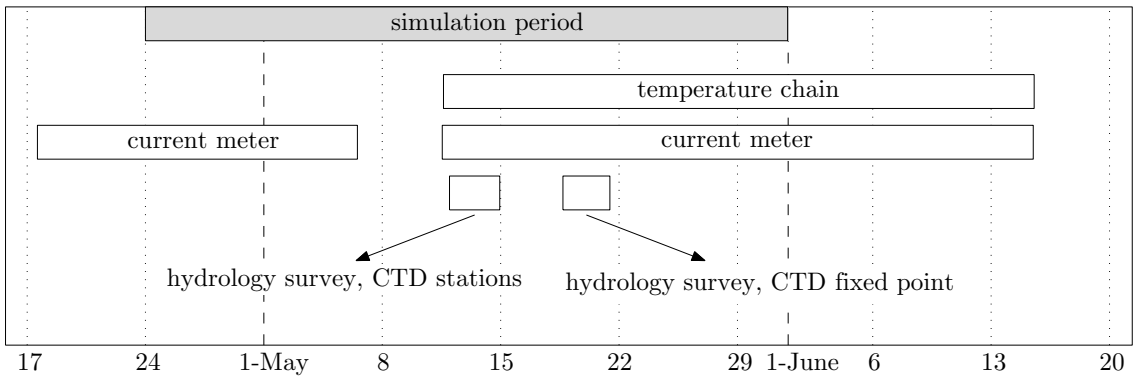

Figure 4.3: Scheme of the ProRecruit cruise observations and its durations, together with the simulation period.

nal curvilinear coordinates in the horizontal and terrain-following s-coordinates in the vertical [Song and Haidvogel, 1994]. The grid used covers the longitudes 12.8° W to 8.4° W and the latitudes 37.6° N to 44.3° N, thus, 360 km in the meridional direction by 740 km in the latitudinal direction. The horizontal resolution increases onshore from about 6 km offshore to 2 km over the shelf. In the south-north direction the grid resolution was kept constant in about 3.3 km. In the vertical, 25 s-levels were used. In order to achieve high resolution near the surface and bottom it was used a maximum depth of 500 m. This was done in order to decrease the computational effort. To use the total depth and keep a good resolution near the surface we would need to use a higher number of vertical levels increasing unnecessarily the computational simulation time. The interest on the shelf region and its independence from offshore allowed such simplification, once some tests with different depths and vertical resolutions produced no significant qualitative and quantitative differences on the shelf results.

The simulation started one week before May 2002 and last until the end of that month, being simultaneous to the period of observations described above.

As initial conditions it was used a profile of temperature and salinity taken from a station offshore, which represents the background stratification of salinity and temperature profile for the season. The model started from rest. Air-ocean bulk fluxes from the NCEP reanalysis database, spatially interpolated to the model grid, were used to force the model (the fluxes are calculated by the model using the variables wind, shortwave

Table 4.1: Model setup parameters

L	122	Number of points points E–W
M	226	Number of points points N–S
N	25	Number of s-levels
h_{max}	500 m	Maximum region depth
h_{min}	5 m	Minimum region depth
θ_s	3	S-coordinates surface control parameter
θ_b	0.4	S-coordinates bottom control parameter
Δx	2→6 km	Resolution in the zonal direction
Δy	3.3 km	Resolution in the meridional direction
Δt	600 s	Baroclinic time step
Δt_f	10 s	Barotropic time step
κ	5×10^{-6} m^2 s^{-1}	Background vertical viscosity
κ_t	5×10^{-6} m^2 s^{-1}	Background vertical diffusivity
r	3×10^{-4} m s^{-1}	Linear bottom drag coefficient
T_{runoff}	13 °C	Rivers runoff temperature
S_{runoff}	30 psu	Rivers runoff salinity
Q_{Minho}	270 m^3 s^{-1}	River Minho runoff
Q_{Douro}	495 m^3 s^{-1}	River Douro runoff
Q_{Vouga}	40 m^3 s^{-1}	River Vouga runoff
Q_{init}	3000 m^3 s^{-1}	One weak spinup rivers runoff

and longwave radiation, air pressure, humidity, temperature and rain fall rate). In the bottom it was used the linear drag and no fluxes. In the four model grid boundaries it was used radiative open boundary conditions (OBC) for tracers and momentum, and gradient OBC for the free surface.

The main rivers runoff was also used, namely the rivers Minho, Douro and Vouga with a climatological outflow for May of 270, 495 and 40 m^3 s^{-1} respectively (values from INAG – Portuguese Water Institute). In order to create the low salinity surface

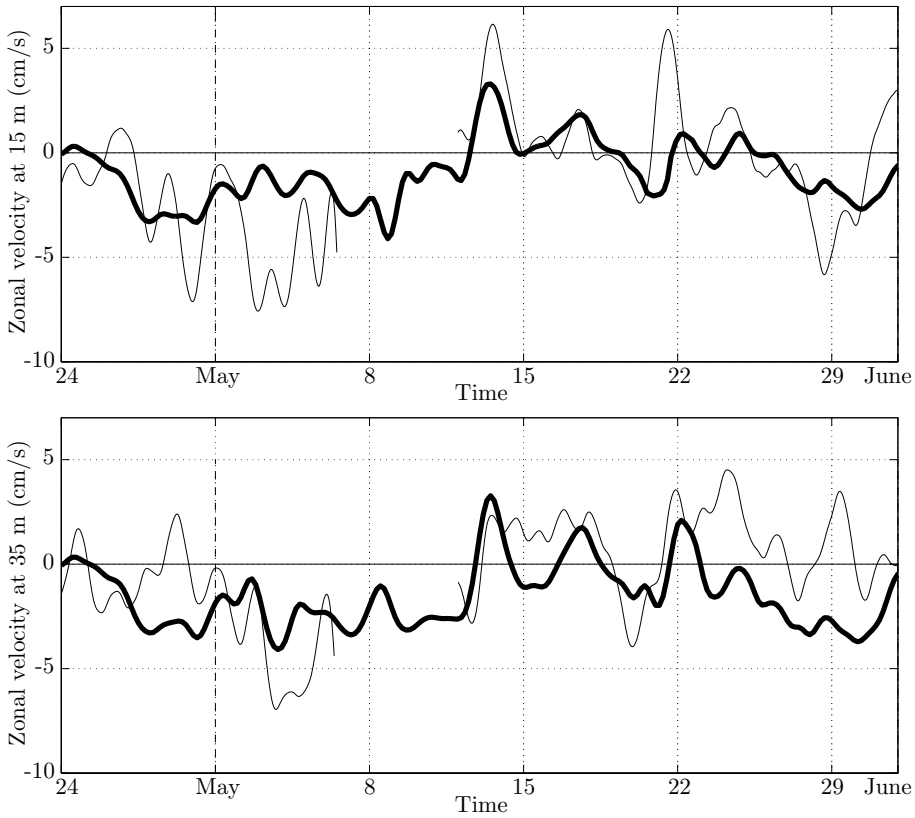

Figure 4.4: Zonal currents at the mooring site, at 15 m (up) at 35 m (down). The thin line represents the observed vales and the bold line indicates the simulation results.

layer, characteristic of the region [Peliz et al., 2005], the rivers outflow in the first weak of simulation was 3000 m^3 s^{-1} for each of the three rivers. The rivers temperature was 13° C and the salinity was 30 psu in order to take into account the mixing of the rivers fresh water with the ocean water inside the estuaries.

The model setup parameters are summarised in Table 4.1.

4.3 Results

In this section the model results are compared with the cruise observations. The mooring observations to be compared with the simulations are the time series of the zonal and meridional currents at 15 (Figure 4.4) and 35 m (Figure 4.5), temperature at 5 m (Figure 4.6) and the simulated and observed temperature chain (Figure 4.7). Between 6 and 12 of May there is no currentmeter observations data due to technical problems

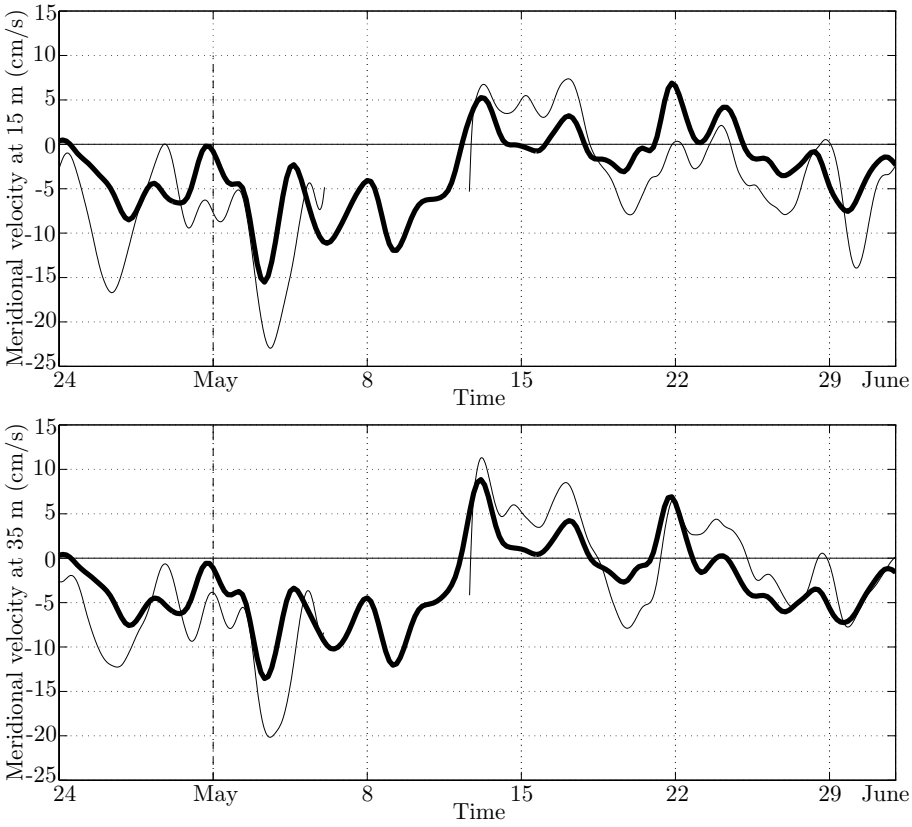

Figure 4.5: Meridional currents at the mooring site, at 15 m (up) at 35 m (down). The thin line represents the observed vales and the bold line indicates the simulation results.

with the mooring devices (Figures 4.4, 4.5 and 4.6, thin line). Respecting the hydrological results, the observed and simulated temperature and salinity at the southern section of the grid of stations, at latitude 40.3° N, are shown in the Figures 4.8. and 4.9. All the data shown (observed and simulated) was filtered with a 33 hours low-pass filter. This is a standard oceanographic filter which uses 1/(33 hours) as the cutoff frequency, and is used primarily to remove tidal energy (or all signal energy with periodicity less than 33 hours).

In the first two and half weeks of simulation the northerly wind (Figure 4.2) gave rise to upwelling negative zonal velocity and southward meridional velocity. The simulated velocities during the first week show qualitative agreement with the observations but with smaller values due to the model spinup. By 12 of May the wind become essentially

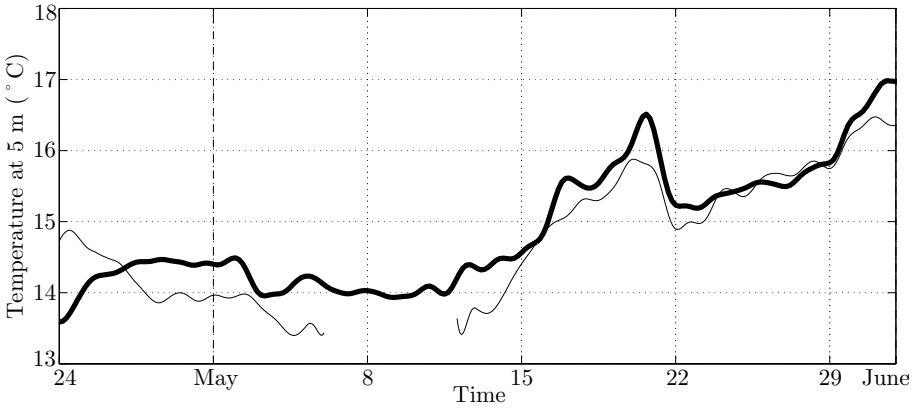

Figure 4.6: Simulated (thin line) and observed (bold line) temperature at 5 m depth at the mooring site.

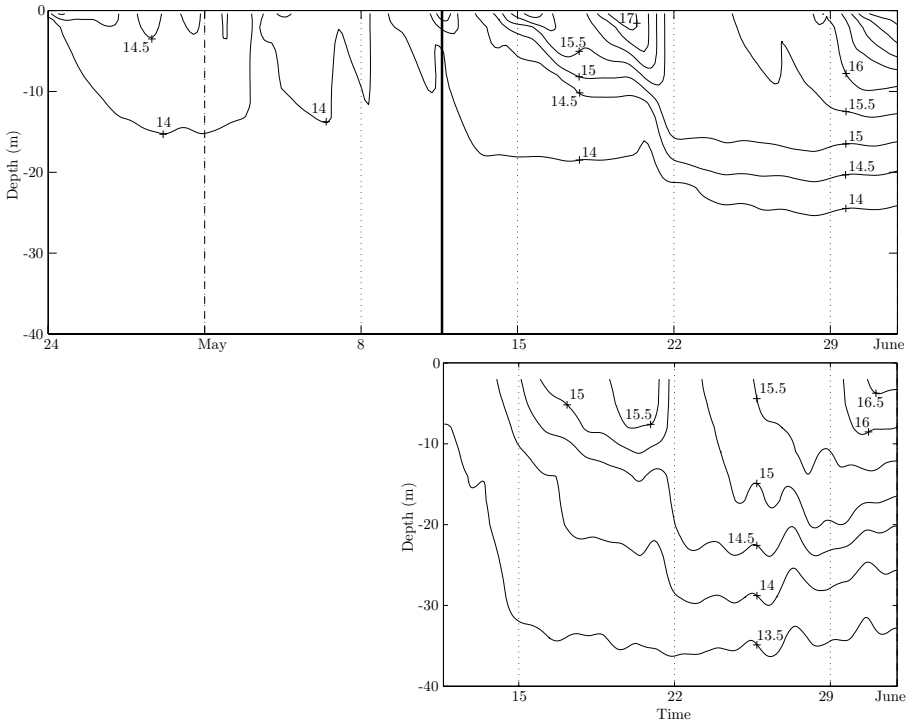

Figure 4.7: Evolution of the vertical profile of temperature at the mooring site: simulation results (up) and temperature chain observations (down). The vertical line in the upper image indicates the beginning of the temperature chain observations.

northward until 25 of May leading to downwelling and northward currents. After this period the wind was southward until the end of the month. Between 22 and 25 of May the wind had a rather complex variability being southward by day 23. This event

created small simulated negative meridional velocities at 35 m depth while at 15 m velocity decreased only until zero. This was however not observed in the currentmeter data. The model results compare with observations but the simulation currents are in general smaller than the observed, which may be due to the inaccuracy of the forcing winds near the coast.

Figure 4.6 compares the mooring time series of temperature with the model result for a depth of 5 m also for the fixed point of mooring. The simulation produced good results taking into account the difference of temperatures at the beginning of the simulation. The differences between the simulation and observed temperature is in general lower than 0.5° C, and qualitatively the observed increase on temperature between the days 12 and 19, and after the day 23 of May compares well with the simulation. The temperature increased continually after 23 of May in spite of the upwelling event after 25 of May, because the cooler upwelled waters didn't reach the mid-shelf (fixed point) during May.

The temperature chain provided the time evolution of the temperature stratification profile. The result is shown in Figure 4.7. The vertical line in the simulation figure (upper one) corresponds to the beginning of the temperature chain observations (lower figure). Model result agrees qualitatively with the observations. Qualitatively, however, the simulations shows higher values of temperature in the first 2, 3 metres depth. The beginning of the temperature chain observations is coincident to the end of the winter regime and the onset of stratification.

The Figure 4.8 shows the cross section of observed and simulated temperature at the latitude 40.3° N in 12 of May, the end of the fully developed winter upwelling season. The model surface temperature is about 15° C which is close to the observed surface temperature. Nevertheless, the model produced higher stratification due to vertical temperature gradients in the first 50 m. Offshore the break, the differences arise from the model initial stratification, which was horizontally homogeneous. From the observed temperature we can conclude that there was lack of evidences of the slope poleward current, which means a strong downwelling of temperature off the shelf break. The circulation, not just in the shelf but also offshore, seems to be mainly controlled by

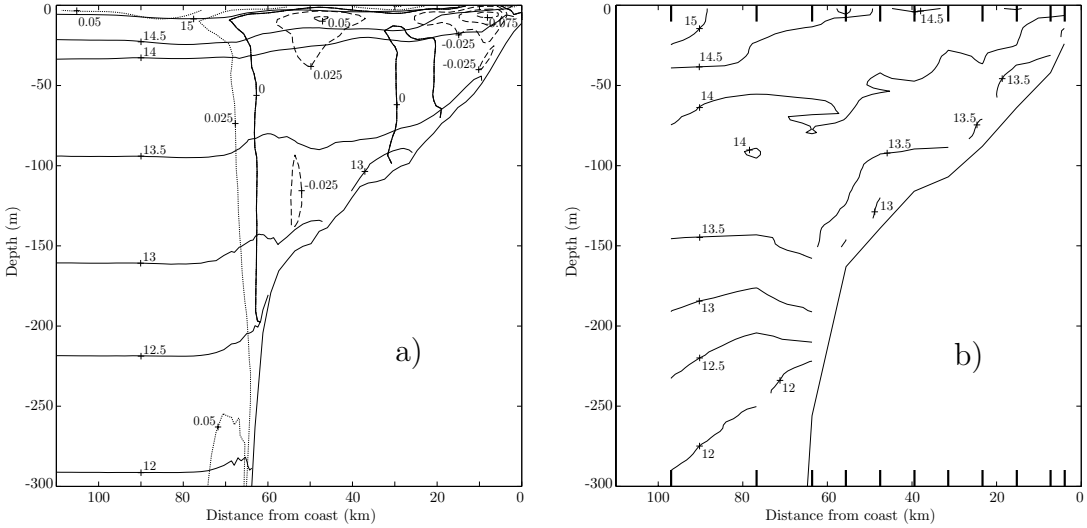

Figure 4.8: Cross-shelf profile of simulated (a) and observed temperatures (b) at the first row (southernmost) of the survey stations. The simulated meridional velocity is also shown, overlaid on the simulated temperatures. The location of the survey stations is indicated in (b) by the bold ticks.

the wind forcing. The cross section of salinity at the same location is shown in Figure 4.9. Values of salinity equal or higher than 37.8 psu are shown as dotted isolines. The cruise observation show the surface low salinity layer of riverine origin around the inner and middle shelf with minimum salinity values of 35.7 psu. Theses low values appear offshore only for depths bellow 150 m. The model gave very similar results with the low salinity plume extending slightly offshore, until the break.

4.4 Discussion and conclusions

A model simulation was done for the Portuguese shelf in parallel with cruise hydrological and currentmeter observations. The period of study was May 2002 which was characterised by the transition from the winter non-upwelling regime to the summer regime with the onset of shelf stratification and beginning of the upwelling regime.

The model was able to simulate the main Portuguese shelf features, being the wind and heat fluxes the main forcing factors. The presence and dynamics of a fresher buoyant plume created by the rivers runoff was also successfully simulated.

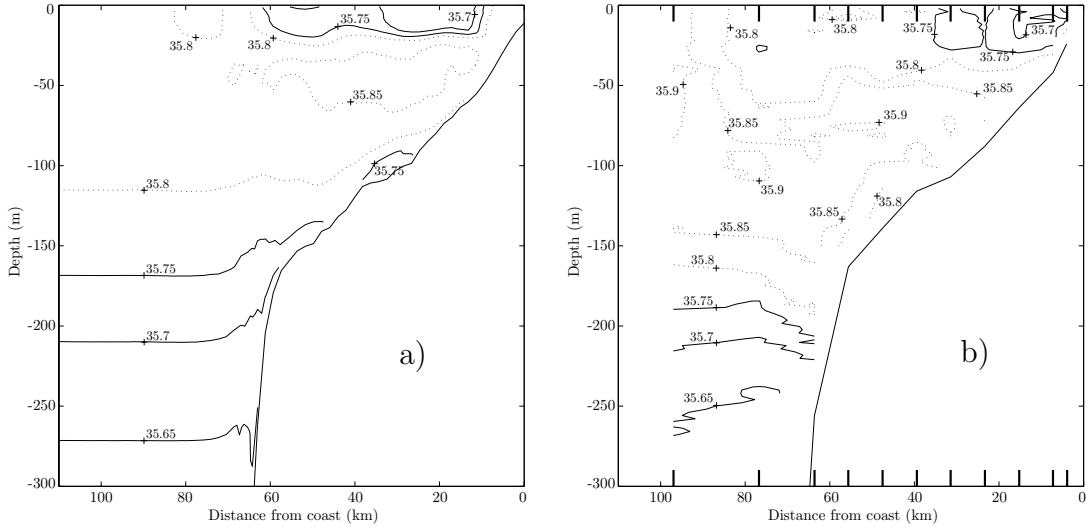

Figure 4.9: Cross-shelf profile of simulated (a) and observed salinities (b) at the southernmost survey stations (shown by the bold ticks in b).

The model was forced by the NCEP air-ocean bulk fluxes and by rivers runoff and provided good results. Some lack of accuracy in the simulated shelf currents was noticed and it should be a consequence of the low resolution of the forcing data near the coast, namely the wind which was certainly weaker than the real one. This leaded to lower simulated velocities than the observed ones during some periods. In spite of this, the results are comparable to the observations and allow to consider the model created a good solution for the northwestern Portuguese shelf, helpful in the better understanding of the observations and ready for future applications.

Chapter 5

Influence of Vertical Migration Pattern on Retention of Crab Larvae Over the Shelf in a Seasonal Upwelling System

Coasts subjected to upwelling are very advective environments where zooplanktonic organisms face the problem of avoiding wastage from the system. Partition of time between a surface layer, which is under the direct influence of the wind, and a deeper layer, dominated by the compensation counterflow, has been proposed as a mechanism that could enhance retention of planktonic organisms in the shelf of upwelling systems. The present study used a three-dimensional numerical model to examine the hypothesis that diel vertical migration is able to retain larvae of the littoral crab *Carcinus maenas* in the shelf of the northwestern Iberian upwelling system, which lacks known retention areas. Simulations contrasted two different wind regimes typical of winter (non-upwelling) and spring (upwelling) and four scenarios of vertical migration: larvae constrained to remain at the surface; passive larvae released with an initial uniform distribution; larvae with nocturnal diel vertical migration (DVM) between the surface and the bottom; and larvae with DVM between an upper and a lower layer. The timing and vertical extent of the DVM scenarios were based on recent observations of vertical

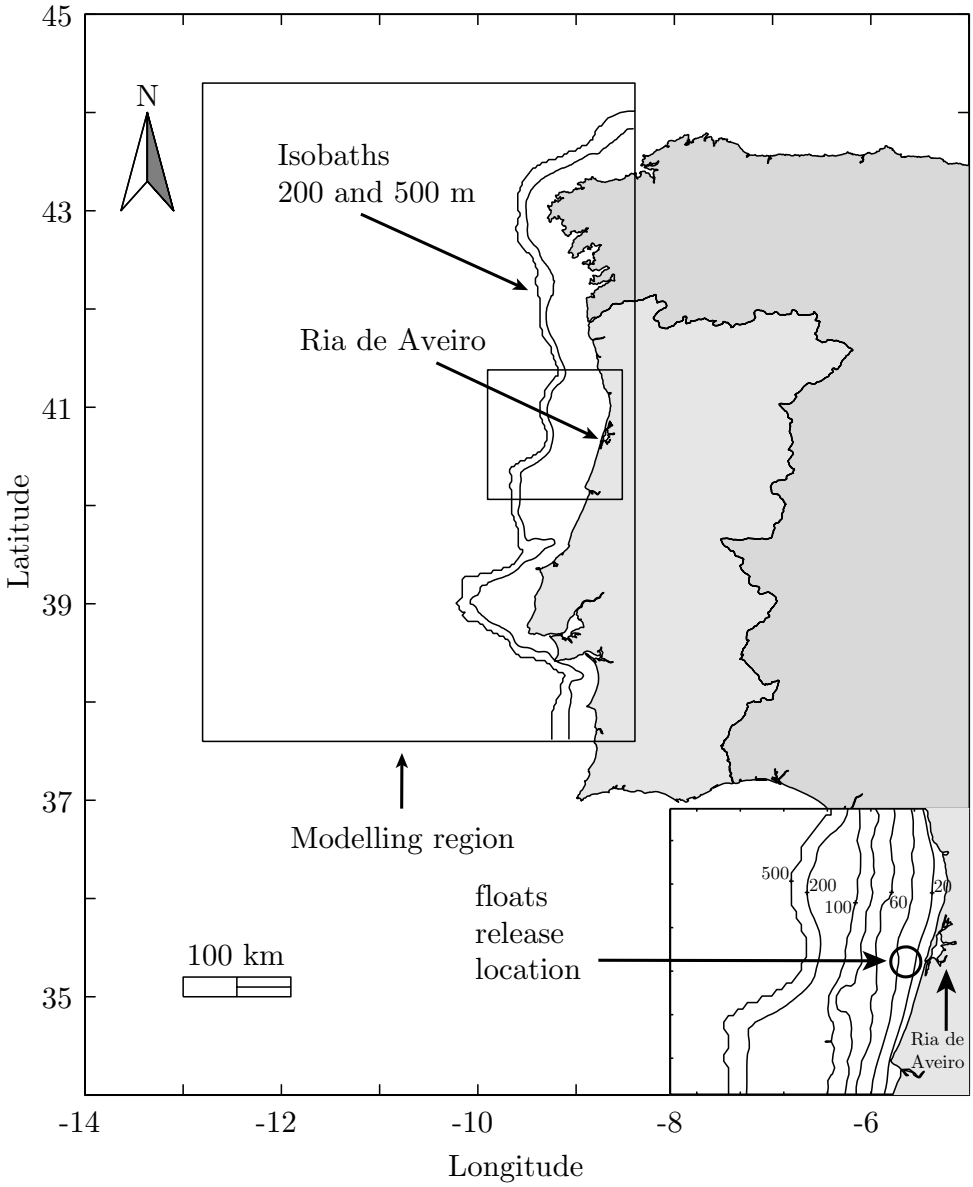

Figure 5.1: Map of the study area with modelling region. The location of the area of release of the particles is shown in the inset map.

distribution of crab larvae in the northwest coast of the Iberian Peninsula. Larvae were simulated as particles released in the model during neap tides at semilunar intervals, to simulate the hatching behaviour of the species, and were followed during 5 weeks, which approximates the average larval development time of the species. The particles from the different migration scenarios showed very different responses to wind forcing. Particles without DVM were more sensitive to wind-driven surface currents and were

often advected seaward of the shelf break, even during winter when upwelling wind events were less frequent and of short duration. Particles with DVM were consistently distributed over the shelf, and were very frequent in the inner shelf during upwelling conditions. This was accomplished by a larger proportion of time spent in the onshore underflow, which dragged the particles shorewards, than at the surface. The results of the simulations show that, for larvae of littoral species showing DVM over a large extent of the water column, upwelling may actually be a mechanism that enhances retention over the shelf.

5.1 Introduction

Temperate coasts subjected to upwelling are very productive systems where mero and holoplanktonic organisms find abundant food and moderate temperatures that favour growth and reproduction. These systems are also very advective environments, where planktonic organisms face a particular problem: how to avoid being swept out of the system by the prevailing seaward circulation at the surface. Several purely physical processes can explain the retention of zooplankton in shelf waters, like the action of eddies [Boehlert et al., 1992; Chiswell and Booth, 1999; Nishimoto and Washburn, 2002], taylor columns [Kloppmann et al., 2001], frontal zones [Werner et al., 1996; Santos et al., 2004] and Ekman convergence/divergence [Lee et al., 1992; Freeland, 1994]. Vertical displacement, either in the form of diel migrations or ontogenic migrations, have been indicated as a behavioural mechanism that improves retention of zooplankton in upwelling systems [Peterson, 1998]. During upwelling the surface waters move offshore due to Ekman transport, while a compensating onshore flow develops in deeper waters. Therefore, any behaviour of planktonic organisms that partitions time between the surface and the deeper layers reduces seaward advection and wastage from the system. The existence of behavioural mechanisms of this kind would constitute a selective advantage for these organisms. The purely physical mechanisms identified above depend to a great extent on local topographic conditions, whereas some kind of vertical migration would provide a general mechanism to increase retention on shelf waters independently

of local topographic singularities.

In this study we used a modelling approach to test the hypothesis that diel vertical migration (DVM) may constitute a mechanism for retention of larvae of littoral invertebrates species in the northwest Iberian upwelling system. Our model is a 3-D numerical model of the circulation in the region and is forced by air-ocean bulk fluxes. Particles were introduced into this model simulating several traits of the larval phase of the portunid crab *Carcinus maenas*. DVM of the nocturnal type is a widespread behaviour in larvae of decapod crustaceans, and these larvae have swimming abilities that allow them to cross vertical distances of the order of several tens of metres during the course of the migrations [reviewed by Queiroga and Blanton, 2004]. The extent of the vertical distribution is also known to change during larval ontogeny, and in some cases the last stage is mostly neustonic [e.g. Zeldis and Jillett, 1982; Shanks, 1986, 1995]. In order to account for uncertainties concerning the vertical migration behaviour of *C. maenas* larvae, several vertical migration scenarios were imposed on the particles (see below). Moreover, series of runs were performed using wind time series typical of non-upwelling and upwelling regimes, in order to contrast the outcome of the different migration scenarios between different wind-forcing conditions.

The Portuguese coast extends approximately south-north along the meridian 9° W and has no significant irregularities in the northern region. The shelf width is about 40 km and the slope is steep (Figure 5.1). The region of study is the shelf adjacent to the estuary of the Ria de Aveiro, northwest Portugal. Ria de Aveiro is a shallow lagoon that harbours a commercially important population of *Carcinus maenas*. It is located in the middle of a sand coast with a single narrow inlet connecting to the sea of 400 m width [Dias et al., 2003]. Tidal heights in the northern Iberian Peninsula coastal region are dominated by the semi-diurnal tidal components M_2 and S_2, which give rise to clear spring-neap cycles modulated by other constituents. Tidal amplitude varies between 0.5 to 1 m during neap tides and 1 m to 2 m during spring tides at the Ria de Aveiro inlet. The wind regime along the Portuguese coast is dependent on the dynamics of the Azores anticyclone whose centre migrates from 27° N in the winter to 33° N in the summer [Fiúza et al., 1982]. This condition originates weak westerly winds during the

winter and northerly winds during the spring and summer. Due to the south-north orientation of the Portuguese coast, the northerly winds give rise to upwelling [Wooster et al., 1976; da Silva, 1992; Peliz et al., 2002]. Huthnance et al. [2002] have computed, based on observed winds, upwelling indices for the west Iberian coast that show average positive values from March to September, with higher values from June to August. Even though these calculations have shown that the variability of northerly winds outside the period June to August is large, the data indicate that upwelling-favourable winds are a recurrent feature of the Portuguese coastal ocean during a protracted period of the year.

Our model species is the littoral portunid crab *Carcinus maenas*. This is the most common crab in northwest Iberia and in coastal waters of the Palaeartic Atlantic, forming large populations in estuaries and rocky shores throughout a native range that extends from Norway and Iceland to Mauritania [d'Udekem d'Acoz, 1999]. This species has become a global invader in the last century, having established successful populations in the east and west coasts of the USA [Almaça, 1962], South Africa [Le Roux et al., 1990] and Australia [Thresher et al., 2003]. *C. maenas* life cycle includes a larval phase composed of four zoeal and one megalopa planktotrophic stages [Rice and Ingle, 1975]. The megalopa is the stage that accomplishes the transition between the planktonic and the benthic phases. Hatching of larvae occurs in estuaries or shallow bays and first stage *C. maenas* zoeae rapidly abandon the release areas and spread into coastal shelf waters where they develop through the next zoeal stages and the megalopa. The megalopa then needs to find appropriate littoral habitats for settlement, metamorphosis and successful juvenile development. The mechanisms by which *C. maenas* leave and reenter the estuaries in northwest Iberia have been studied in recent years and were associated mainly with environmental processes that occur at tidal, diel, and semi-lunar periodicities. In northwest Portugal larval release occurs during night ebb tides. This combination of phase of tide and phase of day takes place during neap tides following the quarter moons, and has thence a semi-lunar periodicity. A rapid export of the first zoea to shelf waters then follows immediately [Queiroga et al., 1994, 1997; Pereira et al., 2000]. Once in shelf waters, development until the megalopa stage

takes about 4 to 6 weeks depending on water temperature [Darwirs, 1985; Mohamedeen and Hartnoll, 1989]. The migration from shelf waters to the estuarine habitat is thought to occur in two steps: *i*) the shoreward transport [Shanks, 1995; Queiroga and Blanton, 2004] and *ii*) the passage through the estuarine inlet and upstream transport until an appropriate settlement environment is found. The mechanisms responsible for step *i*) are not clear, but supply of megalopae to estuaries in northern Portugal has been related to episodes of relaxation/inversion of northerly winds [Almeida and Queiroga, 2003; Queiroga, 2003]. Step *ii*) is accomplished by selective tidal stream transport that takes place during night flood tides [Jones et al., 1984; Queiroga, 1998; Forward Jr. and Tankersley, 2001]. The vertical migration behaviour of *C. maenas* larvae in the shelf is not clearly described, but megalopae of this species are known to migrate to the neuston layer during the night in the British Islands [Zeng and Naylor, 1996]. Moreover, a recent literature review [Queiroga and Blanton, 2004] indicates that diel vertical migration of the nocturnal type, where larvae are closer to the surface during the night, is a very common behaviour in crustacean decapod larvae in shelf waters.

The objective of this work was to investigate the consequences of the active DVM under different wind forcing conditions for the retention and recruitment of larvae in regions without prominent coastal or bathymetric features. The absence of topographic singularities excludes, *à priori*, retention of larvae caused by possible stable and persistent circulations related with the topography. Given the life-cycle characteristics of the species, the available knowledge on critical aspects of its larval biology and its widespread occurrence, we believe *Carcinus maenas* provides a good model to test the retention hypothesis, and that the results of the present work may be important to elucidate aspects of recruitment processes of littoral invertebrates in coastal upwelling areas.

5.2 Methods

5.2.1 Model setup

The influence of the pattern of vertical distribution of larvae on their dispersion and retention in the shelf was studied with a three-dimensional hydrodynamical model that simulates the shelf water dynamics with realistic forcings and stratification. The domain of the model spans from 12.8° W to 8.4° W and 37.6° N to 44.3° N, corresponding to 360 km in the meridional and 740 km in the latitudinal directions (Figure 5.1). The model used was the Regional Ocean Modeling System (ROMS) [Haidvogel et al., 2000] and it was forced by wind and heat fluxes from the NCEP reanalysis database, which were interpolated for the simulation grid.

Useful prediction of oceanographic circulation and advection based on the use of numerical models depend on a proper validation of the models. The model used in the present study was validated by comparing observations, obtained during the ProRecruit cruise carried on in the shelf in front of Ria de Aveiro during May 2002, with model simulations for the same period. Figure 5.2 shows a typical result obtained when current measurements made at 35 m, off the Ria de Aveiro, are compared with model simulations. The simulated instantaneous velocities have a lower variance than the observed values, both for the zonal (across-shore) and meridional (along-shore) components. This results from the fact that NCEP winds do not represent the real winds with high accuracy in the studied region. This conclusion arises from comparison with data from a coastal meteorological station, which shows systematic higher values of observed than NCEP winds. However, simulated residual currents at weekly and longer time scales are similar to the observations. Therefore, the model appears to realistically reproduce transports integrated over the time scales of larval development.

Two simulations were performed, one for the late winter and the other for the spring, covering the months of February to April and April to June 2002, respectively. These periods were chosen because they show contrasting wind regimes between non-upwelling and upwelling season. Figure 5.3 shows the wind for the winter and spring simulations at the release location, off the Ria de Aveiro. The wind was more variable in winter

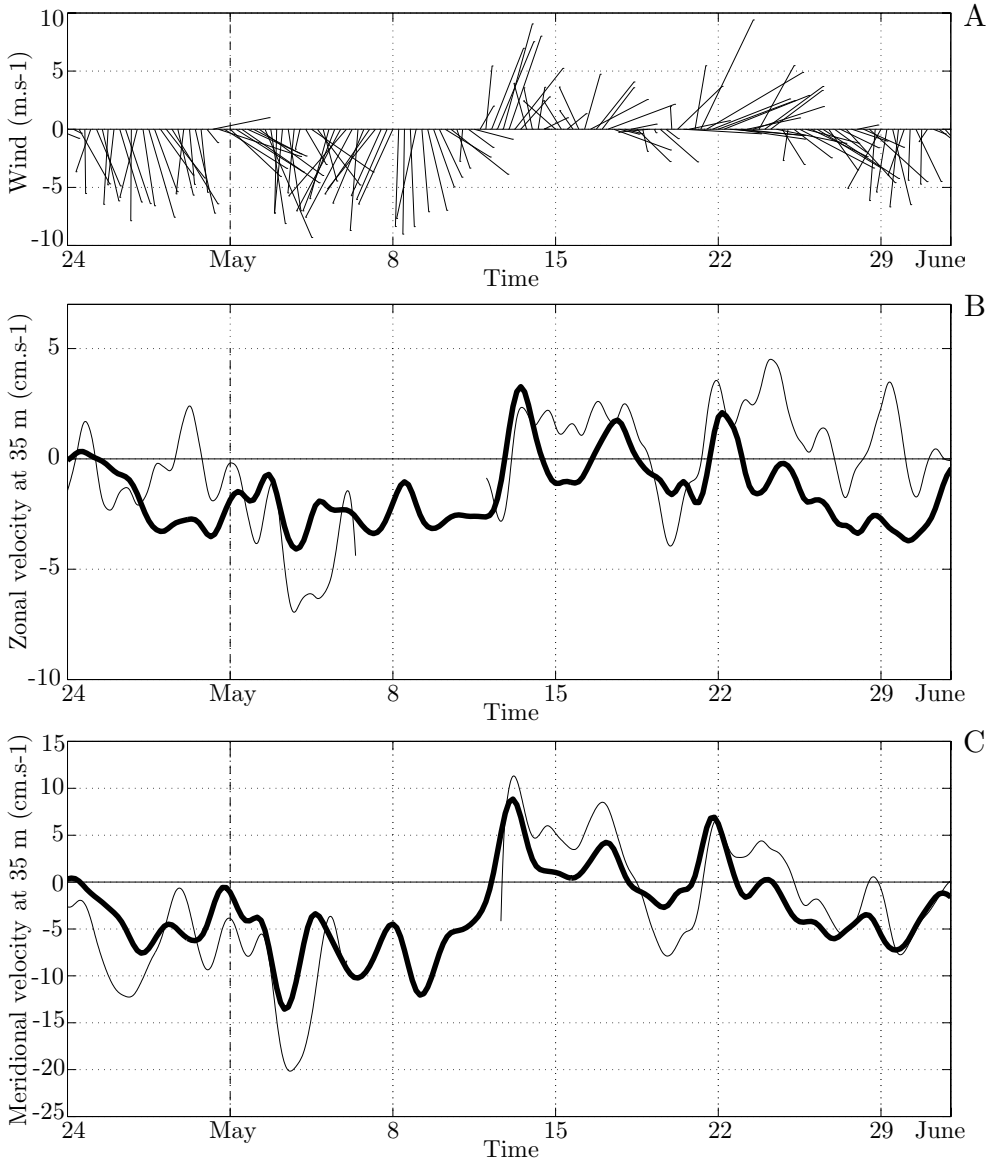

Figure 5.2: Wind (panel A) and simulated and observed across-shelf (panel B) and along-shore (panel C) currents at 35 m depth at the ProRecruit mooring site, off the Ria de Aveiro. In the Y-axis of panel A the positive values refer to southerly wind. In panel B, the bold lines indicate the simulation results and the thin ones, the observations.

than in spring. In February it was southerly in the first week and northerly until day 25. In March there was one episode of northerly wind between day 4 and day 10 and then southerly wind until day 23. During the rest of the month the wind was weaker and more variable, but mainly from the north. Contrasting with this situation, the wind during

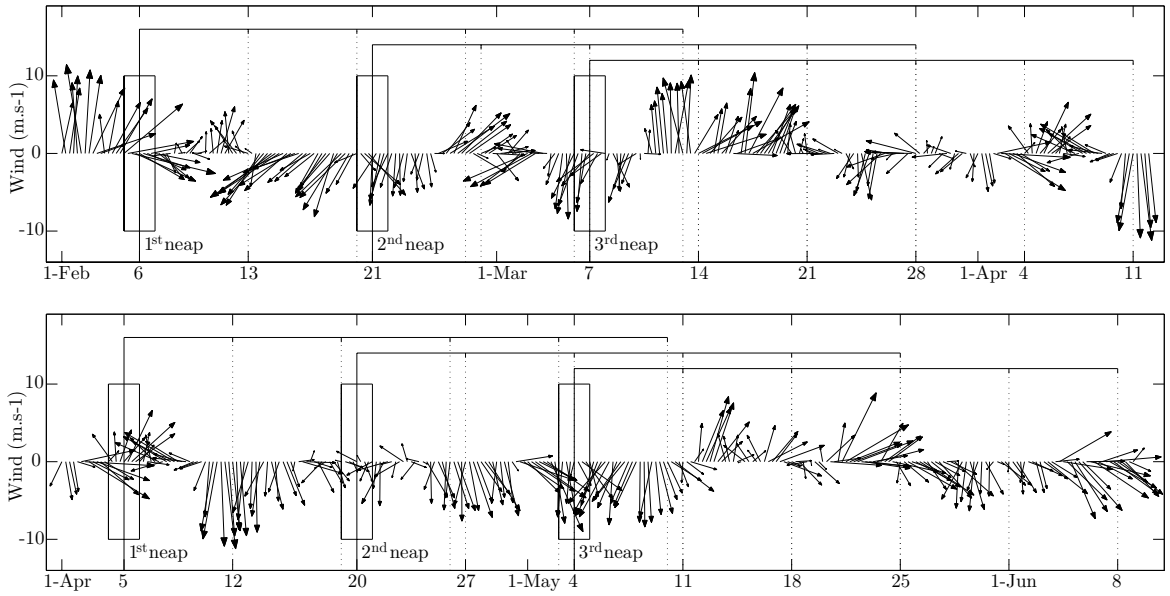

Figure 5.3: Wind near Ria de Aveiro during the winter (February–March, upper chart) and spring (April–May, lower chart) simulation periods. The vertical rectangles indicate the three release days within each neap tide period. The dotted lines represent the five weeks after each release.

the spring simulation was almost always northerly and with an westerly component. The exceptions were between days 4 and 10 of April and between days 12 and 24 of May. The southerly wind in these periods was however weaker than the average northerly wind during the rest of the spring simulation period. The northwesterly wind during the months of April and May are typical of the Portuguese west coast in spring and summer, and drive coastal upwelling in this region.

Tidal forcing was not used in the present study, but preliminary simulations including tides and vertical migration were carried out in order to inspect the sensitivity of the model to interactions between diel vertical migration and tidal currents. The results of those simulations showed that significant net horizontal transport was not observed. Hill [1991b,a, 1995] describes a series of situations where planktonic organisms migrating vertically in the water column on a background of tidal currents would experience considerable horizontal transport, provided the period of the migration is a multiple, or close to a multiple, of the tidal period. Since there is no evidence to suspect that

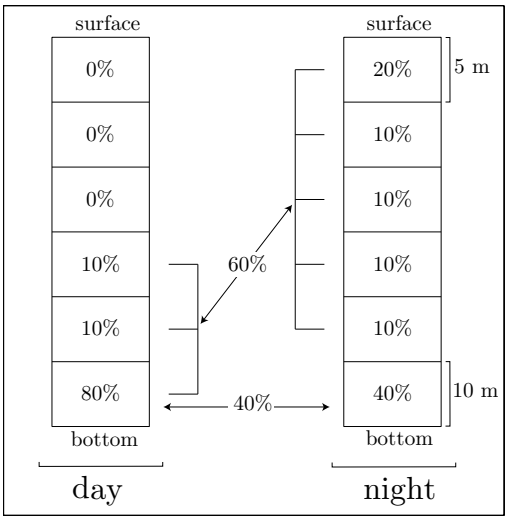

Figure 5.4: Vertical distribution of the particles in the nocturnal DVM scenario between upper and lower layers. See text for explanation.

Carcinus maenas larvae will retain a migration behaviour synchronised with the lunar semi-diurnal tide in shelf waters, horizontal transport by the M_2 tide would not be expected. The 24 h period of the diel migration would interact with the semi-diurnal S_2 constituent, which has a period of 12 h. However, in the area of study this constituent has a small importance relative to the principal lunar M_2. A systematic interaction between tidal currents and vertical migration is expected in places where tides are the main driving mechanism, in opposition to the shelf region of northern Portugal, where wind appears to be the main ocean forcing [Vitorino et al., 2002; Peliz et al., 2003a].

5.2.2 Simulation of larvae behaviours

The larvae were simulated by inserting drifters in the model. The drifters had lagrangean movement in the horizontal, i.e., they had a passive behaviour in terms of horizontal transport. In order to examine the influence of the vertical migration pattern on dispersal, four patterns of distribution were implemented. These were chosen in order to contrast two scenarios with active daily vertical migration with two scenarios without vertical migration. The patterns of vertical movement and the number of particles released each day were as follows. A set of 500 particles was dropped at

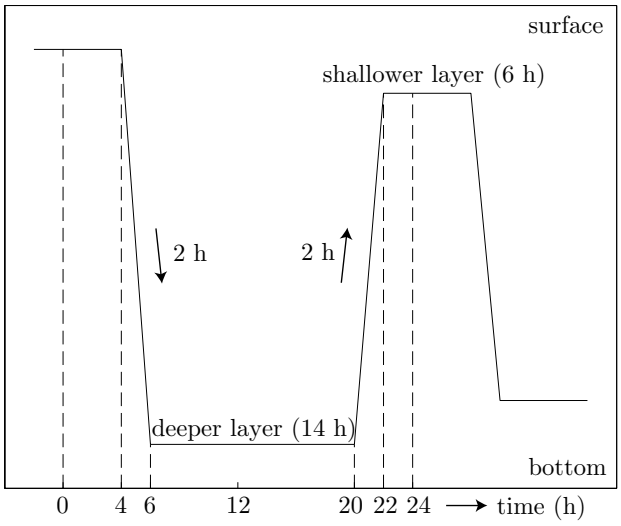

Figure 5.5: Timing of the vertical movements imposed in the scenarios with DVM between surface and bottom (SB) and with DVM between upper and lower layers (UL). The layers labelled shallower and deeper in the figure depend on the migration scenario.

the surface and constrained to remain there. Another set of 500 particles was released with an uniform distribution between the surface and the bottom and left to change vertical position according to the vertical velocities in the model. In a third set of 500 particles, nocturnal vertical migration was imposed making them migrate daily between a surface and a bottom layer, which were arbitrarily set with thicknesses of 5 m and 10 m, respectively. Finally, 1000 particles were released with a more complex pattern of nocturnal vertical migration between an upper and a lower layer, which is detailed in Figure 5.4. In order to force this pattern, the water column was divided into six levels. The surface and the bottom levels were always 5 m and 10 m thick, respectively. The intermediate levels were equal but their thickness depended on the total depth. During the day, 80% of the drifters were in the bottom level and 10% were in each of the next two levels. During the night, half of the particles in the bottom level (i.e., 40% of the total number) remained there. The other 40% plus the 20% in the two levels above the bottom layer moved upwards, reaching a final distribution with 10% in each intermediate level and 20% in the surface one. This last scheme is based on recent observations on the vertical distribution of decapod larval stages made during a cruise conducted

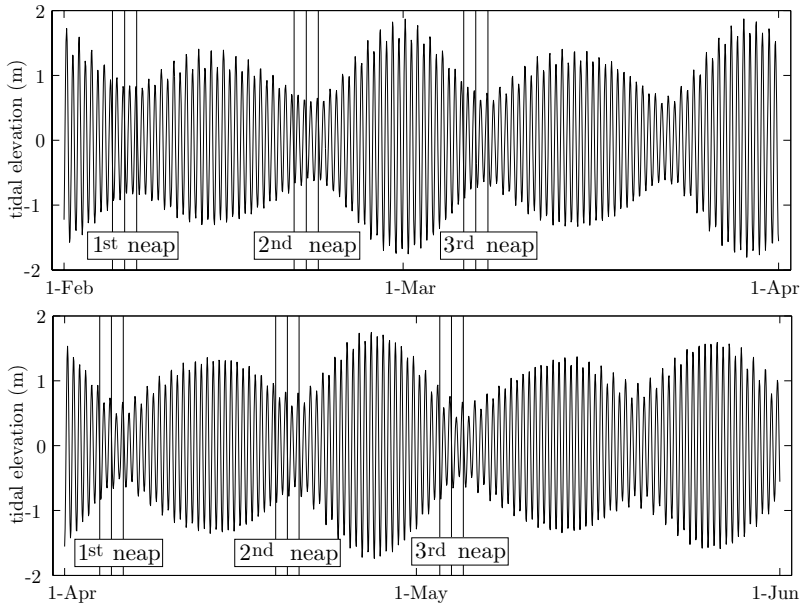

Figure 5.6: Tidal elevation near Ria de Aveiro inlet during the winter (February–March, upper chart) and spring (April–May, lower chart) simulation periods. The vertical lines indicate the three release days within each neap tide period.

in coastal waters off the Ria de Aveiro [dos Santos et al., in preparation]. That study described a very clear nocturnal upward migration of crab larvae during the night that extended along much of a 60 m water column height.

In the two scenarios with vertical migration the particles remained in the deeper levels between 06h00 and 20h00. Then they began the upward movement reaching the shallower levels at 22h00 where they remained until 04h00. At this moment they started a downward movement at a rate that took them back to the deeper levels at 06h00 (Figure 5.5). To facilitate further reference, the four migration scenarios were coded NS for no migration and surface distribution, NU for no migration and uniform distribution, SB for nocturnal diel vertical migration (DVM) between surface and bottom, and UL for nocturnal DVM between upper and lower layers.

Initiation of the particles in the model was programmed to simulate the hatching pattern of *Carcinus maenas*. Larval hatching takes place during nocturnal neap ebb tides which recur in the Portuguese coast with a basic semi-lunar periodicity (see above). Therefore, drifters were released in the model for three consecutive days around

Table 5.1: Time of particles release for the winter and spring simulations. Particles were released during three days at 0 h in the first three neap tides of February–March (winter simulation) and April–May (spring simulation).

neap tide	winter	spring
1st	5,6 and 7 February	4, 5 and 6 April
2nd	20, 21 and 22 February	19, 20 and 21 April
3rd	6,7 and 8 March	3, 4 and 5 May

Table 5.2: Vertical migration scenarios imposed on the particles and the number of particles released per day. At the right column are the insignias used through the text.

drifters/day	migration scenario	
500	none, surface	NS
500	none, uniform	NU
500	surface $\leftrightarrow$ bottom	SB
1000	upper layer $\leftrightarrow$ lower layer	UL

the lowest amplitude tide, during three consecutive neap tide periods (see Figure 5.6). All drifters were released at 0 hours. Tables 5.1 and 5.2 summarise the drifters releasing time and the number of drifters used per release day. For the winter simulation (February and March) the releasing days were 5, 6 and 7 of February (first neap tide), 20, 21 and 22 of February (second neap tide) and 6, 7 and 8 of March (third neap tide). The releasing days in the spring simulation were 5, 6 and 7 of April (first neap tide), 20, 21 and 22 of April (second neap tide) and 6, 7 and 8 of May (third neap tide). By releasing larvae at several consecutive neap tides we hoped to explore possible responses of the larval pool to different wind regimes at the time of initial appearance of the larvae in the shelf. The particles were released in random positions inside a circle of radius 5 km near the Ria de Aveiro inlet (Figure 5.1). This is considered to be a good approximation of the estuarine plume and, therefore, of the larval distribution immediately after they

leave the estuary carried by the ebb current. The number of particles used in each of the two simulations was, thus, 2500 per day, during three days per neap tide period, for three neap tides, summing a total of 45000 drifters' trajectories analysed.

5.2.3 Analysis of dispersal patterns

The analysis of the results was based on four descriptors: *i*) the cross-shelf distribution of the particles, *ii*) the percentage of the particles in the inner shelf, *iii*) the latitudinal distribution of the particles in the inner shelf and *iv*) the dispersion pattern of the particles. The cross-shelf distribution of particles was calculated until the end of the fifth week, at weekly intervals starting one week after the release (using as reference the second day of the release). The period of five weeks was chosen because it corresponds to the average development time of *Carcinus maenas* larvae at the temperature usually found in Portuguese coastal waters during winter and spring [Darwirs, 1985; Mohamedeen and Hartnoll, 1989]. The percentage of particles in the inner shelf was calculated weekly as those within 5 km from the coast, and was chosen in order to obtain a measure of the size of the larval pool available for recruitment to littoral habitats. The latitudinal distribution of these particles was also calculated at weekly intervals. With the aim of measuring the dispersion pattern of the particles, the region of the model was divided into 100×200 boxes (longitudinally $\times$ latitudinally) of equal size and the variance of the resulting matrice of the number of particles was calculated. Since the total number of drifters does not change with time and the boxes are of equal size, the variance $\sum_{i=1}^{b}(n_i - \bar{n})^2/b$ (in individuals^2) is a measure of the particles horizontal dispersion. Because this variance depends on the total number of particles and the UL migration scenario used twice more larvae than the other scenarios, the variance was normalised by $(\frac{N}{b})^2(b-1)$, which is the maximum variance when all particles are inside a single box, i.e., $\sum_{i=2}^{b}(0-\bar{n})^2/b + (N-\bar{n})^2/b$. In these formulas, b is the number of boxes used, n_i is the number of particles in box i, N is the total number of drifters and $\bar{n}$ is the average number of drifters per box, N/b. Thence, high values of the normalised variance correspond to higher aggregation. The calculation of the variance was performed since the third day of release, every day, until the end of the fifth week, separately for each

of the four migration scenarios and for each of the three release periods.

Mortality of the larvae was set to zero.

5.3 Results

The movements of the particles depend on the interaction between their vertical position in the water column and the forcing factors. Since observed winds were the main driving force of the circulation it was expected that trajectories of the particles depended on the migration scenario and on the day of release into the model domain.

Figure 5.7 shows the normalised variance of the particles for all migration scenarios and for the three release periods in the winter and spring simulations. Figures 5.8 to 5.13 show the meridional distribution of the particles in the inner shelf, expressed as the percentage of particles at a distance lower than 5 km from the coast (Panel A), and the cross shelf distribution of the particles (Panel B), calculated at weekly intervals, for the three release periods in the winter (Figures 5.8 to 5.10) and spring (Figures 5.11 to 5.13) simulations. To facilitate the analysis and cross-referencing, all these figures are organised into matrices where rows correspond to the four migration scenarios.

5.3.1 Winter simulation

The normalised variance of the NS scenario in winter showed large fluctuations along time, contrasting with that for the other three vertical migration scenarios (Figure 5.7). As will be seen below, large values of the variance in the NS scenario were always associated with situations when particles hit the coast and remained concentrated there. In the NU, SB and UL scenarios the variance decreased during the five weeks for the three release periods, to levels consistently below 0.03 at the 5^{th} week. Of these, the NU particles showed the lowest values of the variance.

The particles released in the first neap tide of the winter simulation moved southward and offshore (Figure 5.8) onto the middle shelf, for all scenarios. Most of the net displacement took place during the first three weeks, responding to the strong northeasterly wind (Figure 5.3). Retention in the inner shelf was usually below 5% from the

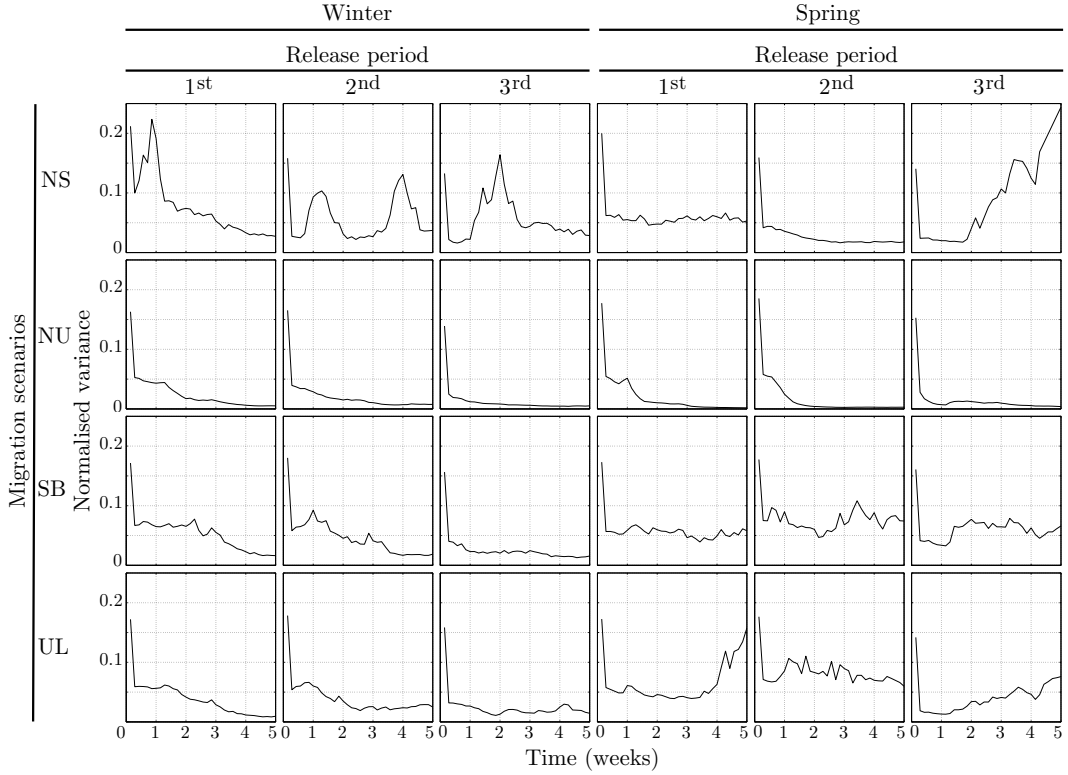

Figure 5.7: Changes in the variance of particles during the first five weeks after release in the model. The first three columns correspond to the three releases of the winter simulation and the last three columns correspond to the three releases of the spring simulation. The four rows correspond to the NS, NU, SB and UL migration scenarios.

4$^{\text{th}}$ week onwards, for all migration scenarios (Figure 5.8, panel A).

In the second neap tide release (Figure 5.9) there were larger differences in the trajectory and dispersion of the particles among the different larval migration scenarios than in the first release. This was caused by the higher variability of the wind in the weeks after the second release (Figure 5.3), leading to different responses of the particles from the different migration schemes. While NS particles move southward in the first two weeks and then northward, all others particles suffered a very small southward transport, but also moved northward after the second week (Figure 5.9, panel A). Two maxima were found in the variance of these particles in the NS scenario (Figure 5.7), one after the first week and the other around the fourth week. These maxima were caused by the interception of the northward trajectory of the particles with the coast

southward (first maximum) and northward (second maximum) of the release location (Figure 5.9). In all other scenarios, particles moved seaward with time until the outer shelf in the 5th week, with concentration maxima at 20 to 40 km from the coast (Figure 5.9, panel B). The contrast between the NS and the other scenarios is evident when the percentage of the particles in the inner shelf is compared (Figure 5.9, panel A). The values were over 60% for the NS particles until the 4th week. The decrease to 0.1% in the 5th week was due to the onset of northerly and easterly wind after the 4th week (Figure 5.3). Percentage of particles in the inner shelf was always below 5% in all other scenarios.

The particles of the third release (Figure 5.10) were subjected to strong southerly wind during about two weeks, and then low and variable wind with an easterly component around the third week (Figure 5.3). The movement of the particles was thus basically northward (Figure 5.10, panel A) and seaward to the middle and outer shelf (Figure 5.10, panel B). A maximum of the variance of the particles occurred two weeks after release in the NS scenario (Figure 5.7) and was again caused by convergence at the coast. While propagating northward, the particles met the coast to the right and remained concentrated there due to a small westerly wind component. This is shown by a peak in concentration near the coast in Figure 5.10, panel B, in week two for this scenario. Particles other than those in the NS scenario are spread through the shelf with concentration maximum around the middle and outer shelf (Figure 5.10, panel B). Except for the very high peak in the percentage of NS particles in the inner shelf, caused by the coast, the values were low and mostly below 2% for the other scenarios after the 2nd week (Figure 5.10, panel A).

5.3.2 Spring simulation

In spring, the normalised variance of the particles in the SB and UL scenarios, both with DVM, remained usually bounded within intermediate levels 0.05 and 0.15 over the five weeks for the three releases (Figure 5.7). This contrasted with the same scenarios in the winter simulation, where variance decreased to lower values. It also contrasted with the NS and NU scenarios both in winter and spring. In the NU scenario, similarly to what

had occurred in the winter simulation, the variance decreased to levels below 0.01. In the NS scenario the pattern of change of the variance with time differed across the three releases, with intermediate and low values for the first and second release and a rise to very high values in the third. Again, the increase in the variance in the NS scenario is associated with the interaction of the shoreward flow with coastal topography.

A few days after the first release (Figure 5.11) the wind turned northerly (Figure 5.3). Thence, a southward and offshore transport was expected for the NS and NU particles, which did actually occur. After the third week the NS particles were southward of the release point, out of the shelf, and kept moving seaward with a small dispersion (Figure 5.11, panel B). The NU particles suffered a smaller offshore transport and were dispersed over the outer shelf and off the break at the fifth week. This dispersion and offshore transport happened because the particles, originally with an uniform distribution between the surface and the bottom, became more concentrated in layers close to the surface due to the upwelling internal return current, which led to an upward transport of the particles. The SB and UL particles also moved southward (Figure 5.11, panel A) but were not advected offshore by the upwelling currents. Instead, they remained in the inner shelf during all the five weeks (Figure 5.11, panel B). Because of the migration schemes that were imposed upon them, these particles spent more time in the lower layers of the water column, where currents are onshore, than in the upper ones. The particles followed an oscillatory trajectory, being transported offshore in the upper layers, but onshore in the lower layers, in spite of the weaker currents at depth. Accordingly, the percentage of the particles close to shore was higher in the SB and UL scenarios than in the other two, with values that reached over 70% after the second week in the UL scenario.

After the second release (Figure 5.12) the particles were subjected to wind conditions similar to those of the first release (Figure 5.3) and behaved very similarly. The main difference is related to the northeasterly wind event in the end of the second week and beginning of the third (between 1 to 4 of May), and also the wind inversion during the fourth and fifth weeks after the release that brought the NS and NU particles, which had moved offshore during the first two weeks, in the shoreward direction (Figure 5.12,

panel B), until the shelf break (NS particles) and middle shelf (NU particles). The percentage of particles in the inner shelf was also similar to that of the previous release, except for the higher values for the SB particles which, now like the UL particles, were retained close to the coast during most of the five weeks (Figure 5.12, panel A).

The particles released in the third neap tide (Figure 5.13) showed a quite different behaviour from the particles of the first and second releases. The wind was northerly during the first, fourth and fifth weeks. After the middle of the second week the wind had a strong westerly component. Because of these events the particles never left the shelf. The NS and NU particles were advected by the upwelling currents only in the first week and moved southward (Figure 5.13, panel A) until the middle shelf (Figure 5.13, panel B). The southwesterly wind then carried the particles onshore, and in the following weeks the NS particles remained attached to the coast while the NU particles dispersed through the inner and middle shelf. The SB and UL particles behaved as in the previous releases, remaining in the inner shelf during the entire simulation period (Figure 5.13, panel B), only exhibiting a smaller southward transport in comparison with the particles from the first and second release (Figure 5.13, panel A). The proportion of particles in the inner shelf was the highest of all releases in both winter and spring simulations and for all the migration scenarios (Figure 5.13, panel A). This happened, however, not because the particles returned to the region near the coast, but because they never left that region in all the simulation period. The variance had very small values for the case of NU particles, as expected, due to the high dispersion they exhibited, and increased with time for the NS particles as a consequence of their shoreward movement and collision with the coast (Figure 5.7).

[†] Figures 5.8 to 5.13, in the next pages, show the latitudinal distribution and percentage (inset value) of the particles within 5 km from the coast (panel A) and the cross-shelf distribution of the total number of particles (panel B). The five columns show the result for one to five weeks after the release. The four rows correspond to the NS, NU, SB and UL migration schemes. In panel A the release point is located at 0 km in the Y-axis and positive values represent particles located to the north of the inlet. In panel B the coast is located at 0 km, on the right at the X-axis. The vertical line in panel B, at 43.1 km, marks the average position of the shelf break calculated over a 300 km stretch of shelf centred on the release location.

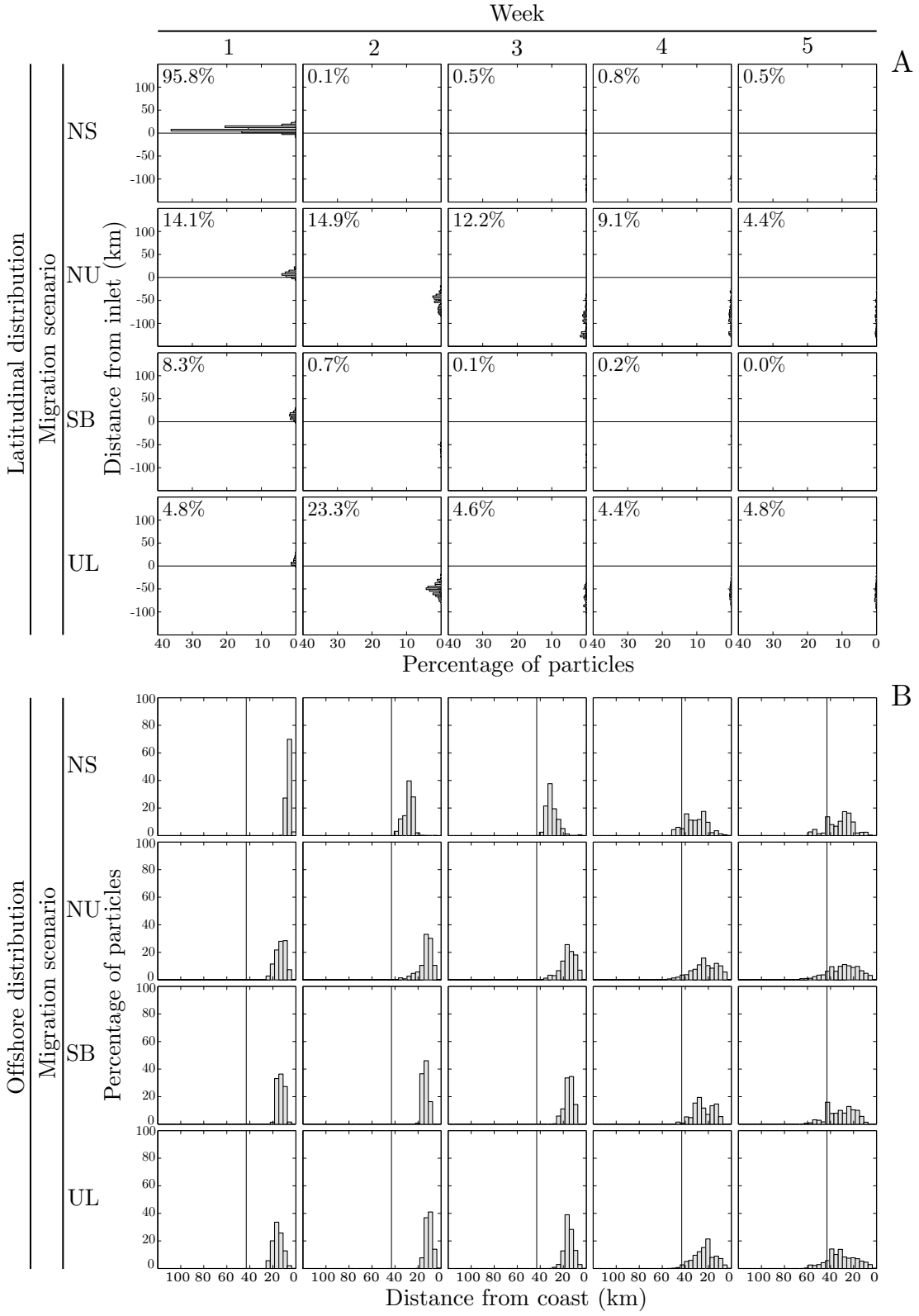

Figure 5.8: Winter simulation, first release. See footnote† at the page 73.

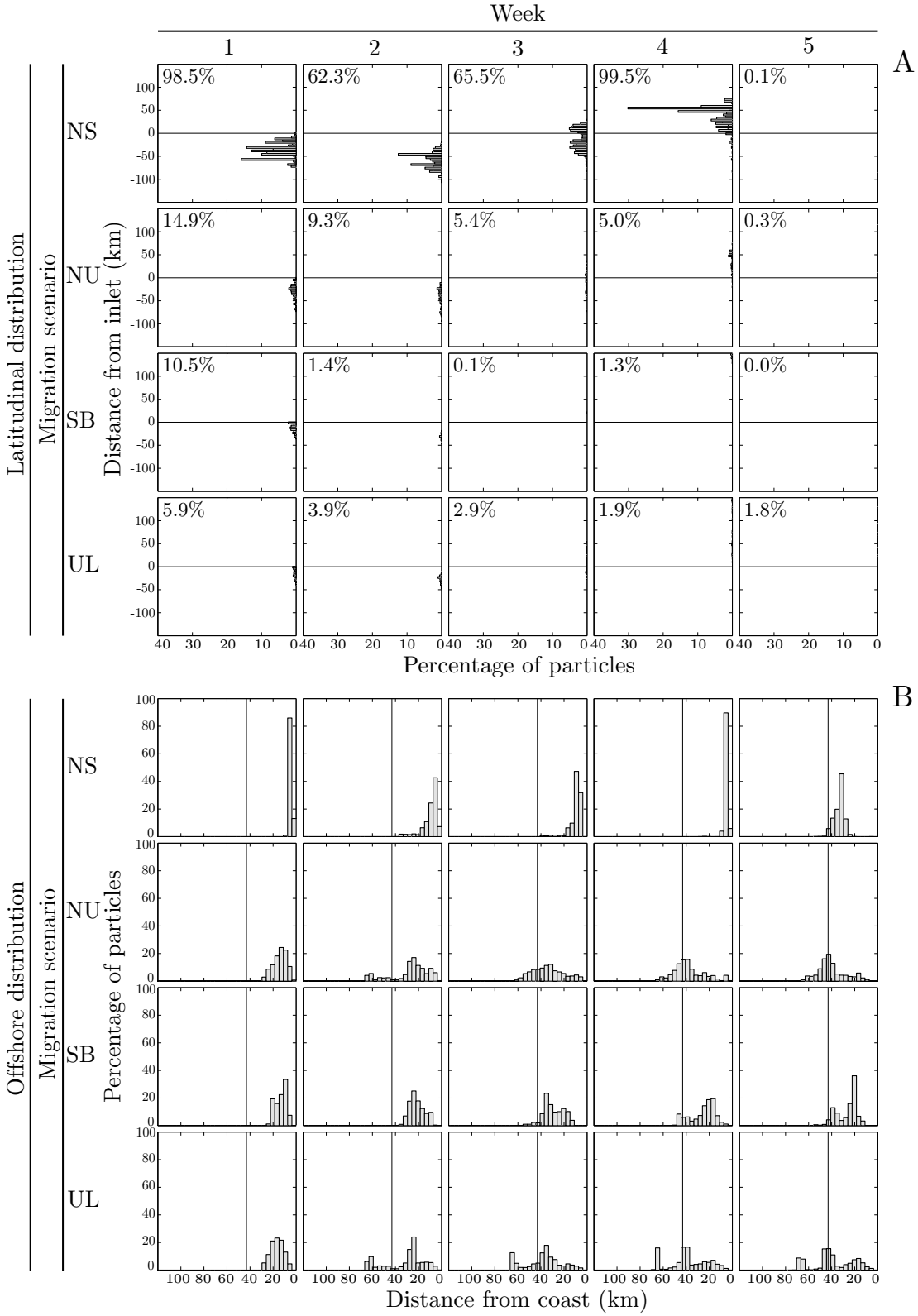

Figure 5.9: Winter simulation, second release. Same as in Figure 5.8.

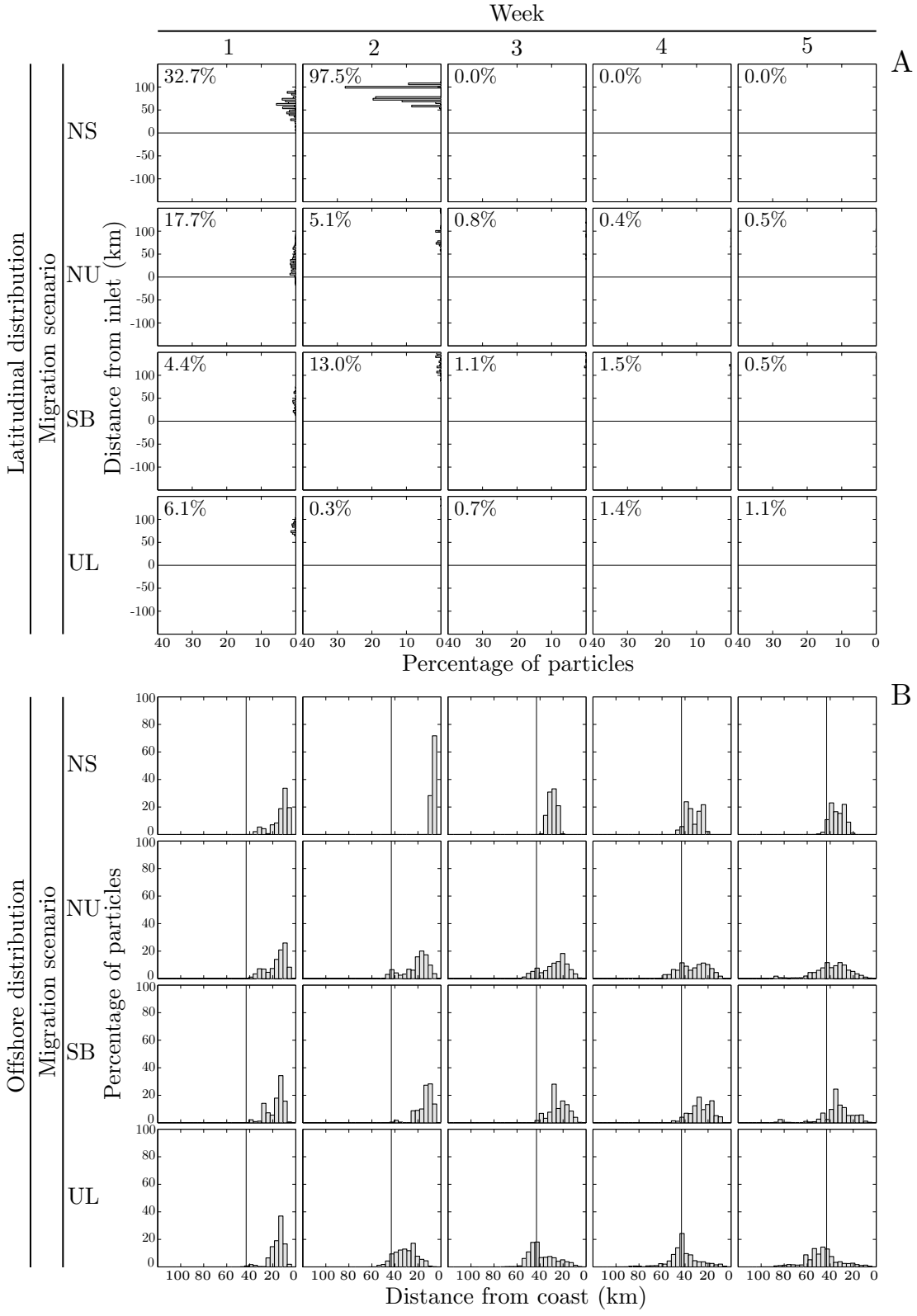

Figure 5.10: Winter simulation, third release. Same as in Figure 5.8.

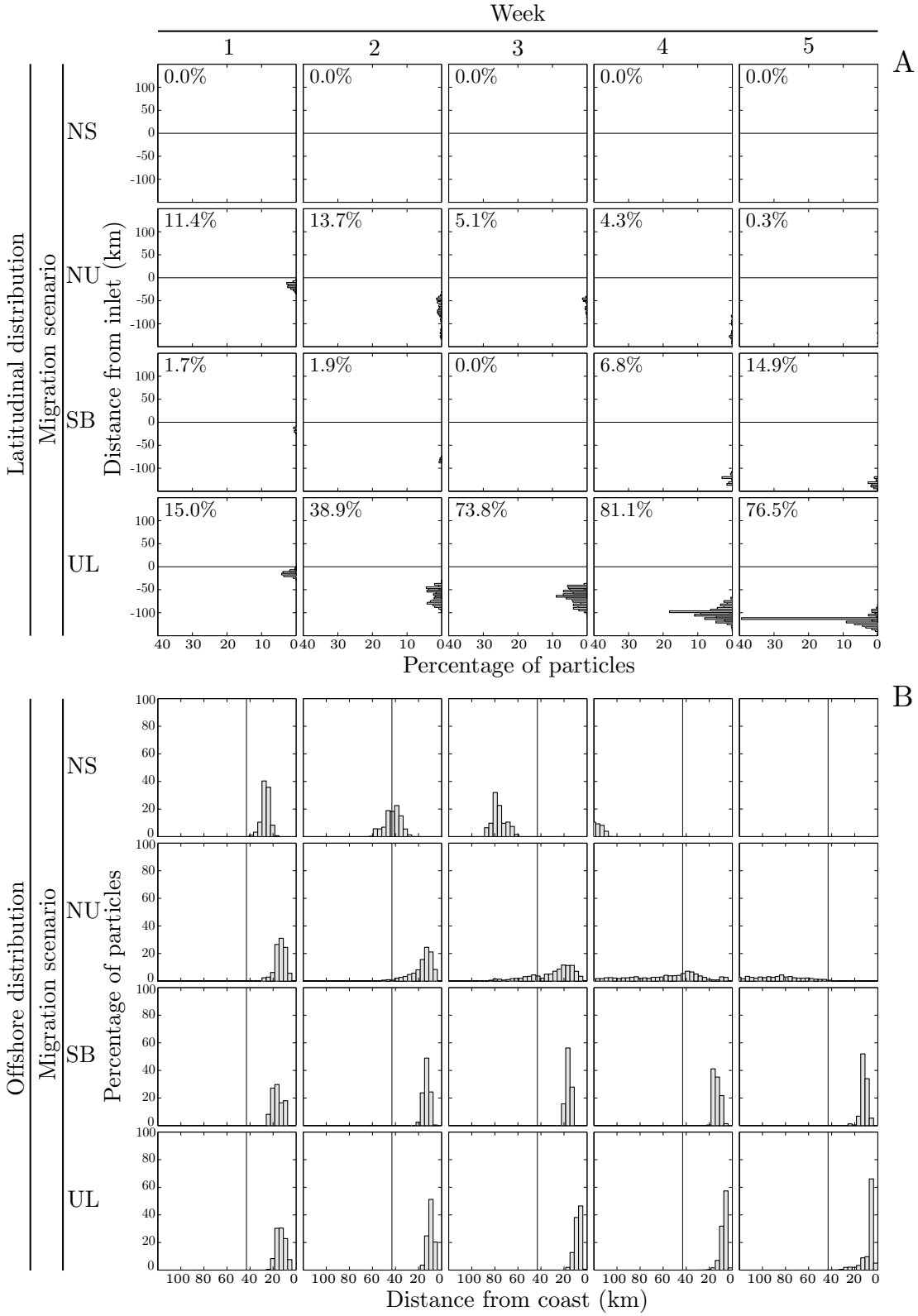

Figure 5.11: Spring simulation, first release. Same as in Figure 5.8.

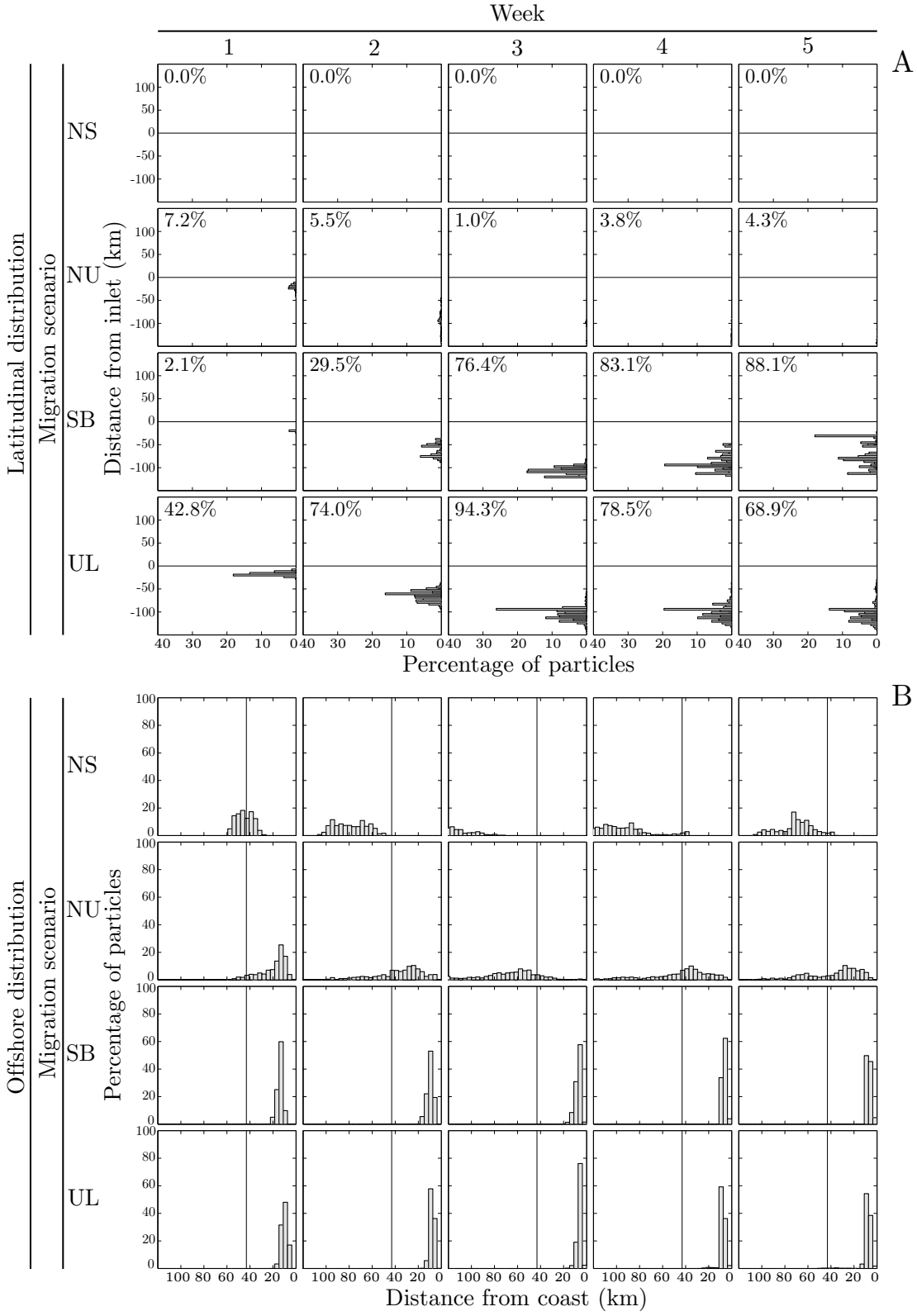

Figure 5.12: Spring simulation, second release. Same as in Figure 5.8.

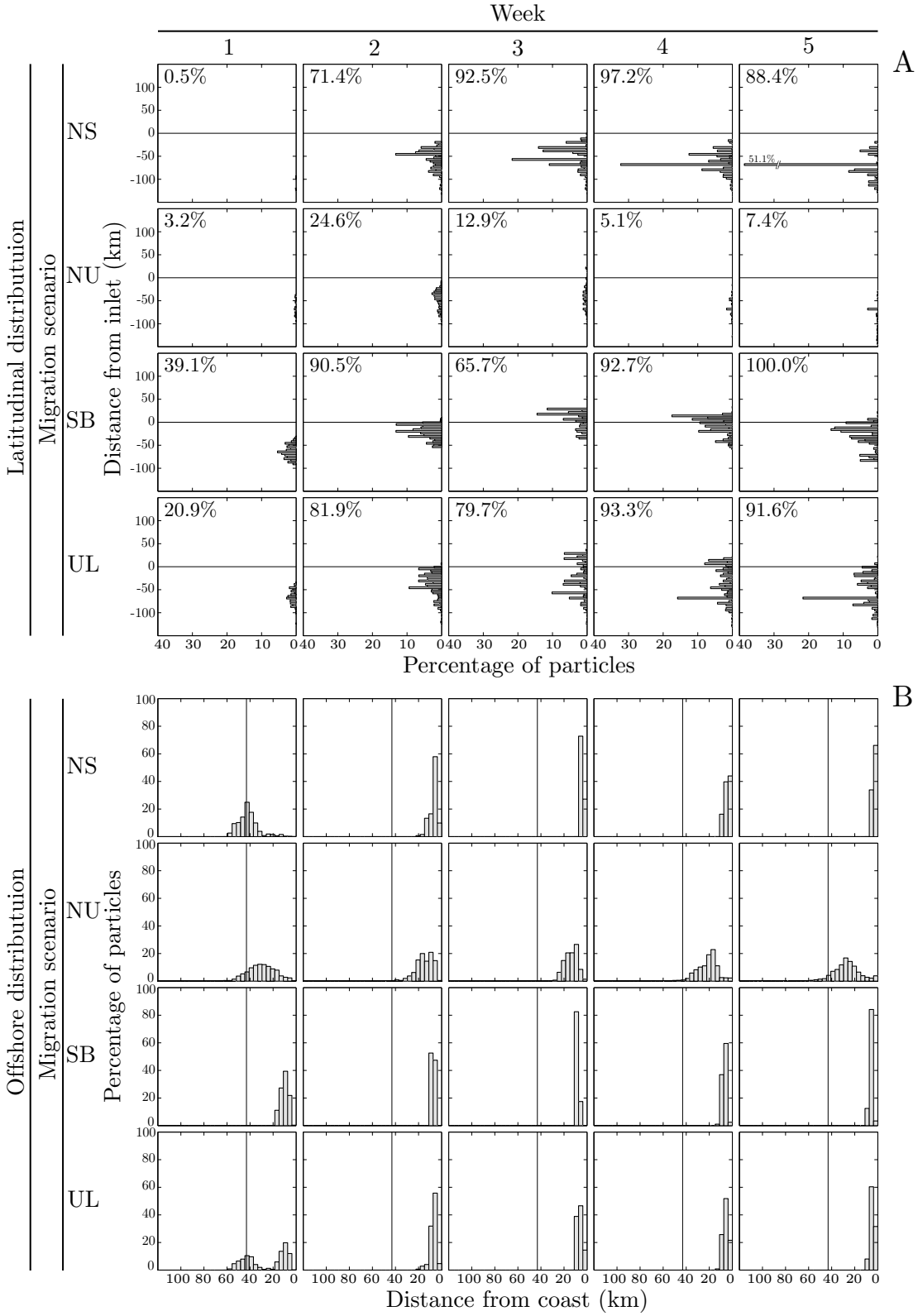

Figure 5.13: Spring simulation, third release. Same as in Figure 5.8.

5.4 Discussion and conclusions

The present study used four different vertical migration scenarios that were kept constant for the duration of all the expected planktonic development of the larvae. This option was taken due to the lack of detailed information necessary to simulate these ontogenetic shifts of distribution in *Carcinus maenas*. This is, however, an unrealistic situation because in most of the cases behavioural reactions of decapod larvae change throughout larval ontogeny, leading to modifications of the average depth of distribution with age [Sulkin, 1984; Queiroga and Blanton, 2004]. Ontogenetic migrations most likely will also affect advection patterns in this species, as suggested for other invertebrate groups [Peterson, 1998]. A second simplification of the model regarding the biology of the larvae is that mortality was not considered. Estimates for decapods indicate that larval mortality may often exceed 90% over the full planktonic period [Morgan, 1995]. Based on data on abundance of first and last stage larvae found inside the Ria de Aveiro [Queiroga, 1995], and assuming that larvae that do not return to the estuary will die, it is possible to estimate an overall mortality value of 99% for *Carcinus maenas*: first zoea produced inside the estuary were 100 times more abundant than the megalopae that recruited into it. Little is known on how these high mortality values are distributed with age of larvae, and on how they change spatially (e.g., concentrations of predators might be higher close to the coast). Setting a constant mortality with time or space is a simplification that would not change the pattern of distribution, it would just decrease the number of drifters returning or retained close to the coast. In our opinion, these imperfections of the model do not impinge on the interpretation of the very clear and distinctive patterns of dispersal produced by the simulations, which depended on the type of migration and on its interaction with wind regime.

The first pattern that emerged from the simulations was that particles with DVM were more retained in the inner shelf during upwelling than in any other combination of migration scenario and wind regime. This arises from the bottom Ekman coastward current characteristic of the upwelling circulation that contrasts with the downwelling regime (Figure 5.14). Both DVM scenarios (between surface and bottom, SB, and

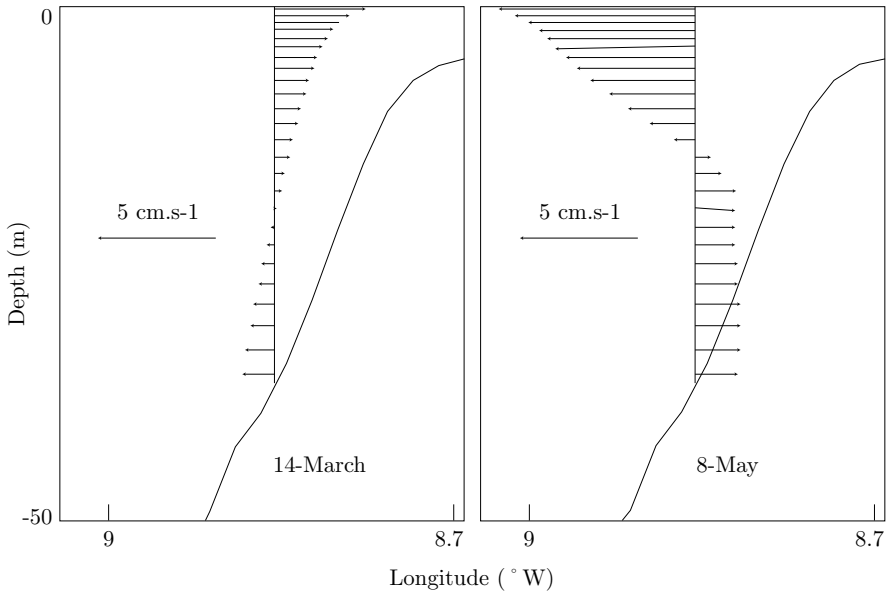

Figure 5.14: Vertical profile of velocity in front of the Ria de Aveiro inlet during one downwelling (left) and upwelling (right) events. The currents shown are averaged on the inertial period in the days 14 of March and 8 of May, respectively.

between upper and lower levels, UL) imposed a longer period of time spent in the deeper layers than at the surface, following observations made in several species [Jamieson and Philips, 1988; Shanks, 1986; Abelló and Guerao, 1999], and coastward advection during the day overcompensating the surface offshore transport during the night. A second pattern was that dispersal was the highest and retention was the lowest in the particles that were not subjected to DVM and released with an uniform vertical distribution (NU). The lowest aggregation resulted from particles at different levels being subjected to different instantaneous currents, thereby being separated from each other. The size of the larval pool in the inner shelf after five weeks under this scenario was typically below 4% independently of the wind regime, while retention under the other scenarios often rose above 50%. Surface particles (NS) originated a third pattern. These particles were more sensitive to the wind, responding more quickly and extensively to wind variations. Aggregation near the coast under this scenario occurred both with non-upwelling and upwelling regimes, and was associated with westerly winds and the resulting convergence of the surface layer to the coast.

The main conclusion of this study is that upwelling conditions do not necessarily lead to offshore transport of larvae. They would in larvae that do not display vertical migration behaviour and would either remain at the surface or be passively redistributed along the water column by the vertical component of the currents. However, decapod larvae seldom, if ever, show these characteristics. In fact, given that nocturnal DVM is the general condition exhibited by these organisms, it may be that in coasts subjected to upwelling, retention in the inner shelf and recruitment to the littoral habitats is enhanced during the upwelling season. In the coast of northwest Iberia, which lacks topographic irregularities that may originate concentration and retention areas, nocturnal migration may constitute an important mechanism to avoid seaward dispersal of the larvae.

Two aspects of the biology of *Carcinus maenas* in the Portuguese coast are consistent with the retention of larvae in the inner shelf through DVM. A study of the distribution of larvae off the Aveiro coast during April [Queiroga, 1996] showed that maximum abundance of all larval stages was located in the middle shelf, and that larvae were not collected beyond the shelf break. The results of the simulations reported in the present study show that the scenarios without DVM resulted in particles distribution that often extended well beyond the shelf break, in sharp contrast with the scenarios with DVM (Figures 5.8 to 5.13, panel B). The other aspect is a temporal mismatch between the initiation of larval production and subsequent recruitment. In the Portuguese coast, large numbers of first zoeae of *C. maenas* can be found from November to July [Gonçalves, 1991; Paula, 1993; Queiroga, 1995; Sprung, 2001], but major recruitment events in the estuaries only take place from April onwards [Queiroga, 1993; Sprung, 2001; Almeida and Queiroga, 2003]. Larval development time cannot account for a delay of several months between production of larvae and recruitment, because *C. maenas* larvae take at most six weeks to develop from hatching to megalopae stage at the temperatures commonly found in Portugal during winter and early spring. This mismatch between larval production and recruitment [Sprung, 2001] could partly be explained if the onset of the upwelling season could aid in the retention of vertical migrating crab larvae in shelf waters. Climatological upwelling indices calculated for

the Portuguese coast [Huthnance et al., 2002] indicate that persistent upwelling events may start as early as March to May, and these could set the conditions for successful recruitment of the species.

Results of the present study concerning the scales of along-shore transport may also be relevant to understand the dynamics of *Carcinus maenas* populations in the region. The west coast of northern Iberia has several estuaries and rias separated by distances of 20 to 60 km, all harbouring populations of the species. The along-shore distribution of the particles retained in the inner shelf showed maxima predominantly located to the north of the inlet of the Ria de Aveiro in winter and to the south in spring (Figures 5.8 to 5.13, panel A). The direction of transport is consistent with the winter and summer oceanographic regimes in the region [Wooster et al., 1976; Mazé et al., 1997; Vitorino et al., 2002; Huthnance et al., 2002; Peliz et al., 2005]. During the simulated period, which lasted five consecutive weeks, the maxima were located typically at distances of 50 to 100 km from the release point. This radius of dispersal is enough to account for the exchange of larvae between adjacent systems, indicating that these populations likely exchange individuals on a regular basis.

Another result of this simulation study that bears on the mechanisms of across-shore transport of larvae is that onshore wind events were responsible for down-the-wind advection of neustonic larvae towards the coast. Correlations between onshore winds and recruitment have been found in several studies of invertebrate larvae [e.g. Hawkins and Hartnoll, 1982; Olmi, 1995], and a recent study showed that surface drifters are advected onshore by sea-breezes [Tapia et al., 2004]. Since megalopae of decapods may occupy the neuston layer during extended periods of time, these larvae may use occasional or persistent onshore winds for return to littoral habitats [Shanks, 1995].

Several studies on recruitment of invertebrate larvae in the upwelling system of California and Oregon [e.g. Johnson et al., 1986; McConnaughey et al., 1995; Wing et al., 1995] stress that the patterns of across- and along-shore dispersal depend on the nature of the interactions between physical forcing and larval behaviour. As in other modelling studies, the predictions of the present work are speculative because of the uncertainties regarding both the ability of the model to realistically represent

the main aspects of oceanography of the area and the details of the behaviour of the larvae. However, the results of the model help in the formulation of hypothesis that can be experimentally addressed in the future. One is that the delay between production of larvae and recruitment depends on the onset of the upwelling season. The other is that there is a regular exchange of larvae between adjacent populations of *Carcinus maenas* on the west coast of northern Iberia. These ideas can be put to test using observational programs on supply of larvae into estuaries and recruitment extending from winter into early summer, and with the use of high resolution genetic markers to describe the genetic structure of the populations along the coast.

Chapter 6

Summary

A three-dimensional ocean numerical model was used to study the influence of the physical conditions on the dispersion and recruitment of larvae with active vertical migration at the northwestern Portuguese shelf region. The work started with the inclusion of drifters in a model for the Western Iberian Peninsula forced by tides. In the drifters it was imposed vertical migration with daily periodicity. It was concluded that the interaction between vertical migration and tidal currents does not produce relevant horizontal transport of the drifters.

The extensive work done with tidal modelling allowed an increment in the knowledge of tidal dynamics in the region. The tidal simulations were done under homogeneous conditions which, for the shelf region, corresponds to the winter situation when the shelf is nearly homogeneous. The tidal currents are dominated by the semi-diurnal harmonic M_2 and are amplified over the shelf. The diurnal components suffer a greater amplification, specially K_1, over the Lisbon Promontory. The analysis of vertical parameters of tidal ellipses showed a clear separation between semi-diurnal and diurnal components, and between the almost barotropic open sea circulation and depth dependent shelf currents.

Once the tidal currents are not responsible for significative horizontal transport of drifters with daily vertical migration, another model was constructed, this time forced by air-ocean bulk fluxes. The model created was able to simulate the main features of the northwestern Portuguese shelf circulation, being the wind and heat fluxes the main

forcing mechanisms. The presence and dynamics of a fresher buoyant plume characteristic of the region, created by the rivers runoff, was also verified. The simulations were done in parallel with hydrological and currentmeters observations and the model results compare with the observations, giving confidence to use the model configuration created in the study of the influence of the diel vertical migration (DVM) and physical forcings on the dispersion and retention of larvae in the shelf. The northwestern Portuguese shelf is a region without prominent bathymetric or coastal features which could origin topography-induced circulation able to retain particles. The retention potential is, thus, a consequence of the physical forcings and the interaction of these forcings with the vertical migration of the larvae. The study used four different vertical migration scenarios that were kept constant for the duration of all the expected planktonic development of the larvae, using *Carcinus maenas* as model species. The results showed that particles with DVM were more retained in the inner shelf during upwelling conditions than in any other combination of migration scenario and wind regime. The DVM imposed a longer period of time spent in the deeper layers than at the surface, and thence coastward advection during the day overcompensating the surface offshore transport during the night. The dispersal was highest and retention was lowest in the particles that were not subjected to DVM and released with an uniform vertical distribution. The lowest aggregation resulted from particles at different levels being subjected to different instantaneous currents, thereby being separated from each other. Particles at the surface were more sensitive to the wind, responding more quickly and extensively to wind variations. Aggregation near the coast under this scenario occurred both with non-upwelling and upwelling regimes, and was associated with westerly winds and the resulting convergence of the surface layer to the coast.

The main conclusion of this study is that upwelling conditions do not necessarily lead to offshore transport of larvae. They would in larvae that do not display vertical migration behaviour and would either remain at the surface or be passively redistributed along the water column by the vertical component of the currents. However, decapod larvae seldom, if ever, show these characteristics. In fact, given that nocturnal DVM is the general condition exhibited by these organisms, it may be that in coasts subjected

to upwelling, retention in the inner shelf and recruitment to the littoral habitats is enhanced during the upwelling season. In the coast of northwest Iberia, which lacks topographic irregularities that may originate concentration and retention areas, nocturnal migration may constitute an important mechanism to avoid seaward dispersal of the larvae.

In addition to the results and conclusions of this thesis it was developed a web page for tidal prediction at the Western Iberian Peninsula and a collection of Matlab utilities for the initialisation, analysis and visualisation of the model simulations. Both are freely available at the server of the Ocean Modelling Group `http://neptuno.fis.ua.pt`.

Bibliography

Abelló, P., Guerao, G., 1999. Temporal variability in the vertical and mesoscale spatial distribution of crab megalopae (Crustacea: Decapoda) in the Northwestern Mediterranean. Est. Coast. Shelf. Sci. 49, 129–139.

Almaça, C., 1962. Sur la distribution géographique du gendre *Carcinus* Leach (Crust. Dec. Brach.). Revista da Faculdade de Ciências (Universidade de Lisboa) 10, 109–113.

Almeida, M. J., Queiroga, H., 2003. Physical forcing of onshore transport of crab megalopae in the northern Portuguese upwelling system. Est. Coast. Shelf. Sci. 57, 1091–1102.

Arakawa, A., Lamb, V., 1977. Computational design of the basic dynamical processes of the UCLA general circulation model and water circulation. Vol. 17 of Methods in Computational Physics. Academic Press, 1977, pp. 174–267.

Batteen, M. L., Martinez, J. R., Bryan, D. W., Buch, E. J., 2000. A modeling study of the coastal eastern boundary current system off Iberia and Morocco. J. Geophys. Res. 105, 14173–14195.

Boehlert, G. W., Watson, W., Sun, L. C., 1992. Horizontal and vertical distributions of larval fishes around an isolated oceanic island in the tropical Pacific. Deep-Sea Res. Part A 39, 439–466.

Chiswell, S. M., Booth, J. D., 1999. Rock lobster *Jasus edwardsii* larval retention by the Wairarapa Eddy off New Zealand. Mar. Ecol. Prog. Ser. 183, 227–240.

da Silva, A. J., 1992. Dependence of upwelling related circulation on wind forcing and stratification over the Portuguese northern shelf. ICES CM (C17).

Darwirs, R. R., 1985. Temperature and development of *Carcinus maenas* (Decapoda) in the laboratory: prediction of larval dynamics in the sea. Mar. Ecol. Prog. Ser. 24, 297–302.

Davies, A. M., Kwong, S. C. M., Flather, R. A., 1997. Formulation of a variable-function three-dimensional model, with applications to the M_2 and M_4 tide on the North-West European Continental Shelf. Cont. Shelf Res. 17, 165–204.

de Mesquita, A. R., 2003. On the harmonic constants of tides and tidal currents of the South-eastern brazilian shelf. Cont. Shelf Res. 23, 1227–1237.

Dias, J. M., Lopes, J. F., Dekeyser, I., 2003. A numerical system to study the transport properties in the Ria de Aveiro lagoon. Ocean Dynamics 53, 220–231.

dos Santos, A., Santos, A. M. P., Loureno, P., Queiroga, H., Conway, D., in preparation. Decapod larvae daily migration to the neuston layer in a coastal upwelling ecosystem.

d'Udekem d'Acoz, C., 1999. Inventaire et Distribution des Crustacés Décapodes de l'Atlantique Nord-Oriental, de la Méditerranée et des Eaux Continentales Adjacentes au Nord de 25 °N. Vol. 40. Muséum National d'Histoire Naturelle, Service Patrimoine Naturel, Collection Patrimoines Naturels, 383 pp.

Durski, S. M., Glenn, S. M., Haidvogel, D. B., 2004. Vertical mixing schemes in the coastal ocean: Comparison of the level 2.5 mellor-yamada scheme with an enhanced version of the k-profile parameterization. J. Geophys. Res. 109, C01015, doi: 10.1029/2002JC001702.

Egbert, G., Bennett, A., Foreman, M., 1994. TOPEX/POSEIDON tides estimated using a global inverse model. J. Geophys. Res. 99, 24821–24852.

Egbert, G. D., Erofeeva, S. Y., 2002. Efficient inverse modeling of barotropic ocean tides. J. Atmos. Ocean. Tech. 19, 183–204.

Fanjul, E. A., Goméz, B. P., Sánchez-Arévalo, I. R., 1997. A descripton of tides in the Eastern North Atlantic. Prog. Oceanogr. 40, 217–244.

Fiúza, A., Macedo, M., Guerreiro, M., 1982. Climatological space and time variation of the Portuguese coastal upwelling. Oceanol. Acta 5, 31–40.

Fiúza, A. F. G., Hamann, M., Ambar, I., del Río, G. D., González, N., Cabanas, J. M., 1998. Water masses and their circulation off western Iberia during May 1993. Deep-Sea Res. Part I 45, 1127–1160.

Fortunato, A., Pinto, L., Oliveira, A., Ferreira, J. S., 2002. Tidally generated shelf waves off the western Iberian coast. Cont. Shelf Res. 22, 1935–1959.

Forward Jr., R. B., Tankersley, R. A., 2001. Selective tidal-stream transport of marine animals. Oceanogr. Mar. Biol. Annu. Rev. 39, 305–353.

Freeland, H., 1994. Ocean circulation at and near Cobb Seamount. Deep-Sea Res. Part I 41, 1715–1732.

Frouin, R., Fiúza, A. F. G., Ambar, I., Boyd, T. J., 1990. Observations of a poleward surface current off the coasts of Portugal and Spain during the winter. J. Geophy. Res. 95, 679–691.

Gonçalves, F., 1991. Zooplanctôn e ecologia larvar de crustáceos decápodes no estuário do Rio Mondego. Ph.D. thesis, Universidade de Coimbra.

Haidvogel, D. B., Arango, H., Hedstrom, K., Beckman, A., Malanotte-Rizzoli, P., 2000. Model evaluation experiments in the North Atlantic Basin: simulations in nonlinear terrain following coordinates. Dyn. Atmos. Oceans 32, 239–281.

Haidvogel, D. B., Beckmann, A., 1999. Numerical Ocean Circulation Modeling. Vol. 2 of Series on Environmental Science and Management. Imperial College Press.

Hawkins, S. J., Hartnoll, R. G., 1982. Settlement patterns of *Semibalanus balanoides* (L.) in the Isle of Man (1977-1981). J. Exp. Mar. Biol. Ecol. 62, 271–283.

Hill, A. E., 1991a. A mechanism for horizontal zooplankton transport by vertical migration in tidal currents. Mar. Biol. 111, 485–492.

Hill, A. E., 1991b. Vertical migration in tidal currents. Mar. Ecol. Prog. Ser. 75, 39–54.

Hill, A. E., 1995. The kinematical principles governing horizontal transport induced by vertical migrations in tidal flows. J. Mar. Biol. Ass. UK 75, 3–13.

Huthnance, J. M., Aken, H. M. V., White, M., Barton, E. D., Cann, B. L., Coelho, E. F., Fanjul, E. Á., Miller, P., Vitorino, J., 2002. Ocean margin exchange – water flux estimates. J. Mar. Syst. 32, 107–137.

Ives, D. C., Zacharias, R. M., 1987. Conformal mapping and orthogonal grid generation. In: AIAA/SAE/ASME/ASEE Joint Propulsion Conference. San Diego, California, paper number 87–2057.

Jamieson, G. S., Philips, A. C., 1988. Ocurrence of *Cancer* crab (*C. magister* and *C. oregonensis*) megalopae off the west coast of Vancouver Island, British Culumbia. Fish. Bull. 86, 525–542.

Johnson, D. F., Botsford, L. W., Methot Jr, R. D., Wainwright, T. C., 1986. Wind stress and cycles in dungeness crab (*Cancer magister*) catch off California, Oregon, and Washington. Can. J. Fish. Aquat. Sci. 43, 838–845.

Jones, F. R. H., Walker, M. G., Arnold, G. P., 1984. Tactics of fish movement in relation to migration strategy and water circulation. Mechanisms of migrations in fishes. Plenum Press, New York, pp. 185–287.

Kloppmann, M., Mohn, C., Bartsch, J., 2001. The distribution of blue whiting eggs and larvae on Porcupine Bank in relation to hydrography and currents. Fish. Res. 50, 89–109.

Large, W. G., McWilliams, J. C., Doney, . C., 1994. Oceanic vertical mixing: A review and a model with nonlocal boundary layer parameterization. Rev. Geophys. 32, 363–403.

Le Roux, P. J., Branch, G. M., Joska, M. A. P., 1990. On the distribution, diet and possible impact of the invasive European shore crab *Carcinus maenas* (L.) along the South African coast. S. Afr. J. Mar. Sci. 9, 85–92.

Lee, T. N., Rooth, C., Williams, E., McGowan, M., Szmant, A. F., Clarke, M. E., 1992. Influence of Florida Current, gyres and wind-driven circulation on transport of larvae and recruitment in the Florida Keys coral reefs. Cont. Shelf. Res. 12, 971–1002.

Mazé, J. P., Arhan, M., Mercier, H., 1997. Volume budget of the eastern boundary layer off the Iberian Peninsula. Deep-Sea Res. Part I 44, 1543–1574.

McConnaughey, R. A., Armstrong, D. A., Hickey, B. M., 1995. Dungeness crab (*Cancer magister*) recruitment variability and Ekman transport of larvae. In: ICES Mar. Sci. Symp. Vol. 199. Copenhagen, pp. 167–174.

Mellor, G. L., Yamada, T., 1982. Development of a turbulence closure model for geophysical fluid problems. Rev. Geophys. 20, 851–875.

Mohamedeen, H., Hartnoll, R. G., 1989. Larval and post-larval growth of individually reared specimens of the common shore crab *Carcinus maenas* (L.). J. Exp. Mar. Biol. Ecol. 134, 1–24.

Morgan, S. G., 1995. Life and death in the plankton: larval mortality and adaptation. Ecology of marine invertebrate larvae. CRC Press, Ch. 9, pp. 279–321.

New, A. L., da Silva, J., 2002. Remote-sensing evidence for the local generation of internal soliton packets in the central Bay of Biscay. Deep-Sea Res. Part I 49, 915–934.

Nishimoto, M. M., Washburn, L., 2002. Patterns of coastal eddy circulation and abundance of pelagic juvenile fish in the Santa Barbara Channel, California, USA. Mar. Ecol. Prog. Ser. 241, 183–199.

Oliveira, P. B., Peliz, Á., Dubert, J., Rosa, T. L., Santos, A. M. P., 2004. Winter geostrophic currents and eddies in the western Iberia coastal transition zone. Deep-Sea Res. Part I 51, 367–381.

Olmi, E. J., 1995. Ingress of blue crab megalopae in the York River, Virginia, 1987-1989. Bull. Mar. Sci. 57, 753–780.

Paula, J., 1993. Ecologia da fase larvar e recrutamento de crustáceos decápodes no estuário do Rio Mira. Ph.D. thesis, Faculdade de Ciências, Universidade de Lisboa.

Pawlowicz, R., Beardsley, B., Lentz, S., 2002. Classic tidal harmonic analysis including error estimates in MATLAB using T_TIDE. Comput. Geosci. 28, 929–937.

Peliz, Á., Dubert, J., Haidvogel, D. B., 2003a. Subinertial response of a density-driven eastern boundary poleward current to wind forcing. J. Phys. Oceanogr. 33, 1633–1650.

Peliz, Á., Dubert, J., Haidvogel, D. B., Cann, B. L., 2003b. Generation and unstable evolution of a density-driven Eastern Poleward Current: The Iberian Poleward Current. Journal of Geophysical Research 108, 3268, doi: 10.1029/2002JC001443.

Peliz, Á., Dubert, J., Santos, M., Oliveira, P., Cann, B. L., 2005. Winter upper ocean circulation in the Western Iberian Basin – Fronts, Eddies and Poleward Flows: an overview. Deep-Sea Res. Part I 1, 621–646.

Peliz, Á., Rosa, T. L., Santos, A. M. P., Pissarra, J. L., 2002. Fronts, jets and counter-flows in the Western Iberian upwelling system. J. Mar. Syst. 35, 61–77.

Pereira, A. F., Beckmann, A., Helmmer, H. H., 2002. Tidal mixing in the southern Weddell Sea: results from a tree-dimensional model. J. Phys. Oceanogr. 32, 2151–2170.

Pereira, F., Pereira, R., Queiroga, H., 2000. Flux of decapod larvae and juveniles at a station in the lower Canal de Mira (Ria de Aveiro, Portugal) during one lunar month. Invertebr. Reprod. Dev. 38, 183–206.

Peterson, W., 1998. Life cycle strategies of copepods in coastal upwelling zones. J. Mar. Syst. 15, 313–326.

Prandle, D., 1982. The vertical structure of tidal currents and other oscillatory flows. Cont. Shelf Res. 1, 191–207.

Prandle, D., 1997a. The influence of bed friction and vertical eddy viscosity on tidal propagation. Cont. Shelf Res. 17, 1367–1374.

Prandle, D., 1997b. Tidal currents in shelf seas – their nature and impacts. Prog. Oceanogr. 40, 245–261.

Pugh, D. T., 1987. Tides, Surges and Mean Sea Level. John Wiley & Sons Ltd.

Queiroga, H., 1993. An analysis of the size structure of *Carcinus maenas* (L.) in canal de Mira (Ria de Aveiro, Portugal) using the probability paper method. BIOS 1, 89–106.

Queiroga, H., 1995. Processos de dispersão e recrutamento das larvas do caranguejo *Carcinus maaenas* (L.) na Ria de Aveiro. Ph.D. thesis, Universidade de Aveiro.

Queiroga, H., 1996. Distribution and drift of *Carcinus maenas* (L.) (Decapoda, Portunidae) larvae over the continental shelf off northern Portugal in April of 1991. J. Plankton Res. 18, 1981–2000.

Queiroga, H., 1998. Vertical migration and selective tidal stream transport in the megalopa of the crab *Carcinus maenas*. Hydrobiologia 375/376, 137–149.

Queiroga, H., 2003. Wind forcing of crab megalopae recruitment to an estuary (Ria de Aveiro) in the northern Portuguese upwelling system. Invertebr. Reprod. Dev. 43, 47–54.

Queiroga, H., Blanton, J., 2004. Interactions between behavior and physical forcing in the control of horizontal transport of decapod crustacean larvae. Adv. Mar. Biol. 47, 107–214.

Queiroga, H., Costlow, J. D., Moreira, M. H., 1994. Larval abundance patterns of *Carcinus maenas* (Decapoda, Brachyura) in Canal de Mira (Ria de Aveiro, Portugal). Mar. Ecol. Prog. Ser. 111, 63–72.

Queiroga, H., Costlow, J. D., Moreira, M. H., 1997. Vertical migration of the crab *Carcinus maenas* first zoea in an estuary: implications for tidal stream transport. Mar. Ecol. Prog. Ser. 149, 121–132.

Ribeiro, A. C., Peliz, Á., Santos, A. M. P., 2005. A study of the response of Chlorophyll-*a* biomass to a winter upwelling event off Western Iberia using SeaWIFS and in situ data. J. Mar. Syst. 53, 87–107.

Rice, A. L., Ingle, R. W., 1975. The larval development of *Carcinus maenas* (L.) and *C. mediterraneous Czerniavsky* (Crustacea, Brachyura, Portinudae) reared in the laboratory. Bull. Br. Mus. (Nat. Hist.) Zool. 28, 103–120.

Røed, L. P., Shi, X. B., 1999. A numerical study of the dynamics and energetics of cool filaments, jets, and eddies off the Iberian Peninsula. J. Geophys. Res. 112, 29817–29841.

Santos, A. M. P., Peliz, A., Dubert, J., Oliveira, P. B., Angélico, M. M., Ré, P., 2004. Impact of a winter upwelling event on the distribution and transport of sardine (*Sardine pilchardus*) eggs and larvae off western Iberia: a retention mechanism. Cont. Shelf. Res. 24, 149–165.

Sauvaget, P., David, E., Soares, C. G., 2000. Modelling tidal currents on the coast of Portugal. Coast. Eng. 40, 393–409.

Shanks, A. L., 1986. Vertical migration and cross-shelf dispersal of larval *Cancer* spp. and *Randallia ornata* (Crustacea, Brachyura) off the coast of southern California. Mar. Biol. 92, 189–200.

Shanks, A. L., 1995. Mechanisms of cross-shelf dispersal of larval invertebrates and fish. Ecology of marine invertebrate larvae. CRC Press, Ch. 10, pp. 323–367.

Shchepetkin, A. F., McWilliams, J. C., 1998. Quasi-monotone advection schemes based on explicit locally adaptive dissipation. Mon. Wea. Rev. 126, 1541–1580.

Shchepetkin, A. F., McWilliams, J. C., 2003. A method for computing horizontal pressure-gradient force in an oceanic model with a non-aligned vertical coordinate. J. Geophys. Res. 108, 1–34.

Shchepetkin, A. F., McWilliams, J. C., 2005. The regional ocean modeling system (ROMS): A split-explicit, free-surface, topography-following coordinates ocean model. Ocean Model. 9, 347–404.

Simpson, J. H., 1997. Physical processes in ROFI regime. J. Mar. Syst. 12, 3–15.

Song, Y., Haidvogel, D., 1994. A semi-implicit ocean circulation model using a generalized topography-following coordinate system. J. Comput. Phys. 115, 228–244.

Song, Y. T., 1998. A general pressure gradient formulation for ocean models. Part I: Scheme design and diagnostic analysis. Mon. Wea. Rev. 126, 3213–3230.

Song, Y. T., White, D. G., 1998. A general pressure gradient formulation for ocean models. Part II: Energy, momentum, and bottom torque consistency. Mon. Wea. Rev. 126, 3231–3247.

Souza, A. J., Simpson, J. H., 1996. The modification of tidal ellipses by stratification in the Rhine ROFI. Cont. Shelf Res. 16, 997–1007.

Sprung, M., 2001. Larval abundance and recruitment of *Carcinus maenas* L. close to its southern geographic limit: a case of match and mismatch. Hydrobiologia 449, 153–158.

Stevens, I., Hamann, M., Johnson, J. A., Fiúza, A. F. G., 2000. Comparisons between a fine resolution model and observations in the Iberian shelf-slope region. J. Mar. Syst. 26, 53–74.

Sulkin, S. D., 1984. Behavioral basis of depth regulation in the larvae of brachyuran crabs. Mar. Ecol. Prog. Ser. 15, 181–205.

Tapia, F. J., Pineda, J., Ocampo-Torres, F. J., Fuchs, H. L., Parnell, P. E., Montero, P., Ramos, S., 2004. High-frequency observations of wind-forced onshore transport at a coastal site in Baja California. Cont. Shelf Res. 24, 1573–1585.

Thresher, R., Proctor, C., Ruiz, G., Gurney, R., MacKinnon, C., Walton, W., Rodriguez, L., Bax, N., 2003. Invasion dynamics of the European shore crab, *Carcinus maenas*, in Australia. Mar. Biol. 142, 867–876.

Vitorino, J., Oliveira, A., Jouanneau, J. M., Drago, T., 2002. Winter dynamics on the northern Portuguese shelf. Part 1: physical processes. Prog. Oceanogr. 52, 129–153.

Werner, F. E., Perry, R. I., Lough, R. G., Naimie, C. E., 1996. Trophodynamic and advective influences on Georges Bank larval cod and haddock. Deep-Sea Res. Part II: 43, 1793–1822.

Wilkin, J., Headström, K. S., 1998. User's manual for an orthogonal curvilinear grid-generation package. Tech. rep., University of Auckland, New Zealand, and Rutgers University, USA.

Wing, S. R., Botsford, L. W., Largier, J. L., Morgan, L., 1995. Spatial structure of relaxation events and crab settlement in the northern California upwelling system. Mar. Ecol. Prog. Ser. 128, 199–211.

Wooster, W. S., Bakun, A., McLain, D. R., 1976. The seasonal upwelling cycle along the eastern boundary of the North Atlantic. J. Mar. Res. 34, 131–141.

Xing, J., Davies, A. M., 1997. Influence of stratification upon diurnal tidal currents in shelf edge regions. J. Phys. Oceanogr. 29, 1803–1831.

Xing, J., Davies, A. M., 1998. A three-dimensional model of internal tides on the Malin-Hebrides shelf and shelf edge. J. Geophys. Res. 103, 27821–27847.

Xing, J., Davies, A. M., 2002. Influence of wind direction, wind waves, and density stratification upon sediment transport in shelf edge regions: The Iberian shelf. J. Geophys. Res. 107, 16–1–16–24.

Zeldis, J. R., Jillett, J. B., 1982. Aggregation of pelagic *Munida gregaria* (Fabricius) (Decapoda, Anomura) by coastal fronts and internal waves. J. Plankton Res. 4, 839–857.

Zeng, C., Naylor, E., 1996. Occurrence in coastal waters and endogenous tidal swimming rhythms of late megalopae of the shore crab *Carcinus maenas*: implications for onshore recruitment. Mar. Ecol. Prog. Ser. 136, 69–79.